Università degli Studi di Milano-Bicocca
Facoltà di Scienze Matematiche, Fisiche e Naturali
Laboratoire des Solides Irradiés, École Polytechnique, Paris

Corso di Laurea Specialistica in Fisica

Ab initio study of microscopic charge fluctuations in graphite

Tesi di Laurea Specialistica

28 Settembre 2009

Giulia Pegolotti

Matricola 064944

Relatore: **Prof. Giorgio BENEDEK**

Relatore esterno: **Dott.ssa Lucia REINING**

Anno Accademico 2008-2009

Merci

Les six mois passés à Paris ont été une expérience unique.
Je remercie tous les gens du bâtiment 411 pour leur accueil chaleureux et leur sympathie, et pour la possibilité qui m'a été donnée de participer aux missions de Zurich et Berlin. Je me suis sentie tout de suite chez moi dans le groupe, malgré la durée relativement courte de mon séjour. Je suis reconnaissante à Lucia, qui m'a donné l'opportunité de travailler avec des personnes aussi compétentes. Elle a toujours été très gentille, disponible et prête à donner de précieux conseils malgré un emploi du temps très chargé. Merci à Ralf pour son aide et sa patience, qui ont été indispensables pour ce travail. Merci aussi à tous les autres: Giovanna, Julien, Feffe, Gaëlle, Arjan, Pina, Francesco, France, Matteo Guzzo, Matteo Gatti, Eleonora, Andrea, Hannes, Christine et Valérie. Les pauses en salle café me manqueront beaucoup, j'espère que je pourrai vous rendre visite et y participer encore quelquefois!
Grazie al Prof. Benedek, senza il cui aiuto non avrei potuto partire per Parigi, né per Londra l'anno prossimo.
Come non ringraziare i miei colocchi parigini, Fritzi, Giulia e Matteo. Anche se verso la fine è stata un po' dura, mi sono divertita ad abitare con voi e sono contenta di come è andata.
Merci anche agli amici di Bicocca, anche quelli che ormai sono parigini dentro: Matty, Fra, Vale, Eleonora, Ilaria, Alberto, Tamby, senza cui questi cinque anni non sarebbero stati gli stessi.
Grazie inoltre a Stefano che ha reso possibile che mi laureassi occupandosi in modo (puramente volontario!) della burocrazia. Grazie alle amichette di sempre, Claudia, Martina, Nicole, Serena, Valentina e Francesca, per tutto quello che abbiamo vissuto assieme e per quello che vivremo. Sono felice di essere diventata grande (forse) insieme a voi.
Grazie alla mia mamma e al mio papà, ai miei fratellini Luca e Tommy, allo zio Gipo, ai nonni Vit, Mariù e Anna: il vostro continuo sostegno è stato punto di partenza e appoggio di tutto quello che sono riuscita a fare.
L'ultimo grazie va a Lorenzo, per il suo supporto, per il bene che ci vogliamo e per le risate che facciamo insieme.
Grazie.

Giulia

Contents

Introduction

Electronic dynamics in atoms and molecules occurs on time scales of tens to ten thousands of attoseconds, corresponding to energies between 1 keV and 1 eV (1 as = 10^{-18} s).
The tools and techniques for observing and controlling this electronic motion are now becoming available and pave the way to the answer to scientific and technological challenges, such as detailed studies about information transport in biomolecules, or electronic currents in nanocircuits [1]. One of these experimental techniques is shown in [2], where electronic dynamics in space and time is deduced starting from frequency domain measurements in a inelastic X-ray scattering experiment (IXS). IXS is a energy-loss technique, like Electron Energy Loss Spectroscopy (EELS): this kind of experiments can be simulated through Theoretical Spectoscopy, which consists in the calculation of electronic excitations and represents a very powerful tool to understand properties of materials.

This work presents an *ab-initio* (i.e. parameter-free) approach to the problem of electronic dynamics, extending the technique adopted in [2] by exploiting the potentialities offered by Theoretical Spectroscopy. The final aim of the project is to give theoretical support and benchmark to future experimental works: this is actually the guiding philosophy of the European Theoretical Spectroscopy Facility [3], to which our laboratory is affiliated.
Electronic excitations, caused for example by light or irradiation by electrons, are in fact the key phenomenon in solid state studies, ranging from bulk systems to atoms, from surface to nanoscale systems. The progress in the technology of experimental spectroscopical techniques has stimulated in the last decades the development of more precise theoretical descriptions; in particular, the joint use of theory and computer simulation has allowed to achieve improvements in the study and prediction of optical properties of both finite and infinite systems.

The ambition of an *ab-initio* condensed matter study - to be able to reproduce and predict physical phenomena, without the need of any experimental parameter - is as much fascinating as expensive. The cost resides not only in the computational time required to carry out big calculations, but also in the quantity of theoretical concepts which necessarily form the basis of any application.
The work starts in Chapter 1 with a brief overview over the dielectric properties of solids as viewed by the classical theory of electromagnetism. Chapter 2 is then devoted to the development of the important link between the macroscopic view of Chapter 1 and the microscopic quantum-mechanical view presented in Chapter 3, with a particular emphasis on the relevance of local field effects, which reflect the microscopic dishomogeneity of crystals. Chapter 3 deals with the many body approach to the problem of electronic correlation: this represents the main obstacle in the calculation of excitations. The way that has been followed is that of density-based methods: density functional theory (DFT) and time dependent density functional theory (TDDFT) are briefly introduced.

Chapter 4 treats the implementation of these theories in codes, and presents some results on graphite, the material that has been chosen for the work. Graphite is a prototype for layered and anisotropic systems, and has already been object of many theoretical studies [4, 5].
Chapter 5 briefly presents the theory of collective excitations, plasmons, which are observed through EELS spectroscopy and then appear also in our simulations.
In Chapter 6 it is shown how the theoretical treatment of the problem allows the access to quantities which are not easily measured by experiments, but are important for the spatial resolution of the dynamics. With the implemented method, it is possible to investigate the importance of these elements, in order to guide experiments similar to that carried out in the reference article [2] to improve the resolution of results. The nature of charge oscillations and their time dependence are also studied, with a particular attention to the connection with plasmon excitations; this to find out which electrons contribute to the excitations.

1
Dielectric properties of solids

The results of this work are obtained with the techniques of Theoretical Spectroscopy [3], which merges the results of ordinary electromagnetic theory with the quantum mechanical microscopical point of view. This chapter gives a brief introduction to the classical optical properties of solids we will have to deal with.

1.1 Introduction

A solid represents an incredibly complicated system from the physical point of view.
The main way to discover the properties of matter is studying its response to an external perturbation, namely an external electromagnetic field, or a particle: this is what spectroscopy studies.
The most important quantity related to spectroscopical measurements is the dielectric function ε, which contains information about internal structure and properties of the material.

Originally, the dielectric function ε was a number (the dielectric constant) giving the extent to which the medium lowers the Coulomb interaction of charges (first definition of *screening*), or increases the capacitance of a capacitor.
Today ε is a frequency-dependent tensor which contains complicated information about the system, such as the inertia in the polarization of the medium, but also its non-locality nature. That is that the polarization at a given point is governed by the amplitude of the field at preceding moments in time, not only at given point, but also in its neighborhood, and all this is included in ε. This latter fact, related to the so-called *local-field effects*, will have an important role in this work.

1.2 Maxwell's Equations

1.2.1 Electromagnetic fields in a medium

Maxwell's equations are the fundamental equations of electromagnetic theory. They relate the space and time derivatives of the electric and magnetic fields to each other and to their sources, the charge and current densities ρ and $\mathbf{j}$. We adopt cgs-Gauss units[1] and express Maxwell's

[1] In cgs-Gaussian units, the constant k_c in the Coulomb expression of electrostatic force in vacuum $F = k_c \frac{q_1 q_2}{r^2}$ is equal to 1. In SI notation, $k_c = \frac{1}{4\pi\varepsilon_0}$.
So to obtain Maxwell'equations in SI units starting from the cgs-Gauss version, one has to replace $4\pi = \frac{1}{\varepsilon_0}$ and $\frac{4\pi}{c^2} = \mu_0$ (this latter coming from the relation $\varepsilon_0\mu_0 = \frac{1}{c^2}$)

equations as follows [6–8]:

$$\nabla \cdot \mathbf{D}(\mathbf{r},t) = 4\pi\rho_{ext}(\mathbf{r},t) \tag{1.1}$$
$$\nabla \cdot \mathbf{B}(\mathbf{r},t) = 0 \tag{1.2}$$
$$\nabla \times \mathbf{E}(\mathbf{r},t) = -\frac{1}{c}\frac{\partial}{\partial t}\mathbf{B}(\mathbf{r},t) \tag{1.3}$$
$$\nabla \times \mathbf{H}(\mathbf{r},t) = \frac{1}{c}\frac{\partial}{\partial t}\mathbf{D}(\mathbf{r},t) + \frac{4\pi}{c}\mathbf{j}_{free}(\mathbf{r},t) \tag{1.4}$$

where $\mathbf{E}(\mathbf{r},t)$ denotes the electric field, $\mathbf{H}(\mathbf{r},t)$ the magnetic field, $\mathbf{D}(\mathbf{r},t)$ the electric displacement and $\mathbf{B}(\mathbf{r},t)$ magnetic induction.

In Eq.(1.1), ρ_{ext} is the charge density of an external source, as opposed to ρ_{ind}, the displacement of charge within the medium.

$$\rho_{tot} = \rho_{ind} + \rho_{ext}$$

In Eq.(1.4), $\mathbf{j}_{free}$ is the current density of electrons free to move around the solid, consisting of two parts: $\mathbf{j}_{cond}$, due to the motion of the conduction electrons in presence of an electric field, and $\mathbf{j}_{ext}$, the current of an external source.
The total current density $\mathbf{j}_{total}$ includes also $\mathbf{j}_{bound}$, arising from the motion of the electrons bound to nuclei.

$$\mathbf{j}_{tot} = \mathbf{j}_{free} + \mathbf{j}_{bound} = (\mathbf{j}_{ext} + \mathbf{j}_{cond}) + \mathbf{j}_{bound} = \mathbf{j}_{ext} + \mathbf{j}_{ind}$$

The electric displacement $\mathbf{D}$ and the magnetic induction $\mathbf{B}$ are connected to the electric field $\mathbf{E}$ and magnetic field $\mathbf{H}$, respectively, by the constitutive equations:

$$\mathbf{D}(\mathbf{r},t) = \mathbf{E}(\mathbf{r},t) + 4\pi\mathbf{P}(\mathbf{r},t)$$
$$\mathbf{H}(\mathbf{r},t) = \mathbf{B}(\mathbf{r},t) - 4\pi\mathbf{M}(\mathbf{r},t)$$

where $\mathbf{P}(\mathbf{r},t)$ and $\mathbf{M}(\mathbf{r},t)$ are the polarization and magnetization of the medium.

The dielectric constant

Let us begin in this introductory chapter with the simplest possible case of response, which does not depend neither on position nor on direction: this is the case of an homogeneous and isotropic medium. Let the response be also local and time-independent, and the linear approximation be valid (see Appendix A).
If all these conditions are fulfilled, the connection between $\mathbf{E}(\mathbf{r},t), \mathbf{H}(\mathbf{r},t)$ and $\mathbf{D}(\mathbf{r},t), \mathbf{B}(\mathbf{r},t)$ is given by the simple relations

$$\mathbf{D}(\mathbf{r},t) = \varepsilon_M \mathbf{E}(\mathbf{r},t) \tag{1.5}$$
$$\mathbf{B}(\mathbf{r},t) = \mu \mathbf{H}(\mathbf{r},t)$$

where ε_M and μ are called the *dielectric* and the *permeability constants* (which are actually functions if our simplifying hypothesis are dropped)[2].

[2]The subscript M for the dielectric constant stands for macroscopic. The importance of this specification will be clarified throughout the work.

Also $\mathbf{P}(\mathbf{r},t)$ and $\mathbf{M}(\mathbf{r},t)$ and the conduction part of the current $\mathbf{j}_{cond}(\mathbf{r},t)$ can be expressed within these approximations as

$$\begin{aligned}\mathbf{P}(\mathbf{r},t) &= \chi_e \mathbf{E}(\mathbf{r}',t')\\ \mathbf{M}(\mathbf{r},t) &= \chi_m \mathbf{H}(\mathbf{r}',t')\\ \mathbf{j}_{cond}(\mathbf{r},t) &= \sigma \mathbf{E}(\mathbf{r}',t')\end{aligned}$$

where χ_e is the electric susceptibility, χ_m the magnetic susceptibility and σ the optical conductivity.

By combining the previous equations, we get the relation between the response functions χ_e, χ_m and ε_M, μ:

$$\varepsilon_M = 1 + 4\pi\chi_e \tag{1.6}$$

$$\mu = 1 + 4\pi\chi_m \tag{1.7}$$

For non-magnetic materials the magnetization can be omitted, so that $\mathbf{H}(\mathbf{r},t) = \mathbf{B}(\mathbf{r},t)$. This corresponds to setting $\mu = 1$ and $\chi_m = 0$, as we will do in this work.

1.2.2 Light-medium interaction: complex refraction index and absorption coefficient

When considering the interaction of light with a medium, we can set $\rho_{ext} = 0$ and $\mathbf{j}_{ext} = 0$ in Maxwell's Equations (1.1), because external sources can be considered far away.
Using the relations in Eqs.(1.5) and supposing as before isotropic, homogeneous and non-magnetic media we can write:

$$\nabla \cdot \mathbf{D} = 0$$

$$\nabla \cdot \mathbf{H} = 0$$

$$\nabla \times \mathbf{E} = -\frac{1}{c}\frac{\partial \mathbf{H}}{\partial t} \tag{1.8}$$

$$\nabla \times \mathbf{H} = \frac{\varepsilon_M}{c}\frac{\partial \mathbf{E}}{\partial t} + \frac{4\pi\sigma}{c}\mathbf{E} \tag{1.9}$$

From the vector identity

$$\nabla \times \nabla \times \mathbf{E} = \nabla(\nabla \cdot \mathbf{E}) - \nabla^2 \mathbf{E}$$

and Eqs. (1.8) and (1.9) we obtain the wave equation for a plane wave propagating in an energy-absorbing medium:

$$\nabla^2 \mathbf{E} = \frac{\varepsilon_M}{c^2}\frac{\partial^2 \mathbf{E}}{\partial t^2} + \frac{4\pi\sigma}{c^2}\frac{\partial \mathbf{E}}{\partial t} \tag{1.10}$$

As there is no net charge density, $\nabla \cdot \mathbf{E} = 0$ and solutions are necessarily restricted to transverse plane waves.
The general solution to Eq.(1.10) is

$$\mathbf{E} = \mathbf{E}_0 e^{i(\mathbf{q}\cdot\mathbf{r} - \omega t)} \tag{1.11}$$

Note that we may assume a sinusoidal (plane wave) variation of $\mathbf{E}$ only in a region large compared with the lattice constant.

Substituting Eq. (1.11) in (1.10) we find

$$\hat{q}^2 = \frac{\omega^2}{c^2}\left(\varepsilon + i\frac{4\pi\sigma}{\omega}\right) \tag{1.12}$$

Usually a *complex refractive index* $\hat{n}$ is defined such that

$$\hat{q} = \frac{\omega}{c}\hat{n} = \frac{\omega}{c}(n + ik) \tag{1.13}$$

where n is the refraction index, responsible for the dispersive optical phenomena, and k is the extinction coefficient, related to the phenomena of light absorption. This is evident if we use Eq.(1.13) to rewrite Eq.(1.11) as a damped wave:

$$\mathbf{E} = \mathbf{E}_0 \exp\left[-\frac{\omega}{c}\mathbf{k}\cdot\mathbf{r}\right] \exp\left[i\left(\frac{\omega}{c}\mathbf{n}\cdot\mathbf{r} - \omega t\right)\right] \tag{1.14}$$

The first exponential factor in Eq.(1.14) describes the attenuation of wave amplitude with distance. The *absorption coefficient*, which describes the fractional decrease in intensity with distance, is defined as

$$\alpha = -\frac{1}{I}\frac{dI}{dr} \tag{1.15}$$

where I is the intensity. Since the intensity is proportional to the square of the wave amplitude, we find from Eqs (1.14) and (1.15) that

$$\alpha = \frac{2\omega k}{c} \tag{1.16}$$

The second exponential factor in Eq.(1.14) describes a wave travelling with phase velocity $\frac{c}{n}$, hence the earlier identification of n as the refractive index.
Using Eqs. (1.12) and (1.13) we can obtain expressions for ε_M and σ in terms of n and k. Thus,

$$\begin{aligned} \varepsilon_M &= n^2 - k^2 \\ \frac{4\pi\sigma}{\omega} &= \frac{2nk}{\mu} \end{aligned} \tag{1.17}$$

We now define a complex dielectric function $\hat{\varepsilon}_M$ as

$$\hat{\varepsilon}_M = \varepsilon_{M1} + i\varepsilon_{M2} = \hat{n}^2$$

where ε_{M1} is the old ε of Eq.(1.17), the ε that appears in the usual versions of Maxwell's Equations when the properties of the medium are included. Thus,

$$\varepsilon_{M1} = n^2 - k^2 \tag{1.18}$$

$$\varepsilon_{M2} = 2nk = \frac{nc\alpha}{\omega} = \frac{4\pi\sigma}{\omega} \tag{1.19}$$

Eqs. (1.18) and (1.19) show that ε_{M1} and ε_{M2} are not independent quantities. In fact ε_{M1} and ε_{M2}, as well as n and k, are related in a quite fundamental way by means of the Kramers Kronig dispersion relations (see Appendix A).

1.2.3 External Fields and Induced Responses

Maxwell's equations in the form of Eqs.(1.1)-(1.4) are written in the common notation of electromagnetic theory, but we can also look at them from the point of view of the study of optical properties of solids.
A light wave incident on a sample can be described by its electric field. This electric field acts as a probe and induces another electric field in the material. The total field given by the sum of the induced and external fields is the electric field $\mathbf{E}$ appearing in Maxwell's equations, but the field that can be controlled is the external field, which actually acts as a perturbation on the system. Then we can write:

$$\mathbf{E}_{tot} = \mathbf{E}_{ext} + \mathbf{E}_{ind}$$

where $\mathbf{E}_{tot}$ is the $\mathbf{E}$ that appears in Eq. (1.3) and $\mathbf{E}_{ext}$ is the displacement in Eq. (1.1).

$$\mathbf{E} = \mathbf{E}_{tot} \qquad \mathbf{D} = \mathbf{E}_{ext} \tag{1.20}$$

The presence of an induced field in a material results in an induced charge density ρ_{ind} if the divergence of this induced field is nonzero.

1.2.4 Fourier Analysis of Maxwell's Equations

We assume that all the fields and sources can be decomposed into a complete set of plane waves varying as $e^{i(\mathbf{q}\cdot\mathbf{r}-\omega t)}$ for all $\mathbf{q}$ and ω. As the properties of solids are mostly studied in the reciprocal space, we are interested the form taken by Maxwell's Equations in the momentum-frequency domain.
We use the general convention (see Appendix B for the case of crystals)

$$f(\mathbf{r}) = \frac{1}{(2\pi)^3}\int \mathrm{d}\mathbf{q}\, e^{i\mathbf{q}\cdot\mathbf{r}}\widehat{f}(\mathbf{q}) \qquad \widehat{f}(\mathbf{q}) = \int \mathrm{d}\mathbf{r}\, e^{-i\mathbf{q}\cdot\mathbf{r}} f(\mathbf{r}) \tag{1.21}$$

$$f(t) = \int \mathrm{d}\omega\, e^{-i\omega t}\widehat{f}(\omega) \qquad \widehat{f}(\omega) = \frac{1}{2\pi}\int \mathrm{d}t\, e^{i\omega t} f(t) \tag{1.22}$$

Thus, for example[3]

$$\begin{aligned}\mathbf{E}(\mathbf{r},t) =& \frac{1}{(2\pi)^3}\int \mathrm{d}\mathbf{q}\int \mathrm{d}\omega\, \mathbf{E}(\mathbf{q},\omega)e^{i(\mathbf{q}\cdot\mathbf{r}-\omega t)}\\ \mathbf{E}(\mathbf{q},\omega) =& \frac{1}{2\pi}\int \mathrm{d}\mathbf{r}\int \mathrm{d}t\, \mathbf{E}(\mathbf{r},t)e^{-i(\mathbf{q}\cdot\mathbf{r}-\omega t)}\end{aligned}$$

Taking the Fourier Transform of Maxwell's equations as given by Eqs. (1.1)-(1.4) and considering the observation (1.20) we obtain:

$$\begin{aligned} i\mathbf{q}\cdot\mathbf{E}_{ext}(\mathbf{q},\omega) &= 4\pi\rho_{ext}(\mathbf{q},\omega)\\ \mathbf{q}\times\mathbf{E}_{tot}(\mathbf{q},\omega) &= \frac{\omega}{c}\mathbf{H}(\mathbf{q},\omega)\\ \mathbf{q}\cdot\mathbf{H}(\mathbf{q},\omega) &= 0\\ i\mathbf{q}\times\mathbf{H}(\mathbf{q},\omega) &= -\frac{i\omega}{c}\mathbf{E}_{tot}(\mathbf{q},\omega) + \frac{4\pi}{c}\mathbf{j}_{free}(\mathbf{q},\omega)\end{aligned}$$

[3]From now on, the hat on the transformed function will be implicitly assumed when the variables are $\mathbf{q}$ and ω: $f(\mathbf{q},\omega) \equiv \widehat{f}(\mathbf{q},\omega)$

The reciprocal space version of Maxwell's equations is very useful in many cases. For example, consider the case of a single plane wave

$$\mathbf{E} = \mathbf{E_0} e^{-i(\omega t - \mathbf{q}\cdot\mathbf{r})} \tag{1.23}$$

Taking the curl and the divergence of Eq. (1.23) we get

$$\nabla \times \mathbf{E} = i\mathbf{q} \times \mathbf{E}$$
$$\nabla \cdot \mathbf{E} = i\mathbf{q} \cdot \mathbf{E}$$

If we now write the electric field in terms of its transverse and longitudinal parts we obtain

$$\nabla \times (\mathbf{E^T} + \mathbf{E^L}) = i\mathbf{q} \times (\mathbf{E^T} + \mathbf{E^L})$$
$$\nabla \cdot (\mathbf{E^T} + \mathbf{E^L}) = i\mathbf{q} \cdot (\mathbf{E^T} + \mathbf{E^L})$$

The wave vector $\mathbf{q}$ is parallel to the direction of propagation, as is $\mathbf{E^L}$, but $\mathbf{E^T}$ is perpendicular to the direction of propagation. Thus,

$$\nabla \times \mathbf{E^L} = 0$$
$$\nabla \cdot \mathbf{E^T} = 0$$

and then

$$\nabla \times \mathbf{E} = \nabla \times \mathbf{E^T}$$
$$\nabla \cdot \mathbf{E} = \nabla \cdot \mathbf{E^L}$$

This holds for any vector field, and it is not strictly necessary to use a plane wave.
So if we work in reciprocal space, the electric field is easily decoupled in its transverse and longitudinal components, with $\mathbf{E^L}$ irrotational and $\mathbf{E^T}$ divergenceless.

1.3 Optical absorption and EELS Spectroscopies

Two spectroscopic techniques are particularly important in the theory we will be considering: optical absorption and Electron Energy Loss Spectroscopy. We will see that the calculations of the two spectra are closely related, even if they imply two different kind of perturbations, one transverse (absorption) and one longitudinal (EELS).

1.3.1 Absorption

From the classical point of view, the absorption of electromagnetic radiation by a sample is simply described by Beer-Lambert law, which relates the intensity of the radiation ad a depth r with the initial intensity I_0.

$$I(r) = I_0 e^{-\alpha(\omega) r}$$

$\alpha(\omega)$ is the absorption coefficient defined in §1.2.2. As we have seen, it is related to the imaginary part of the dielectric function by

$$\alpha(\omega) = \frac{\omega \varepsilon_{M2}}{nc}$$

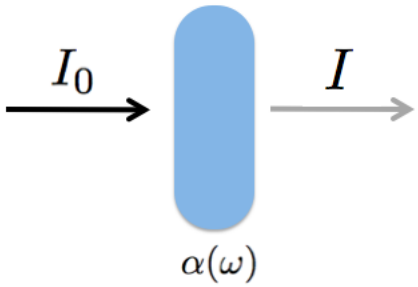

Figure 1.1: Schematical representation of an absorption experiment

Then we see that the absorption spectrum is related to the imaginary part of the dielectric function:

$$\boxed{\text{Abs} \propto \text{Im}\{\varepsilon_M\}}$$

If we switch to the quantum-mechanical point of view, one finds [9] using Fermi's Golden Rule that the absorption coefficient α is given by

$$\alpha(\omega) = \frac{4\pi^2}{\nu\omega c} \sum_{i,f} |\hat{\mathbf{e}} \cdot \langle f|e^{i\mathbf{q}\cdot\mathbf{r}}|i\rangle|^2 \delta(E_f - E_i - \omega)$$

where $\hat{\mathbf{e}}$ is the polarization vector and $\mathbf{q}$ is the wave-vector of the radiation.
In a single particle picture, and if the system is a solid, the many-body level i can be substituted by a double index containing band and wave vector $(v, \mathbf{k})$. Moreover, since the wavelenght of light is very small ($\sim 5 \cdot 10^{-2}$ nm^{-1}) the transmitted momentum can usually be neglected[4]. Therefore we consider only vertical transitions, i.e. from an occupied state $(v, \mathbf{k})$ to an empty state $(c, \mathbf{k})$ and we work in reciprocal space. From the relation (1.16) we can obtain the part of the dielectric function related to absorption:

$$\varepsilon_2(\omega) = 2\frac{4\pi^2}{\Omega} \lim_{\mathbf{q}\to 0} \frac{1}{q^2} \sum_{v,c,\mathbf{k}} |\langle c, \mathbf{k}+\mathbf{q}|e^{i\mathbf{q}\cdot\mathbf{r}}|v, \mathbf{k}\rangle|^2 \delta(\epsilon_{c,\mathbf{k}+\mathbf{q}} - \epsilon_{v,\mathbf{k}} - \omega) \tag{1.24}$$

Notice that the subscript M in this case is missing: ε has been obtained in this case with a microscopic approach, and its relation with the macroscopic ε_M we have been dealing with so far is a subtle problem, and will be the subject of the next chapter.

1.3.2 Electron Energy Loss

In Electron Energy Loss Spectroscopy, the probe is a high-energy electron that experiences a scattering interaction with the sample. In such experiments, one observes the energy spectrum of kilovolt electrons either as they emerge from a thin solid film, or after they are reflected from a solid surface. What is measured is the energy transfer to the electrons in the solid.

To find an expression for the EELS spectra, we first start with some very general concepts. Given a generic external charge density $\rho^{ext}(\mathbf{r}, t)$, we can obtain the external potential V_{ext} by using the Poisson equation[9]

$$\nabla^2 V_{ext}(\mathbf{r}, t) = -4\pi\rho^{ext}(\mathbf{r}, t) \tag{1.25}$$

[4]This also means that we do not need to consider the difference between longitudinal and trasverse part of ε

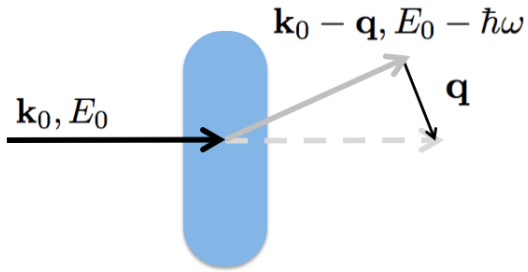

Figure 1.2: Schematical representation of an EELS experiment

In Fourier space, the external charge becomes $\rho^{ind}(\mathbf{q},\omega)$ and Eq.(1.25) is rewritten as

$$q^2 V_{ext}(\mathbf{q},\omega) = 4\pi\rho^{ext}(\mathbf{q},\omega) \tag{1.26}$$

The external perturbation V_{ext} can in turn induce a charge density ρ_{ind}, which is related to the external potential by the response function χ.
As we will see in more detail in the next chapters, in the linear response formalism we can write

$$\rho_{ind}(\mathbf{q},\omega) = \int \mathrm{d}\mathbf{q}'\, \chi(\mathbf{q},\mathbf{q}',\omega) V_{ext}(\mathbf{q}',\omega) \tag{1.27}$$

Using once again Poisson equation:

$$q^2 V_{ind}(\mathbf{q},\omega) = 4\pi\rho^{ind}(\mathbf{q},\omega) \tag{1.28}$$

The effective potential acting on the sistem is given by the sum of V_{ext} and V_{ind}. Using Eqs.(1.26) and (1.27) we obtain:

$$\begin{aligned} q^2 V_{tot}(\mathbf{q},\omega) &= 4\pi\left[\rho_{ind}(\mathbf{q},\omega) + \rho_{ext}(\mathbf{q},\omega)\right] = \\ &= 4\pi\left[\int \mathrm{d}\mathbf{q}'\, \chi(\mathbf{q},\mathbf{q}',\omega) V_{ext}(\mathbf{q}',\omega) + \frac{q^2}{4\pi} V_{ext}(\mathbf{q},\omega)\right] \end{aligned}$$

and

$$V_{tot}(\mathbf{q},\omega) = \left[1 + \frac{4\pi}{q^2}\chi(\mathbf{q},\omega)\right] V_{ext}(\mathbf{q},\omega) = \varepsilon_M^{-1}(\mathbf{q},\omega) V_{ext}(\mathbf{q},\omega)$$

where we have used

$$V_{ext}(\mathbf{q},\omega) = \varepsilon_M(\mathbf{q},\omega) V_{tot}(\mathbf{q},\omega) \tag{1.29}$$

The relation between the external charge and the total potential acting on the system is the given by

$$V_{tot}(\mathbf{q},\omega) = \frac{4\pi}{k^2}\varepsilon^{-1}(\mathbf{q},\omega)\rho_{ext}(\mathbf{q},\omega)$$

Now we can specify the external perturbation ρ_{ext} in the attempt of modelling EELS spectroscopy. The charge density of a particle (an electron e^-) moving with velocity $\mathbf{v}$ can be expressed as

$$\rho_{ext}(\mathbf{r},t) = e\delta(\mathbf{r} - \mathbf{v}t)$$

which becomes in Fourier space

$$\begin{aligned}\rho_{ext}(\mathbf{q},\omega) &= \frac{e}{(2\pi)^4}\iint \mathrm{d}\mathbf{r}\mathrm{d}t\, e^{-i(\mathbf{q}\cdot\mathbf{r}-\omega t)}\delta(\mathbf{r}-\mathbf{v}t) \\ &= \frac{e}{(2\pi)^4}\iint \mathrm{d}\mathbf{r}\mathrm{d}t\, e^{-i(\mathbf{q}\cdot\mathbf{v}t-\omega t)} = \frac{e}{(2\pi)^4}\delta(\omega-\mathbf{q}\cdot\mathbf{v})\end{aligned}$$

Now we make the important assumption that the probe, the fast electron, could be treated classically. This justifies the use of the previous classical derivation for the induced potential and allows to simply derive the total electric field as

$$\begin{aligned}\mathbf{E}_{tot}(\mathbf{r},t) &= -\nabla V_{tot}(\mathbf{r},t) \\ \mathbf{E}_{tot}(\mathbf{q},\omega) &= -i\mathbf{q}V_{tot}(\mathbf{q},\omega) \\ &= -\frac{ie}{2\pi^2 q^2}\varepsilon_M^{-1}(\mathbf{q},\omega)\delta(\omega-\mathbf{q}\cdot\mathbf{v})\mathbf{q}\end{aligned} \tag{1.30}$$

We want to find an expression for the energy lost by the electron in unit time

$$\frac{\mathrm{d}W}{\mathrm{d}t} = \int \mathrm{d}\mathbf{r}\,\mathbf{j}_{ext}\cdot\mathbf{E}_{tot}$$

Eq. (1.30) in real space is

$$\mathbf{E}_{tot}(\mathbf{r},t) = \iint \mathrm{d}\mathbf{q}\mathrm{d}\omega\, e^{i(\mathbf{q}\cdot\mathbf{r}-\omega t)}\mathbf{E}(\mathbf{q},\omega)$$

Merging the last two expressions one can obtain [9] the electron energy loss rate per unit time, with $\omega = \mathbf{v}\cdot\mathbf{q}$:

$$\frac{\mathrm{d}W}{\mathrm{d}t} = -\frac{e^2}{\pi^2}\int \mathrm{d}\mathbf{q}\,\frac{1}{q^2}\mathrm{Im}\left\{\frac{\omega}{\varepsilon_M(\mathbf{q},\omega)}\right\}$$

The function $-\mathrm{Im}\{\varepsilon_M^{-1}\}$ is called the loss function, and it is what basically determines the EELS spectrum:

$$\boxed{\text{EELS} \propto \mathrm{Im}\{\varepsilon_M^{-1}\}}$$

2
Microscopic-Macroscopic Connection

In the previous chapter we have introduced quantities such as the refraction index n or the absorption coefficient α (§1.2.2) that can be experimentally measured. In Chapter 3 we will see the kind of quantities we are able to calculate with many-body theory, such as the microscopic polarizability χ and the microscopic dielectric function ε.
A key problem in our theoretical framework is the connection between these two points of view: this chapter presents the important problem of averages required by the connection between the macroscopic and microscopic view [10–13].

2.1 The dielectric function

So far we have been considering the very simple case of the local, linear and time independent response of an homogeneous and isotropic medium; all these hypothesis lead to a scalar dielectric constant ε_M.
Things are obviously more complex than this, and in this work results will be obtained retaining just the linear response approximation, while dropping the others. This fact is reflected in the form of ε_M in a way that can be summed up as follows:

- If the medium is isotropic, *non-homogeneous* and the response is local ε_M becomes a scalar function depending on position $\varepsilon_M(\mathbf{r})$;
- If we consider a *non-local* response for an homogeneous and isotropic medium we get a scalar dielectric function depending on distance $\varepsilon_M(\mathbf{r}-\mathbf{r}')$ and expressions like Eq.(1.5) take the form
$$\mathbf{D}(\mathbf{r},t) = \int \mathrm{d}\mathbf{r}' \varepsilon_M(\mathbf{r}-\mathbf{r}')\mathbf{E}(\mathbf{r}',t);$$
- If the medium is isotropic, *non-homogeneous* and the response is *non-local*, the spatial dependence of the dielectric function takes the general form $\varepsilon_M(\mathbf{r},\mathbf{r}')$;
- If we finally consider also *time dependence*, which is important because it corresponds to the frequency dependence in Fourier space, we have $\varepsilon_M(\mathbf{r},\mathbf{r}',t-t')$ and
$$\mathbf{D}(\mathbf{r},t) = \int \mathrm{d}t' \int \mathbf{r}'\, \varepsilon_M(\mathbf{r},\mathbf{r}',t-t')\mathbf{E}(\mathbf{r}',t')$$
where the form of time dependence comes from the fact that time is homogeneous;
- If the medium is *anisotropic*, ε_M becomes a tensor $\underline{\underline{\varepsilon}}_M$ to include the dependence on direction.

2.1.1 Longitudinal and transverse parts: Dielectric Constant Tensor

We are now interested in spending a few lines for this last point, which is actually related to the existence of longitudinal and trasverse field components that have been introduced in §1.2.4. For this purpose, it is more convenient to consider the Fourier space version of ε_M, given by $\varepsilon_M(\mathbf{q}, \mathbf{q}', \omega)$.

In an isotropic medium, there is no coupling between the longitudinal and transverse components, so that a purely longitudinal electric field induces a longitudinal current and a purely transverse electric field induces a transverse current [7, 11].
For example, in the case of a free-electron gas a longitudinal (transverse) current cannot be induced by a transverse (longitudinal) electric field.

In an anisotropic medium, which is the general case of a solid, the polarization and induced currents generally lie in a direction different from that of the electric field; it is then possible, for example, to generale a longitudinal current with a purely transverse electric field. This situation can be handled by representing the dielectric function as a tensor, defined by [11]

$$\mathbf{j}_{ind}(\mathbf{q}, \omega) = \frac{i\omega}{4\pi}\Big[1 - \underline{\underline{\varepsilon}}_M(\mathbf{q}, \omega)\Big]\mathbf{E}_{tot}(\mathbf{q}, \omega)$$

where now $\underline{\underline{\varepsilon}}_M$ is a complex tensor with a general form

$$\underline{\underline{\varepsilon}}_M(\mathbf{q}, \omega) = \begin{bmatrix} \varepsilon_M^{\mathbf{LL}}(\mathbf{q}, \omega) & \varepsilon_M^{\mathbf{LT}}(\mathbf{q}, \omega) \\ \\ \varepsilon_M^{\mathbf{TL}}(\mathbf{q}, \omega) & \varepsilon_M^{\mathbf{TT}}(\mathbf{q}, \omega) \end{bmatrix}.$$

The off-diagonal elements $\varepsilon_M^{\mathbf{LT}}(\mathbf{q}, \omega)$ and $\varepsilon_M^{\mathbf{TL}}(\mathbf{q}, \omega)$ describe, respectively, the longitudinal (transverse) current induced by a transverse (longitudinal) electric field.

2.1.2 Dielectric function in crystals

When considering a solid, another degree of complexity is added to the form of the dielectric function.
In the most general case, the dielectric function is a frequency dependent matrix $\varepsilon(\mathbf{r}, \mathbf{r}', \omega)$, called *microscopic dielectric function*. Notice that in this case we have dropped the subscript M because we are explicitly speaking of microscopic quantities.
Properties of solids are often treated in Fourier space; the symmetry properties of the system can be used (see Appendix B) to show that ε takes the form

$$\varepsilon_{\mathbf{G}\mathbf{G}'}(\mathbf{q}_\mathbf{r}, \omega) = \begin{bmatrix} \varepsilon_{\mathbf{G_0}\mathbf{G_0}}(\mathbf{q}_\mathbf{r}, \omega) & \varepsilon_{\mathbf{G_0}\mathbf{G_1}}(\mathbf{q}_\mathbf{r}, \omega) & \cdots & \varepsilon_{\mathbf{G_0}\mathbf{G_N}}(\mathbf{q}_\mathbf{r}, \omega) \\ \varepsilon_{\mathbf{G_1}\mathbf{G_0}}(\mathbf{q}_\mathbf{r}, \omega) & \varepsilon_{\mathbf{G_1}\mathbf{G_1}}(\mathbf{q}_\mathbf{r}, \omega) & \cdots & \varepsilon_{\mathbf{G_1}\mathbf{G_N}}(\mathbf{q}_\mathbf{r}, \omega) \\ \vdots & & & \\ \varepsilon_{\mathbf{G_N}\mathbf{G_0}}(\mathbf{q}_\mathbf{r}, \omega) & \varepsilon_{\mathbf{G_N}\mathbf{G_1}}(\mathbf{q}_\mathbf{r}, \omega) & \cdots & \varepsilon_{\mathbf{G_N}\mathbf{G_N}}(\mathbf{q}_\mathbf{r}, \omega) \end{bmatrix}$$

where $\mathbf{G}$ and $\mathbf{G}'$ are reciprocal lattice vectors and $\mathbf{q}_\mathbf{r}$ is a vector in the first Brillouin zone of the crystal.

2.2 Macroscopic average and local-field effects

We have seen that the key quantity for both absorption and EELS spectrum is the dielectric function ε. A dielectric function appears in §1.2.1, in Maxwell's equations: in this case it is a

macroscopic quantity, as it represents the relation between macroscopic quantities.
On the other hand, the ε appearing in Eq.(1.24) is determined by the elementary excitations of the medium (interband and intraband transitions, as well as collective excitations): these are microscopic properties, related to the band structure and to the quantum mechanical nature of our system. The two ε's are not the same!
So we can guess that the key to a macroscopic-microscopic connection is a link between the microscopic dielectric function we can compute from theory and the macroscopic dielectric function we get from experiments: this means that we are looking for a way to do an average.

2.2.1 Definition of macroscopic

First of all, let us define what we mean by macroscopic quantities. At long wavelenghts, external fields are slowly varying over the unit cells of the crystal, having volume Ω:

$$\lambda = \frac{2\pi}{q} \gg (\Omega_{cell})^{\frac{1}{3}}$$

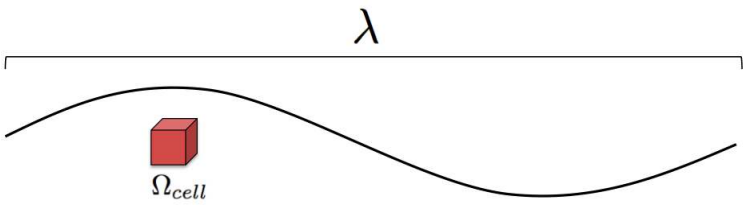

Figure 2.1: Long wavelength perturbation compared with a unit cell

On the microscopic scale, instead, total and induced fields are rapidly varying: they include the contribution from electrons in all regions of the cell. The contribution of electrons close to or far from the nuclei will be very different, and we expect large and irregular fluctuations over the atomic scale.
So, in order to obtain macroscopic quantities from the microscopic ones we have to average over distances large compared to the cell diameter, but small compared to the wavelenght of the external perturbation.
The procedure to do that is to average over a unit cell whose origin is at $\mathbf{r}$, and take $\mathbf{r}$ as the continous coordinate appearing in Maxwell's equations.
The physical meaning of this averaging procedure lies in the distinction between the local field producing charge polarization and the macroscopic field. The fact that these two fields are not the same gives rise to the so called local field effects (LFE) [13].
In fact, the electrons in the solid respond not just to $\mathbf{E}^{ext} = \mathbf{D}$, but to the total field $\mathbf{E}^{tot} = \mathbf{E}$ which includes the induced field due to the other electrons as well. $\mathbf{E}^{tot}$ will be rapidly varying over the unit cell, and its macroscopic average therefore will be different from the field which polarizes the charge in the crystal.

2.2.2 Procedure

Functions having the crystal symmetries $V(\mathbf{r}+\mathbf{R}) = V(\mathbf{R})$, where $\mathbf{R}$ is any vector of the Bravais lattice, can be represented by the Fourier series

$$V(\mathbf{r},\omega) = \sum_{\mathbf{q},\mathbf{G}} V(\mathbf{q}+\mathbf{G},\omega)e^{i(\mathbf{q}+\mathbf{G})\cdot\mathbf{r}} = \sum_{\mathbf{q}} V(\mathbf{r};\mathbf{q},\omega)e^{i\mathbf{q}\cdot\mathbf{r}}$$

where we have defined the periodic function

$$V(\mathbf{r};\mathbf{q},\omega) = \sum_{\mathbf{G}} V(\mathbf{q}+\mathbf{G},\omega)e^{i\mathbf{G}\cdot\mathbf{r}}$$

This function contains all the G-harmonics of the field, and varies strongly even if the original wave has a long wavelength and is nearly constant within each cell.
If we suppose a long wavelength perturbation ($\mathbf{q}\to 0$) the average can be done only on the latter quantity:

$$\begin{aligned} V(\mathbf{R},\omega) &= e^{i\mathbf{q}\cdot\mathbf{r}}\langle V(\mathbf{r};\mathbf{q},\omega)\rangle_{\mathbf{R}} = \\ &= e^{i\mathbf{q}\cdot\mathbf{r}}\frac{1}{\Omega}\int \mathrm{d}\mathbf{r}\sum_{\mathbf{G}} V(\mathbf{q}+\mathbf{G},\omega)e^{i\mathbf{G}\cdot\mathbf{r}} = \\ &= e^{i\mathbf{q}\cdot\mathbf{r}}V(\mathbf{q}+\mathbf{0},\omega) \end{aligned}$$

So we see that the macroscopic average corresponds to the $\mathbf{G}=0$ component. This is a truncation that eliminates all wave vectors outside the first Brillouin zone, that is to say, microscopic fields.
Macroscopic quantities all have their $\mathbf{G}$ components equal to zero, except the $\mathbf{G}=0$ component. The average has been done in the limit of long wavelength (i.e. $\mathbf{q}\to 0$). If the external applied field is not macroscopic and has a very short wavelength, the averaging procedure for the response function of the material has no meaning. In this case, one has to consider an average procedure based on the statistical and quantum mechanical point of view.

2.2.3 The longitudinal case

In the longitudinal case, all the fields can be expressed in terms of potentials ($\mathbf{E} = \nabla V$) and the longitudinal dielectric function is defined as

$$V_{ext}(\mathbf{q}+\mathbf{G},\omega) = \sum_{\mathbf{G}'} \varepsilon^{\mathbf{LL}}_{\mathbf{GG}'}(\mathbf{q},\omega)V_{tot}(\mathbf{q}+\mathbf{G}',\omega)$$

As V_{ext} is a macroscopic quantity,

$$V_{ext}(\mathbf{q}+\mathbf{G},\omega) = V_{ext}(\mathbf{q},\omega)\delta_{\mathbf{G0}}$$

This is not the case for $V_{tot}(\mathbf{q}+\mathbf{G},\omega)$, then:

$$V_{ext}(\mathbf{q},\omega) = \sum_{\mathbf{G}'} \varepsilon^{\mathbf{LL}}_{\mathbf{0G}'}(\mathbf{q},\omega)V_{tot}(\mathbf{q}+\mathbf{G}',\omega) \neq \varepsilon^{\mathbf{LL}}_{\mathbf{00}}(\mathbf{q},\omega)V_{tot}(\mathbf{q},\omega)$$

If we consider the inverse, we have the relation

$$V_{tot}(\mathbf{q}+\mathbf{G},\omega) = \sum_{\mathbf{G}'} \varepsilon^{\mathbf{LL}^{-1}}_{\mathbf{GG}'}(\mathbf{q},\omega)V_{ext}(\mathbf{q}+\mathbf{G}',\omega)$$

where $\varepsilon^{\mathbf{LL}^{-1}}$ is the inverse dielectric function:

$$\sum_{\mathbf{G}''} \varepsilon^{\mathbf{LL}}_{\mathbf{GG}''}(\mathbf{q},\omega)\varepsilon^{\mathbf{LL}^{-1}}_{\mathbf{G}''\mathbf{G}'}(\mathbf{q},\omega) = \delta_{\mathbf{GG}'}$$

As V_{ext} is macroscopic, we have

$$V_{tot}(\mathbf{q}+\mathbf{G},\omega) = \varepsilon^{\mathbf{LL}^{-1}}_{\mathbf{G0}}(\mathbf{q},\omega)V_{ext}(\mathbf{q},\omega)$$

and then

$$V_{tot}(\mathbf{q}+0,\omega) = \varepsilon^{\mathbf{LL}^{-1}}_{\mathbf{00}}(\mathbf{q},\omega)V_{ext}(\mathbf{q},\omega)$$

Let us compare this with the macroscopic relation (see also Eq.(1.29))

$$V_{ext}(\mathbf{q},\omega) = \varepsilon_M(\mathbf{q},\omega)V_{tot}(\mathbf{q},\omega)$$

where ε_M is the one that appears in Maxwell's Equations, and is a longitudinal quantity.
Thus we get the important relation, valid in the longitudinal long wavelength case:

$$\varepsilon_M(\omega) = \lim_{\mathbf{q}\to 0} \frac{1}{\varepsilon^{\mathbf{LL}^{-1}}_{\mathbf{00}}(\mathbf{q},\omega)} \tag{2.1}$$

At first sight Eq.(2.1) might appear redundant, but it is not: this is due to the tensorial nature of the microscopic dielectric function $\varepsilon(\mathbf{q},\omega)$.
Eq.(2.1) implies that the calculation of the macroscopic $\varepsilon_M(\mathbf{q},\omega)$ starting from the microscopic $\varepsilon(\mathbf{q},\omega)$ requires the inversion of the full dielectric matrix $\varepsilon_{\mathbf{GG}'}(\mathbf{q},\omega)$, and only at the end of the inversion the $\mathbf{G} = \mathbf{G}' = 0$ component is taken. In this way, *all* the microscopic quantities of the induced field will couple together to produce the macroscopic response. This is one of the mathematical expressions of local field effects. $\varepsilon_{\mathbf{00}}$ is *not* the true dielectric function, but the dielectric function neglecting crystal local fields, i.e. the off-diagonal terms corresponding to the rapidly oscillating contributions to the microscopic total potential. Taking the mere diagonal of ε means in that in real space the dielectric function depends only on the distance between $\mathbf{r}$ and $\mathbf{r}'$: $\varepsilon(|\mathbf{r}-\mathbf{r}'|)$.

The relation (2.1) tells us how we have to average microscopic quantities in order to be compared with experimental results: it is now clear that the dielectric function has a microscopic expression (related to quantum mechanics) and a macroscopic expression (related to Maxwell's equations).

2.3 Summary: from micro to macro

We know from §2.1.1 that in the general case the dielectric constant is more complicated than what considered so far and has a tensorial nature.
Anyway, it can be shown [10] that the expression for the longitudinal dielectric function ε_M(2.1) defines entirely the optical response (also the transverse part) in the long wavelength limit ($\mathbf{q}\to 0$)[1].
For non-vanishing momentum, Eq.(2.1) defines only the longitudinal response.

[1] For non-cubic crystals it is necessary to pay attention to the choice of the axis system.

As in this work we will be working with EELS, we will be concerned only with the longitudinal response, and our average is definitely given by Eq.(2.1)[11, 12]:

$$\boxed{\varepsilon_M(\omega) = \lim_{\mathbf{q}\to 0} \frac{1}{[\varepsilon^{-1}(\mathbf{q},\omega)]_{\mathbf{G}=\mathbf{G}'=\mathbf{0}}}} \tag{2.2}$$

Following §1.3, the imaginary parts of ε_M and ε_M^{-1} determine the measured absorption and Electron Energy Loss spectra:

$$\text{Abs} \propto \text{Im}\{\varepsilon_M\} \qquad \text{EELS} \propto -\text{Im}\left\{\frac{1}{\varepsilon_M}\right\} \tag{2.3}$$

As we will see later in more detail, in the equation for the absorption (1.24) an average different from (2.2) was implicitly taken:

$$\varepsilon'_M(\omega) = \lim_{\mathbf{q}\to 0} \varepsilon(\mathbf{q},\omega)_{\mathbf{G}=\mathbf{G}'=0} \tag{2.4}$$

and this corresponds to neglecting local field effects: matrix elements are no longer mixing because no inversion is performed.
Another physical reason why this is not correct is that, as seen in §1.2.3, the total electric field $\mathbf{E}^{tot} = \mathbf{E}$ is related to the external applied field $\mathbf{E}^{ext} = \mathbf{D}$ via $\mathbf{E} = \varepsilon^{-1}\mathbf{D}$, and the correct and physically meaningful average is to be taken on ε^{-1}.

3

The Many-Body Problem and Density Functional Theory

In the first two chapters we have seen that what we basically want to do is to calculate the microscopic dielectric function ε, from which we will be able to obtain the macroscopic ε_M and to predict absorption and EELS spectra.
We will do this with *ab initio* calculations: no experimental data will be needed to obtain our results.
The basic tool we will be using is Density Functional Theory (DFT), whose aim is to treat inhomogeneous interacting many-body systems, taking the electronic density as the basic variable [14–16].
DFT is a powerful and very successful method to calculate ground state total energies. Actually,the two fundamental articles about DFT [14, 16] are the most cited papers ever in the history of APS Journals[1]. We need to calculate total energies because all physical properties are related to total energies or to difference between total energies. For instance, the equilibrium lattice constant of a crystal may be determined by minimization of total energy, and total-energy techniques also have proven successful in predicting with accuracy bulk moduli, phonons, piezoelectric constants, and phase-transition pressures and temperatures [17].

This chapter aims at briefly presenting the evolution of the *ab-initio* approach, starting from Hartree-Fock theory before landing to DFT. In order to calculate the dielectric properties we are interested in, a time-dependent version of the DFT is needed [18, 19], which will be also presented at the end of this chapter.

3.1 The Many-Particle Problem

The fundamental problem of condensed matter physics is the determination of the eigenstates of the Hamiltonian[2]:

$$H(\{\mathbf{r},\mathbf{p}\};\{\mathbf{R},\mathbf{P}\}) = \sum_{i=1}^{N}\frac{\mathbf{p}_i^2}{2} + \sum_{I=1}^{M}\frac{\mathbf{P}_I^2}{2M_I} + \sum_{i<j}\frac{1}{|\mathbf{r}_i-\mathbf{r}_j|} - \sum_{i,I}^{N,M}\frac{Z_I}{|\mathbf{r}_i-\mathbf{R}_I|} + \sum_{I<J}\frac{Z_I Z_J}{|\mathbf{R}_I-\mathbf{R}_J|}$$

This describes the evolution of any system composed of electrons (coordinates $\mathbf{r}_i$, momenta $\mathbf{p}_i$ and mass m) and nuclei ($\mathbf{R}_I$, $\mathbf{P}_i$,M_I and atomic number Z_I).

[1] June 2009: more than 7400 citations for [14] and more than 9000 for [16]!
[2] In this work atomic units will be used, so that $m_e = e = \hbar = a_0 = 1$ and everything is simpler.

The problem is enourmously complex because of the large number of objects and interactions involved: fortunately it is possibile to introduce some approximations based on the differences of energy scales between the processes involved.
The first and most common approximation allows to separate the motion of nuclei from the one of electrons and it is called Born-Oppenheimer (or adiabatic) approximation, which is based on the idea that nuclei can be assumed at fixed positions as they are much heavier than the electrons [20, 21].

3.1.1 The N-electron Problem

The Born Oppenheimer approximation leaves us with the problem of solving the Schrödinger equation for a system of interacting electrons in the external field generated by the ions frozen in their positions $\{\mathbf{R}_I\}$. The solution to this N-electron Hamiltonian represents still a difficult task that requires other approximations.

Let us consider an inhomogeneous electronic system, where in principle we want to solve the many-electron Schrödinger equation

$$\left[-\sum_i^N \frac{\nabla_i^2}{2} + \frac{1}{2}\sum_{i\neq j}^N \frac{1}{|\mathbf{r}_i - \mathbf{r}_j|} + \sum_i^N V_{ext}(\mathbf{r}_i) \right] \psi = E\psi \tag{3.1}$$

The indices run over the N electrons, the first term giving their kinetic energy, the second term the electron-electron Coulomb interaction, and the third term the interaction with an external potential $W = \sum_i^N V_{ext}(\mathbf{r}_i)$ (e.g. due to the nuclei, in the Born-Oppenheimer approximation).
The ground state energy E_0 and wavefunction ψ_0 can be found from the variational principle, by minimizing $\langle\psi|H|\psi\rangle$ with the normalization requirement on ψ; the complicated part is that ψ is a function of $3N$ spatial variables.

3.1.2 Hartree-Fock Method and Mean-Field Theory

Before we get on to DFT, we look at the Hartree-Fock method, which is the "best" single-particle description of the electronic wavefunction: a single particle description because each electron occupies a one-electron wavefunction, and the best in the sense that it minimizes the energy of the system.
Hartree-Fock belongs to an important class of approximations that reduce the problem to the study of a Hamiltonian of *non interacting* particles like

$$H_0 = \sum_i H_i$$

The many-electron wavefunction in Hartree-Fock is written as a so-called Slater determinant of occupied one-electron wavefunctions ψ_i:

$$\Psi(\mathbf{x}_1, \mathbf{x}_2, \cdots, \mathbf{x}_N) = \frac{1}{\sqrt{N!}} \begin{vmatrix} \psi_1(\mathbf{x}_1) & \psi_2(\mathbf{x}_1) & \cdots & \psi_N(\mathbf{x}_1) \\ \psi_1(\mathbf{x}_2) & \psi_2(\mathbf{x}_2) & \cdots & \psi_N(\mathbf{x}_2) \\ \vdots & & & \\ \psi_1(\mathbf{x}_N) & \psi_2(\mathbf{x}_N) & \cdots & \psi_N(\mathbf{x}_N) \end{vmatrix}.$$

Here the electron coordinate $\mathbf{x}_i$ includes the spin coordinate ξ as well as the spatial coordinate $\mathbf{r}_i$. The total wavefunction is antisymmetric with respect to interchanging electronic coordinates,

as required by Fermi-Dirac statistics, and it vanishes if two electrons are occupying the same state.
To find the "best" single-particle wavefunctions, we vary the ψ_i's to minimize the energy, i.e. to minimize the expectation value of the Hamiltonian[3]:

$$\begin{aligned}\langle\Psi|H|\Psi\rangle = \sum_i \int \mathrm{d}\mathbf{x}\psi_i^*(\mathbf{x})\left[-\frac{\nabla^2}{2} + V_{ext}(\mathbf{r})\right]\psi_i(\mathbf{x}) + \\ + \frac{1}{2}\sum_{i,j}\int \mathrm{d}\mathbf{x}\int \mathrm{d}\mathbf{x}'\psi_i^*(\mathbf{x})\psi_j^*(\mathbf{x}')\frac{1}{|\mathbf{r}-\mathbf{r}'|}\psi_i(\mathbf{x})\psi_j(\mathbf{x}') + \\ - \frac{1}{2}\sum_{i,j}\int \mathrm{d}\mathbf{x}\int \mathrm{d}\mathbf{x}'\psi_i^*(\mathbf{x})\psi_j^*(\mathbf{x}')\frac{1}{|\mathbf{r}-\mathbf{r}'|}\psi_i(\mathbf{x}')\psi_j(\mathbf{x})\end{aligned} \tag{3.2}$$

subject to the normalization constraints on the one-electron wavefunctions.
This can be done using Lagrangian multipliers, minimizing without constraints the functional

$$E[\Psi] = \langle\Psi|H|\Psi\rangle - \sum_i \epsilon_i\langle\psi_i|\psi_i\rangle \tag{3.3}$$

Substituting the espression (3.2) we found for $\langle\Psi|H|\Psi\rangle$ in Eq. (3.3) and varying the wavefunctions gives that each wavefunction ψ_i must satisfy:

$$\begin{aligned}\left[-\frac{\nabla^2}{2} + V_{ext}(\mathbf{r})\right]\psi_i(\mathbf{x}) + \sum_j \int \mathrm{d}\mathbf{x}'\psi_j(\mathbf{x}')\psi_j^*(\mathbf{x}')\frac{1}{|\mathbf{r}-\mathbf{r}'|}\psi_i(\mathbf{x}) + \\ - \sum_j \int \mathrm{d}\mathbf{x}'\psi_i(\mathbf{x}')\psi_j^*(\mathbf{x}'))\frac{1}{|\mathbf{r}-\mathbf{r}'|}\psi_j(\mathbf{x}) = \epsilon_i\psi_i(\mathbf{x})\end{aligned} \tag{3.4}$$

This is an effective one-electron Schrödinger equation containing, in addition to the external potential v, a *mean field* form of potential. This consists of two parts, first the *Hartree* potential due to the smeared-out charge density of the outer electrons:

$$V_H(\mathbf{r}) = \sum_j \int \mathrm{d}\mathbf{x}'\psi_j(\mathbf{x}')\psi_j^*(\mathbf{x}')\frac{1}{|\mathbf{r}-\mathbf{r}'|}$$

and also the *exchange* potential, which comes from the antisymmetric structure of the wavefunction Ψ and which operates non-locally on ψ_i:

$$\int \mathrm{d}\mathbf{x}'V_x(\mathbf{x},\mathbf{x}')\psi_i(\mathbf{x}') = -\sum_j \int \mathrm{d}\mathbf{x}'\psi_i(\mathbf{x}')\psi_j^*(\mathbf{x}')\frac{1}{|\mathbf{r}-\mathbf{r}'|}\psi_j(\mathbf{x})$$

Taking the expectation value of the Hamiltonian the ground state energy is given by

$$\begin{aligned}E = \langle\Psi|H|\Psi\rangle = \\ = \sum_i \epsilon_i - \frac{1}{2}\sum_{i,j}\int \mathrm{d}\mathbf{x}\int \mathrm{d}\mathbf{x}'\psi_i^*(\mathbf{x})\psi_j^*(\mathbf{x}')\frac{1}{|\mathbf{r}-\mathbf{r}'|}\psi_i(\mathbf{x})\psi_j(\mathbf{x}') + \\ - \frac{1}{2}\sum_{i,j}\int \mathrm{d}\mathbf{x}\int \mathrm{d}\mathbf{x}'\psi_i^*(\mathbf{x})\psi_j^*(\mathbf{x}')\frac{1}{|\mathbf{r}-\mathbf{r}'|}\psi_j(\mathbf{x})\psi_i(\mathbf{x}')\end{aligned} \tag{3.5}$$

[3]The braket implies an integration on all the $\mathbf{x}_N$. The number of variables remaining in each term depends on the number of spatial variables in the operator; all the other go away because of the normalization condition. The minus sign comes from the second part of the determinant.

This is a sum of one-electron energies ϵ_i, corrected by subtracting off the Hartree and exchange energies which are otherwise counted twice: the energy ϵ_i includes the Hartree and exchange interactions of the electron in orbital i with all other electrons, in particular the electron in orbital j; but ϵ_j also includes the Hartree and exchange interactions with i, hence the need to correct for double counting.
Characteristic of this mean-field approach is the fact that the field - the Hartree and exchange potentials - depends on the wavefunctions themselves, so Eq.(3.4) must be solved (numerically) self-consistently: starting from a guess for the Hartree and exchange potentials, the eigenfunctions and eigenvalues of (3.4) are found. The N states of low one-electron energies are occupied and the potentials calculated: the process is repeated until the input potentials are similar to the output ones within a certain tolerance, giving us the self-consistent potential (a potential whose wavefunctions generate back the same potential). From the variational principle, this self-consistent procedue generates the ground state of the system in Hartree-Fock, with expression (3.5) minimized.

This method gives quite good total energies and equilibrium geometries; in atoms and molecules, Hartree-Fock works well because the electrons tend to be kept apart by the shell structure, and corrections to Hartree Fock (*correlation* effects) are not as important as in solids. While Hartree-Fock single particle solutions represent approximate solutions, the DFT allows us to reduce the initial problem to an *exact* non-interacting particles problem, with an evident conceptual advantage.

3.1.3 Excited states in HF

Expression (3.5) is the energy of the ground state with the Hartree-Fock trial wavefunction. In fact, the eingevalues ϵ_i have a direct physical interpretation as the change in energy of the system when an electron is removed from orbital i: this is the so-called Koopman's Theorem. It can be shown [15] that in Hartree Fock theory the ionization[4] energy of the removal of an electron from the orbital l, assuming that the other orbitals do not relax, is given by:

$$I = E^{N-1} - E = -\epsilon_l$$

Thus the energy of an occupied orbital in Hartree Fock represents the energy needed to remove an electron from that state, assuming no relaxation of the other electrons.
Koopman's theorem thus gives us a direct, physical meaning for the eigenvalues - and one which is accessible experimentally.

The main problem with HF theory is that dynamic correlations between electrons are not included: the fundamental problem of many electron physics is to solve the correlation problem and find an accurate ground state energies and excitations. Methods to deal with this include configuration interaction in quantum chemistry and Green function methods in electron gas theory. The approach we shall now consider is density functional theory for the inhomogeneous electron gas.

[4]The ionization energy of an atom is the work required to remove (to infinity) the topmost electron when the atom is isolated in free space and is in its ground electronic state.

3.2 Density Functional Theory

3.2.1 Hohenberg and Kohn Theorems

DFT is based upon two main theorems proposed by Hohenberg and Kohn [14, 15]. The main idea of this theory is to treat electronic density as the main variable, which decreases the degrees of freedom to be considered with respect to the use of wavefunctions.

HK Theorem I *There is a one-to-one relationship between the external potential W in the many-electron Hamiltonian (3.1) and the ground state electron density $\rho_0(\mathbf{r})$, assuming a non degenerate ground state.*

It is obvious that given a potential, the ground state electron density is completely determined. To show the one-to-one relationship we proceed with a *reductio ad absurdum*.
Assume that there are two external potentials, W and W', corrisponding to the Hamiltonians H and H', with different ground states Ψ_0 ans Ψ_0', but the same ground state electron density $\rho_0(\mathbf{r})$. Following the variational principle we can write

$$\langle\Psi_0|H|\Psi_0\rangle < \langle\Psi_0'|H|\Psi_0'\rangle = \langle\Psi_0'|H' + W - W'|\Psi_0'\rangle$$
$$E < E' + \int \mathrm{d}\mathbf{r}(W - W')\rho_0(\mathbf{r})$$

But we can similarly reason that

$$E' < E - \int \mathrm{d}\mathbf{r}(W - W')\rho_0(\mathbf{r})$$

Adding the last two expressions we get an evidently absurd result:

$$E + E' < E + E'$$

Hence $\rho_0(\mathbf{r})$ cannot be the ground state density of two different Hamiltonians, and we conclude that $\rho_0(\mathbf{r})$ corresponds uniquely to $v(\mathbf{r})$. Since $\rho_0(\mathbf{r})$ determines the potential, it also determines the ground state wavefunction Ψ_0 and the all the other electronic properties of the system.

We now consider all possible electron densities leading to different external potentials. As the ground state wavefunction Ψ_0 is a functional of $\rho_0(\mathbf{r})$, the expectation value of the kinetic plus Coulomb energies is also a functional of electron density:

$$F[\rho_0(\mathbf{r})] = \langle\Psi_0|T + U|\Psi_0\rangle \tag{3.6}$$

Consider now the N interacting electrons moving in a fixed external potential V_{ext}.

HK Theorem II *The total energy functional defined by*

$$\begin{aligned} E_v[\rho_0'(\mathbf{r})] &= F[\rho_0'(\mathbf{r})] + W[\rho_0'(\mathbf{r})] \\ &= F[\rho_0'(\mathbf{r})] + \int \mathrm{d}\mathbf{r} V_{ext}(\mathbf{r})\rho_0'(\mathbf{r}) \end{aligned} \tag{3.7}$$

is minimum for $\rho_0'(\mathbf{r}) = \rho_0(\mathbf{r})$, the actual electron density.

This follows from the fact that ρ_0' corresponds to some external potential W' different from W, with a ground state wavefunction Ψ_0'. But from the variational principle:

$$E_{V_{ext}}[\rho_0'(\mathbf{r})] = \langle \Psi_0' | T + U + W | \Psi_0' \rangle \tag{3.8}$$
$$> \langle \Psi_0 | T + U + W' | \Psi_0 \rangle \tag{3.9}$$

Hence:

$$E_{V_{ext}}[\rho_0'(\mathbf{r})] > E_{V_{ext}}[\rho_0(\mathbf{r})] \tag{3.10}$$

Then treating the ground state energy $E_{V_{ext}}$ as a functional of the electron density, this takes a minimum value at the actual ground state density: this represents a huge semplification because the density is a function only of the 3 components of $\mathbf{r}$ compared with $3N$ in the wavefunction. If $F[\rho(\mathbf{r})]$ were a known and sufficiently simple functional of the density, the problem of determining the ground-state energy in a given external potential would be rather easy: the major part of the complexities of the many-electron problems are associated with the determination of the universal functional $F[\rho(\mathbf{r})]$.

3.2.2 Kohn and Sham Equations

The minimization of a functional of the density appears as a convenient approach from the computational point of view. The practical usefulness of DFT was definitely made clear by the work of Kohn and Sham [16] who reformulated the theory in order to use a self-consistent field scheme similar to Hartree-Fock methods, and proposed a very simple approximation, namely the local density approximation, which already yielded good results.

The idea of Kohn and Sham was considering an auxiliary system of *non-interacting* electrons, whose density would be the same of the associated interacting-electron system.
The Hamiltonian of this auxiliary system will be

$$H' = T' + W'$$

where T' is the kinetic energy of a non-interacting electron gas with the same density $\rho_0(\mathbf{r})$ as the interacting system and W' is the so called KS potential.
The fact that the two densities are the same means that

$$\rho(\mathbf{r}) = \rho'(\mathbf{r}) = \sum_{i}^{occ} |\phi_i(\mathbf{r})|^2 \tag{3.11}$$

with ϕ_i single particle orbitals of the non-interacting system. Associated to this auxiliary system are the N exact single-particle equations

$$\left[-\frac{\nabla_i^2}{2} + V_{tot}(\mathbf{r}) \right] \phi_i(\mathbf{r}) = \epsilon_i \phi_i(\mathbf{r}) \tag{3.12}$$

which are called Kohn and Sham equations.
To find an expression for V_{tot}, let us consider the HK functional of the real system, which is, by Eq.(3.7),

$$E[\rho(\mathbf{r})] = F[\rho(\mathbf{r})] + \int \mathrm{d}\mathbf{r} V_{ext}(\mathbf{r}) \rho(\mathbf{r}) \tag{3.13}$$

while that of the auxiliary system is

$$E'[\rho(\mathbf{r})] = T'[\rho(\mathbf{r})] + \int \mathrm{d}\mathbf{r} V_{tot}(\mathbf{r}) \rho(\mathbf{r}) \tag{3.14}$$

with

$$T'[\rho(\mathbf{r})] = \sum_{i}^{occ} \langle \psi_i | - \frac{\nabla_i^2}{2} | \psi_i \rangle \tag{3.15}$$

Consider now the quantity

$$T'[\rho(\mathbf{r})] + \frac{1}{2} \int \mathrm{d}\mathbf{r} \int \mathrm{d}\mathbf{r}' v(\mathbf{r}, \mathbf{r}') \rho(\mathbf{r}) \rho(\mathbf{r}') \tag{3.16}$$

where

$$\int \mathrm{d}\mathbf{r}' v(\mathbf{r}, \mathbf{r}') \rho(\mathbf{r}') = \int \mathrm{d}\mathbf{r}' \frac{1}{|\mathbf{r} - \mathbf{r}'|} \rho(\mathbf{r}') = V_H \tag{3.17}$$

is the Hartree potential.
Adding and subtracting eq.(3.16) to eq.(3.13), the HK functional becomes

$$\boxed{E[\rho(\mathbf{r})] = T'[\rho(\mathbf{r})] + \int \mathrm{d}\mathbf{r} V_{ext}(\mathbf{r}) \rho(\mathbf{r}) + \frac{1}{2} \int \mathrm{d}\mathbf{r} \int \mathrm{d}\mathbf{r}' v(\mathbf{r}, \mathbf{r}') \rho(\mathbf{r}) \rho(\mathbf{r}') + E_{xc}[\rho(\mathbf{r})]} \tag{3.18}$$

with

$$E_{xc}[\rho(\mathbf{r})] = T[\rho(\mathbf{r})] + U[\rho(\mathbf{r})] - \frac{1}{2} \int \mathrm{d}\mathbf{r} \int \mathrm{d}\mathbf{r}' v(\mathbf{r}, \mathbf{r}') \rho(\mathbf{r}) \rho(\mathbf{r}') - T'[\rho(\mathbf{r})] \tag{3.19}$$

which represents the *exchange-correlation energy*.
If we impose the stationarity condition $\delta E[\rho(\mathbf{r})] = 0$:

$$\delta T'[\rho(\mathbf{r})] + \int \mathrm{d}\mathbf{r} \delta\rho(\mathbf{r}) \left[V_{ext}(\mathbf{r}) + \int \mathrm{d}\mathbf{r}' v(\mathbf{r}, \mathbf{r}') \rho(\mathbf{r}) \rho(\mathbf{r}') + \frac{\delta E_{xc}[\rho(\mathbf{r})]}{\delta \rho(\mathbf{r})} \right] = 0$$

and use, from Eq.(3.14)

$$\delta T'[\rho(\mathbf{r})] = - \int \mathrm{d}\mathbf{r} V_{tot}(\mathbf{r})$$

we find

$$V_{tot}(\mathbf{r}) = V_{ext}(\mathbf{r}) + \int \mathrm{d}\mathbf{r}' v(\mathbf{r}, \mathbf{r}') \rho(\mathbf{r}') + V_{xc}([\rho(\mathbf{r}), \mathbf{r}]) \tag{3.20}$$

where

$$\frac{\delta E_{exc}[\rho]}{\delta \rho(\mathbf{r})} = V_{xc} \tag{3.21}$$

is the *exchange correlation potential*. The central equation of this procedure is Eq.(3.18), which is composed of four terms:

- the kinetic energy of the auxiliary non-interacting system T'
- the energy associated to the external potential V_{ext}
- the Hartree energy (the classic electrostatic energy of the electron distribution)
- the rest that we do not know, which we define as the exchange-correlation energy $E_{xc}[\rho(\mathbf{r})]$. The accuracy of DFT calculations depends on the choice of the approximation for this unknown term, which takes into account all the effects that go beyond Hartree theory.

The problem one has to face at this point is to find the functional dependence of E_{xc} on ρ.

3.2.3 Local Density Approximation (LDA)

The first and simplest approximation for the exchange-correlation energy is the Local-Density Approximation (LDA) proposed by Kohn and Sham in [16]. This approximation assumes that the functional dependence of of E_{xc} on ρ can be approximated by a local relation:

$$E_{xc}^{LDA}[\rho(\mathbf{r})] \simeq \int \mathrm{d}\mathbf{r}\rho(\mathbf{r})\varepsilon(\rho(\mathbf{r})) \tag{3.22}$$

where $\varepsilon(\rho(\mathbf{r}))$ is the exchange-correlation energy per electron in a homogeneous electron gas of density ρ.
The $\varepsilon(\rho(\mathbf{r}))$ is known exactly in the high-density limit and can be accurately computed for any density using Quantum Monte Carlo simulations [22–24]. It is by construction exact for the homogeneous electron gas and can be expected to be a good approximation for systems where density has small spatial variations or where the electron-electron interaction is well screened.
LDA proved successful in systems which are well beyond the nearly-free electron gas and accurate results can be obtained for ground state energies of inhomogeneous systems like atoms or molecules.

Why does LDA work?

The reason why the local density approximation for E_{xc} and V_{xc} works so well even in systems in which the electron gas is rather inhomogeneous is that the exchange-correlation energy comes from the electrostatic interaction of an electron with the dynamic exchange-correlation hole in the electron distribution. In an inhomogeneous system, this hole is very far from the spherically symmetric hole in the homogeneous electron gas (as assumed in the LDA), but as the spherical average of the hole is taken in calculating the electrostatic interaction, this does not matter very much.

3.2.4 Excited States in DFT

The one-particle energies ϵ_i appearing in Eq.(3.12) are actually Lagrange multipliers with the constraint of the normalization condition and have a very ambigous physical meaning. The intepretation of KS eigenvalues appears to be much more complicated in DFT than that of eigenvalues in the traditional schemes of quantum chemistry. For example in Hartree-Fock theory, the Koopmans' Theorem gives a clear meaning to the eigenvalues of the HF single equations (see §3.1.3):

$$\epsilon_i^{HF} = E(f_1, \ldots, f_i, \ldots, f_n) - E(f_1, \ldots, f_i - 1, \ldots, f_n)$$

where ϵ_i^{HF} is a HF eigenvalue and $E(f_1, \ldots, f_i, \ldots, f_n)$ the total energy of a system of $N = f_1 + \ldots + f_n$ electrons.
In DFT this correspondence between KS eigenvalues and excitation energies is not valid. It has been shown that the eigenvalue of the highest occupied state, in an exact DFT scheme, gives a correct work function for a metal, or the ionization energy for a finite system [25, 26]. The only thing we can write for all the other KS eigenvalues is Janak Theorem [27]:

$$\epsilon_i(f_1, \ldots, f_n) = \frac{\partial E}{\partial f_i} \tag{3.23}$$

Eq.(3.23) means that

$$E(f_1,\ldots,f_i,\ldots,f_n) - E(f_1,\ldots,f_i-1,\ldots,f_n) = \int_0^1 \mathrm{d}f \cdot \epsilon_i(f_1,\ldots,f_i+f-1,\ldots,f_n)$$

rather different from the result of Koopman's Theorem.
In spite of the lack of a formal justification, the ϵ_i's are often treated as excitation energies, particularly in solid state applications where DFT band structures are often calculated and compared with experimental measurements (using photoemission or inverse photoemission). Agreement is frequently excellent, though a known problem is the fact that the energy gap between occupied and onuccupied states in DFT band structures is too small by typically 50% [28], while HF theory largely overestimates band gap energy[9].

Band gap problem

The error in the band gap seems surprising. It is not an intrinsic feature of DFT nor of the LDA, but rather of the KS-formalism.
As already said, the highest occupied DFT-KS eigenvalue $\epsilon_N^{(N)}$ obtained with the exact exchange-correlation potential in an N-electron system equals the true ionization energy of the system [26]. The band gap is given by the difference in ionization potential and electron affinity[5] for the N-electron system with the valence band completely full:

$$E_{gap} = E_N^{ion} - E_N^{aff}$$

But the electron affinity for the N-electron system is the same as the ionization energy for the $N+1$-electron system with an extra electron in the conduction band, so:

$$E_{gap} = E_N^{ion} - E_{N+1}^{ion}$$

From DFT, these ionization energies are given by the highest occupied eigenvalue for the N and $N+1$-electron systems respectively:

$$E_{gap} = \epsilon_i^{(N+1)} - \epsilon_i^N$$

As the eigenvalues come from Schrödinger equations in which the only difference is in V_H and V_{xc} due to an extra electron (among a vast number), we would expect this to be equal to the energy gap E_{gap}^{DFT} from the single-electron DFT band-structure calculation. This is wrong: there is in fact a discontinuity Δ in V_{xc} in going from the system in which the valence band is completely full and the conduction band is completely empty, to one with an extra electron in the conduction band:

$$V_{xc}^{(N+1)}(\mathbf{r}) - V_{xc}^N(\mathbf{r}) = \Delta$$

This discontinuity shifts the whole bad-structure of the $N+1$-electron system relative to the N-electron system, so:

$$E_{gap} = E_{gap}^{DFT} + \Delta$$

This non-analytic behaviour of V_{xc} as a function of the number of electron should sound as a cautionary note about treating E_{xc} as a relatively simple functional of the electron density.
In general DFT band-structures have to be corrected via the self-energy to give the actual one-electron excitation energies [28].

[5]The electron affinity of an atom is the energy required to detach an electron from a singly charged negative ion, i.e., the energy change for the process $X^- \rightarrow X + e^-$.

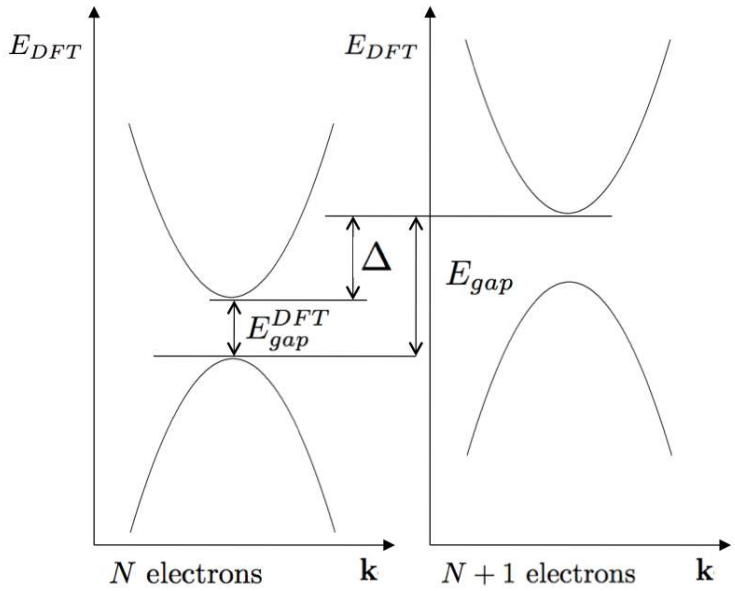

Figure 3.1: Band structures for the N- and $N+1$-electron systems in a semiconductor, showing the effect of the discontinuity Δ in V_{exc}

3.2.5 Success and Failures of DFT

DFT, even in the simplest LDA approximation, turns out to be much more successful than one could expect. LDA is computationally much simpler than Hartree-Fock, but it yields results of similar quality in atoms and molecules. Structural and vibrational properties of solids are in general accurately described and the correct crystal structure is usually found to have the lowest energy.
LDA also has some well-known problems. Some can be avoided by using better functionals, some others have a deeper and more fundamental nature.

Accuracy of LDA and gradient corrections

The accuracy of LDA is often considered satisfactory in condensed-matter systems, but it is much less so in atomic and molecular physics, for which highly accurate experimental data are available. Also, LDA badly overestimates cohesive energies and bond strengths in molecules and solids, and as a consequence bond lengths are often underestimated. Such problems are mostly corrected by the introduction of *gradient corrections*, in which the exchange correlation functional is written as a function of the local density and of the local gradient of the density [29].

The weak van der Waals forces between closed-shells systems are still beyond the reach of DFT. The van der Waals (or dispersive) interactions have a non-local character: they are due to charge fluctuations on one system, inducing a dipole on the other. This phenomenon is absent by construction from LDA, as well as from any functional based on the local density and on its local derivatives: these can reproduce only phenomena due to charge overlap. Since however LDA overestimates the attractive potential coming from the overlap of the tails of the charge density, closed-shell systems in LDA are actually bound with binding energies and binding distances in apparent agreement with experimental results. This is a fictitious result (and the dependence on the separation distance is wrong) that disappear if better-behaved gradient-corrected functionals

are used [30].

3.3 Time Dependent DFT

The theory developed in the last section is a ground-state time-independent theory, which is not generally applicable to problems involving a time dependence, such as the calculation of optical properties and electronic spectra.
The generalization of the basic formalism of DFT to the time-dependent case is due to Runge, Gross and Kohn [18, 19], who developed a method similar to the Hohenberg-Kohn-Sham Theory for time-dependent potentials.

3.3.1 TDDFT Theorems

Consider a N-electron system, described by the Schrödinger equation

$$H(t)\varphi(t) = i\hbar\frac{\partial\phi(t)}{\partial t}$$

with

$$H(t) = T + U + W(t) = -\sum_{i=1}^{N}\frac{\nabla_i^2}{2} + \frac{1}{2}\sum_{i\neq j}^{N}\frac{1}{|\mathbf{r}_i - \mathbf{r}_j|} + \sum_{i=1}^{N}V_{ext}(\mathbf{r},t)$$

sum of the kinetic, Coulomb and external (time-dependent) potential energy. Suppose that the external potential is expandable in Taylor series around t_0.

TDDFT Theorem I *The densities $\rho(\mathbf{r},t)$ and $\rho'(\mathbf{r},t)$ evolvng from the common initial state $\varphi(t_0) = \varphi_0$, under the influence of two external potentials $V_{ext}(\mathbf{r},t)$ and $V'_{ext}(\mathbf{r},t)$, both Taylor expandable around t_0, are always different provided that the external potentials differ by more than a purely time-dependent function $c(t)$.*

This is the time-dependent analogue of HK theorem I: the time-dependent density uniquely determines the external potential up to a purely time-dependent function $c(t)$. On the other hand the potential determines the time-dependent wavefunction, unique functional of the density up to a purely time-dependent phase:

$$\varphi(t) = e^{-i\alpha(t)}\varphi[\rho,\varphi_0](t)$$

For an operator $\hat{O}(t)$, which is a function of time but not of any derivative or integral operators on t, the phase factor calcels out when taking the expectation value, which is hence a unique functional of the density:

$$\langle\varphi(t)\hat{O}(t)|\varphi(t)\rangle| = O[\rho](t)$$

TDDFT Theorem II *The analogue of HK Theorem II, where the variational principle is used for the total energy, is given in the time-dependent theory by the stationary principle of the Hamiltonian action integral.*
In quantum mechanics the time-dependent Schrödinger equation, with the initial condition $\varphi(t_0) = \varphi_0$ corresponds to a stationary point of the quantum mechanical action integral

$$A = \int_{t_0}^{t_1}\mathrm{d}t\langle\varphi(t)|i\hbar\frac{\partial}{\partial t} - H(t)|\varphi(t)\rangle$$

A is a functional of the density and has a stationary point at the correct time-dependent density, which can be obtained solving the Euler equations

$$\frac{\partial A[\rho(\mathbf{r},t)]}{\partial \rho(\mathbf{r},t)} = 0$$

with the appropriate initial conditions. Following the same procedure than in the time-independent case, we find the time-dependent Kohn-Sham equations:

$$\left[-\frac{\nabla_i^2}{2} + V_{tot}(\mathbf{r},t)\right]\phi_i(\mathbf{r},t) = i\frac{\partial}{\partial t}\phi_i(\mathbf{r},t) \tag{3.24}$$

where

$$V_{tot}(\mathbf{r},t) = V_{ext}(\mathbf{r},t) + \int \mathrm{d}\mathbf{r}' v(\mathbf{r},\mathbf{r}')\rho(\mathbf{r}',t) + V_{xc}(\mathbf{r},t) \tag{3.25}$$

which are analogous to Eqs. (3.12) and (3.20).

3.3.2 Time Dependent Density Response Functional Theory

The solutions of Eq.(3.24) are the KS orbitals which yield the true charge density. This means that any property which depends only on the density can be exactly obtained, in principle, by the Kohn-Sham formalism. We are interested in excitation energies and polarizabilities within linear response, which leads to some simplifications.
The linear response theory can be applied here to study the effect of a small perturbation $V_{ext}(\mathbf{r},t)$ on the system. In the linear approximation the induced charge density is related to the external potential

$$\rho_{ind}(\mathbf{r},t) = \int \mathrm{d}\mathbf{r}' \int \mathrm{d}t' \chi(\mathbf{r},\mathbf{r}',t-t')V_{ext}(\mathbf{r}',t') \tag{3.26}$$

via the *response function* $\chi(\mathbf{r},\mathbf{r}',t-t')$, which is called full polarizability. Due to the causality condition, χ is non-zero only for $t > t'$.
In the time-dependent KS scheme it is also possibile to describe the response of the system to an *effective* total potential V_{tot}, given by Eq. (3.25), containing also the exchange-correlation contribution, via the

$$\rho_{ind}(\mathbf{r},t) = \int \mathrm{d}\mathbf{r}' \int \mathrm{d}t' \chi^0(\mathbf{r},\mathbf{r}',t-t')V_{tot}(\mathbf{r}',t')$$

where the indipendent particle polarizability χ^0 is the linear response of the fictitious Kohn-Sham system (non-interacting) and has the form (see Appendix A)

$$\chi^0(\mathbf{r},\mathbf{r}',\omega) = \sum_{vc} \frac{(f_v - f_c)\phi_v^*(\mathbf{r})\phi_c(\mathbf{r})\phi_c^*(\mathbf{r}')\phi_v(\mathbf{r}')}{\omega - (\epsilon_c - \epsilon_v) + i\eta} \tag{3.27}$$

in the real space and frequency domain[6] and

$$\begin{aligned}\chi^0(\mathbf{q},\mathbf{G},\mathbf{G}',\omega) &= \frac{2}{\Omega}\sum_{i,j,\mathbf{k}} \frac{(f_{i,\mathbf{k}+\mathbf{q}} - f_{j,\mathbf{k}})\langle i,\mathbf{k}|e^{-i(\mathbf{q}+\mathbf{G})\cdot\mathbf{r}}|j,\mathbf{k}+\mathbf{q}\rangle\langle j,\mathbf{k}+\mathbf{q}|e^{i(\mathbf{q}+\mathbf{G}')\cdot\mathbf{r}'}|i,\mathbf{k}\rangle}{\omega - (\epsilon_{i,\mathbf{k}} - \epsilon_{j,\mathbf{k}}) + i\eta} \\ &= \frac{2}{N_\mathbf{k}}\sum_{i,j,\mathbf{k}} \frac{(f_{j,\mathbf{k}+\mathbf{q}} - f_{i,\mathbf{k}})\tilde{\rho}_{ij\mathbf{k}}(\mathbf{q},\mathbf{G})\tilde{\rho}^*_{ij\mathbf{k}}(\mathbf{q},\mathbf{G}')}{\omega - (\epsilon_{j,\mathbf{k}+\mathbf{q}} - \epsilon_{i,\mathbf{k}}) + i\eta}\end{aligned} \tag{3.28}$$

[6]The pure imaginary part $i\eta$ is insterted in order to make the Fourier Transform feasible. The formula is valid for $\eta \to 0$

in reciprocal space and frequency, explicitly including the band structure of the system. In these equations f_j and f_i are the Fermi occupation numbers, ϵ_j and ϵ_i the KS eigenvalues and the sums run over all KS orbitals.

The two response functions χ and χ^0 are related by Eq. (3.25), giving

$$\chi = \frac{\delta\rho}{\delta V_{ext}} = \frac{\delta\rho}{\delta V_{tot}}\frac{\delta V_{tot}}{\delta V_{ext}} = \chi^0\left[\frac{\delta V_{ext}}{\delta V_{ext}} + \frac{\delta V_H}{\delta V_{ext}} + \frac{\delta V_{xc}}{\delta V_{ext}}\right] = \tag{3.29}$$
$$= \chi^0\left[1 + \frac{\delta V_H}{\delta\rho}\frac{\delta\rho}{\delta V_{ext}} + \frac{\delta V_{xc}}{\delta\rho}\frac{\delta\rho}{\delta V_{ext}}\right]$$

Introducing the variations of the Hartree and exchange-correlation potentials

$$v = \frac{\delta V_H}{\delta\rho} \qquad f_{xc} = \frac{\delta V_{xc}}{\delta\rho}$$

Eq.(3.29) becomes

$$\boxed{\chi = \chi^0 + \chi^0(v + f_{xc})\chi} \tag{3.30}$$

which has the form of a Dyson equation and can be written more explicitly as

$$\chi(\mathbf{r},\mathbf{r}',\omega) = \chi^0(\mathbf{r},\mathbf{r}',\omega) + \int d\mathbf{r}'' \int d\mathbf{r}''' \left[\chi^0(\mathbf{r},\mathbf{r}'',\omega)\Big(v(\mathbf{r}'',\mathbf{r}''') + f_{xc}(\mathbf{r}'',\mathbf{r}''',\omega)\Big)\chi(\mathbf{r}''',\mathbf{r}',\omega)\right]$$

The presence of the two variations v and f_{xc} in the response function derives from the fact that the total perturbation acting on the system is calculated self-consistently.
The quantity

$$f_{xc}(\mathbf{r},\mathbf{r}',t,t') = \frac{\delta V_{xc}([\rho(\mathbf{r})],\mathbf{r},t)}{\delta\rho(\mathbf{r}',t')}$$

is called exchange-correlation kernel and takes into account all dynamical exchange and correlation effects to linear order in the perturbation potential.
A frequently used approximation to solve Eq.(3.30) is the Random Phase Approximation (RPA), which will be treated in more detail later. In RPA $f_{xc} = 0$ and Eq. (3.30) takes the form

$$\boxed{\chi = \chi^0 + \chi^0 v\chi} \tag{3.31}$$

in which only the Coulomb potential v is left in the self-consistent part.

3.3.3 Excited states in TDDFT

We have seen that the interpretation of one-particle eigenvalues as quasi-particle energies has no formal justification in static DFT.
Time-dependent DFT is one of the methods that allow to solve this problem and calculate che excited state energies of a many-body system [31, 32].

If we rewrite Eq.(3.30) in the form

$$\Big[1 - \chi^0(v + f_{xc})\Big]\chi = A(\omega)\chi = \chi^0 \tag{3.32}$$

one can observe that while χ has poles at the true excitation energies

$$\Omega_j = (E_j^N - E_0^N)$$

where E_0^N is the ground state energy and E_j^N a j^{th} excited state energy of a N-particle system, χ^0 has poles at the one-particle excitation energies

$$\epsilon_i - \epsilon_j$$

(KS eigenvalue differences), which are different from the true excitation energies.
This implies that the relation (3.32) holds only if the operator $A(\omega)$ is not invertible at frequencies $\omega = \Omega_j$: this because zeroes of $A(\omega)$ must cancel the singularities of χ.
We see that the problem of finding the excitation energies of a N-particle system can be solved by finding the frequencies for which $A(\omega)$ is not invertible, $\omega = \Omega_j$.

3.4 Calculating the spectra

We have developed all the theory we need to use many-body theory to calculate electronic spectra.
To finally make the microscopic-macroscopic connection we have to define a dielectric function ε, which relates in the linear approximation the effective potential V_{tot} to the external potential V_{ext} via

$$V_{tot}(\mathbf{r}, \omega) = \int \mathrm{d}\mathbf{r}' \varepsilon^{-1}(\mathbf{r}, \mathbf{r}', \omega) V_{ext}(\mathbf{r}', \omega)$$

where the inverse dielectric function ε^{-1} acts as a screening for the external potential. The previous expression and Eqs. (3.25) and (3.26) contain the connection between the dielectric function and the polarizability.

An expression for ε^{-1}

We rewrite Eq.(3.25) as

$$\delta V_{tot} = \delta V_{ext} + \delta V_H + \delta V_{xc}$$

from which we obtain

$$\begin{aligned} \frac{\delta V_{tot}}{\delta V_{ext}} = \varepsilon^{-1} &= 1 + \frac{\delta V_H + \delta V_{xc}}{\delta V_{ext}} = \\ &= 1 + \left[\frac{\delta V_H}{\delta \rho} + \frac{\delta V_{xc}}{\delta \rho} \right] \frac{\delta \rho}{\delta V_{ext}} = \\ &= 1 + (v + f_{xc})\chi \end{aligned} \tag{3.33}$$

The portion of screening that has to be included in ε^{-1} depends on the probe.
We can see this in two steps:

1. The external perturbation V_{ext} induces a charge density $\rho_{ind} = \chi V_{ext}$, where the response function χ depends only on the nature of the system; in this case, we are dealing with a gas of interacting electrons, so

$$\chi = \frac{\chi^0}{1 - \chi^0 v - \chi^0 f_{xc}} \tag{3.34}$$

2. The induced charge creates a screening described by ε^{-1} which, instead, depends on the perturbation to be screened: if the perturbation is a test-particle, it has no exchange-correlation effects with the responding electron gas. On the other hand an electron will feel not only an induced classical potential $v\rho_{ind}$ but also an induced exchange-correlation potential $V_{xc} = f_{xc}\rho_{ind}$. Then

$$\varepsilon_{TP}^{-1} = 1 + v\chi$$
$$\varepsilon_{TE}^{-1} = 1 + v\chi + f_{xc}\chi$$

for the two cases.

In the case of the test-particle dielectric matrix, one can explicitly obtain the microscopic dielectric function as

$$\boxed{\varepsilon^{-1}_{\mathbf{GG'}}(\mathbf{q},\omega) = \delta_{\mathbf{GG'}} + v_{\mathbf{G}}(\mathbf{q})\chi_{\mathbf{GG'}}(\mathbf{q},\omega)}$$

And an expression for ε

We can see things in a different way by considering the inverse of Eq. (3.33). Let us put $\delta V_{xc} = 0$ from the beginning. This means that we are considering $\delta V_{ind} = \delta V_H$, and the test particle case (photon or fast electron whose exchange correlation interaction is negligible, since it starts to interact from far away).

$$\begin{aligned}\frac{\delta V_{ext}}{\delta V_{tot}} = \varepsilon &= 1 - \frac{\delta V_H}{\delta V_{tot}} = \\ &= 1 - \frac{\delta V_H}{\delta \rho}\frac{\delta \rho}{\delta V_{tot}} \\ &= 1 - vP\end{aligned}$$

where the polarizability $P = \dfrac{\delta_\rho}{\delta V_{tot}}$ has been introduced[7].
One should notice that while χ is an experimentally accessible quantity, because it represents the variation of charge with respect to the macroscopic potential V_{ext}, P cannot be measured, because it involves the variation with respect to the *microscopic* potential V_{tot}, that we do not know[8]. Anyway P allows us to write another expression for the microscopic ε:

$$\varepsilon_{\mathbf{GG'}}(\mathbf{q},\omega) = \delta_{\mathbf{GG'}} - v_{\mathbf{G}}(\mathbf{q})P_{\mathbf{GG'}}(\mathbf{q},\omega)$$

3.4.1 Approximations

Of course, the exact time dependent exchange-correlation potential and kernel appearing in Eq.(3.30) are unknown and realistic calculations rely on some approximations.
From the expressions used in the previous paragraph, it can be shown[9] that the link between P and χ is given by another Dyson-like equation

$$\chi = P + Pv\chi \tag{3.35}$$

Considering together Eqs.(3.35) and (3.30), another similar relation involving χ^0 can be obtained:

$$P = \chi^0 + \chi^0 f_{xc} P \tag{3.36}$$

Now we are ready to present the different approximations, considering an increasing grade of complexity.

[7] P is called *irreducible* polarizability, as opposed to χ, which is called *reducible*. The distintion between these two is clearer in the GW theory, another kind of excited state theory, which is beyond the scope of this work.
[8] Incidentally, this is again related with the fact that the physically relevant quantity is ε^{-1} and not ε.

Indipendent Particles (RPA without LFE)

We first consider the simplest possible approximation, the independent particle picture of the DFT-KS scheme.
Actually, DFT is a ground state theory and that there is no formal justification in using it to study the excited states, but we can anyway try to consider a first investigation of electronic spectra. Once the DFT-KS band structure has been found by solving Eq.(3.12), the polarizability that can be calculated is χ^0, which comes from static DFT as a sum over *independent transitions*:

$$\chi^0(\mathbf{q},\omega) = 2\sum_{i,j} \frac{|\langle\phi_j|e^{i\mathbf{q}\cdot\mathbf{r}}|\phi_i\rangle|^2}{\omega - (\epsilon_j - \epsilon_i) + i\eta} \tag{3.37}$$

with ϕ_i, ϵ_i KS eigenfunctions and eigenvalues, respectively.
χ^0 describes the response of the fictituos Kohn-Sham system of independent electrons to the effective Kohn-Sham potential:

$$\chi^0 = \frac{\delta\rho}{\delta V_{tot}}$$

In the case of independent particles there are no dynamical correlation effects, so $f_{xc} = 0$: this alone is the Random Phase Approximation already mentioned. From Eq.(3.30) we see that

$$P_{IPA} = \chi^0$$

In this simple approximation we also neglect local field effects, so what we obtain for the microscopic ε and macroscopic ε_M is

$$\begin{aligned}
&\varepsilon = 1 - v\chi^0 \quad \text{(IPA)} \\
&\varepsilon_M(\omega) = \varepsilon_M^{NLF}(\omega) = \lim_{\mathbf{q}\to 0} \varepsilon_{\mathbf{00}}(\mathbf{q},\omega) \quad \text{(neglecting LFE)}
\end{aligned}$$

The electronic spectra calculated with Eqs.(2.3) are then

$$\begin{aligned}
\text{Abs} &= \text{Im}\{\varepsilon_M\} = \Im\{1 - v\chi^0\} = -v\Im\{\chi^0\} \\
\text{EELS} &= -\text{Im}\left\{\frac{1}{\varepsilon_M}\right\} = -v\Im\left\{\frac{\chi^0}{1 - v\chi^0}\right\}
\end{aligned} \tag{3.38}$$

Applying the relation

$$\lim_{\eta\to 0} \frac{1}{x \pm i\eta} = \text{pv}\left(\frac{1}{x}\right) \mp i\pi\delta(x) \tag{3.39}$$

to the (3.37) expression for χ^0, we see that for the absorption spectrum we have, more explicitly

$$\text{Abs} \propto \text{Im}\{\varepsilon\} \propto \sum_{v,c} |\langle\phi_c|e^{i\mathbf{q}\cdot\mathbf{r}}|\phi_v\rangle|^2 \delta(\omega - (\epsilon_c - \epsilon_v))$$

with the sum over all independent transitions and the delta function representing the conservation of energy. This last expression corresponds to the one-electron approximation of Fermi's golden rule we had in Eq.(1.24): then, as already said in §2.3, Fermi's golden rule applied to absorption correspond to an IP-RPA calculation without local-field effects.

Random Phase Approximation with LFE

The next step beyond the independent particle approximation, which is the one made throughout this work, is the Random Phase Approximation, in which f_{xc} is set to zero, but local field effects are taken into account. In this case, the microscopic ε has the same form as in the previous step, but the macroscopic ε_M is calculated with the right average (2.2).

$$\varepsilon = 1 - v\chi^0 \quad \text{(RPA)}$$
$$\varepsilon_M(\omega) = \lim_{\mathbf{q}\to 0} \frac{1}{[\varepsilon^{-1}(\mathbf{q},\omega)]_{\mathbf{G}=\mathbf{G}'=\mathbf{0}}} \quad \text{(considering LFE)}$$

Adiabatic Local Density Approximation

A more sophisticated kind of approximation with respect to RPA is the so called adiabatic[9] local density approximation (ALDA), in which f_{xc} is taken as the functional derivative of the static LDA exchange-correlation potential described in §3.2.3.

$$f_{xc}^{ALDA}(\mathbf{r},\mathbf{r}',t,t') = \delta(\mathbf{r}-\mathbf{r}')\delta(t-t')\frac{\partial V_{xc}^{LDA}[\rho(\mathbf{r}),\mathbf{r}]}{\partial\rho(\mathbf{r})}$$

The ALDA approximation has proven to be quite successful in applications to finite systems, such as molecules or clusters. However, for the graphite system considered in this work, it does not lead to remarkable improvements with respect to RPA (see Chapter 4 and [4, 5]).

[9] In this case, the term adiabatic refers to the independence from ω

3.4.2 Summary

We can summarize the steps leading to the determination of a spectrum with TDDFT used in this work.

1. **A Ground state calculation** is done within the static DFT framework, where a reasonable exchange-correlation potential V_{xc} has been chosen, usually V_{xc}^{LDA}. We obtain the single-particle eigenfunctions ϕ_i and eigenvalues ϵ_i.
   The approximations involved are the choice of V_{xc} and the use of pseudopotentials.

2. **The Independent-Particle polarizability** χ_0 is calculated with eigenfunctions and eigenvalues obtained in step 1 via Eq.(3.28):

$$\chi^0_{\mathbf{GG'}}(\mathbf{q},\omega) = \frac{2}{\Omega}\sum_{v,c,\mathbf{k}} \frac{(f_{v,\mathbf{k+q}} - f_{c,\mathbf{k}})\langle\phi_{v,\mathbf{k}}|e^{-i(\mathbf{q}+\mathbf{G})\cdot\mathbf{r}}|\phi_{c,\mathbf{k+q}}\rangle\langle\phi_{c,\mathbf{k+q}}|e^{i(\mathbf{q}+\mathbf{G'})\cdot\mathbf{r'}}|\phi_{v,\mathbf{k}}\rangle}{\omega - (\epsilon_{v,\mathbf{k}} - \epsilon_{c,\mathbf{k}}) + i\eta} \tag{3.40}$$

   The approximation is just the linear response framework.

3. **The full polarizability** χ can be obtained with Eq.(3.30), if there is an expression for f_{xc}:

$$\chi_{\mathbf{GG'}}(\mathbf{q},\omega) = \chi^0_{\mathbf{G},\mathbf{G'}}(\mathbf{q},\omega) + \sum_{\mathbf{G}_1\mathbf{G}_2} \chi^0_{\mathbf{GG}_1}(\mathbf{q},\omega)\cdot\left[v_{\mathbf{G}_1}(\mathbf{q})\delta_{\mathbf{G}_1\mathbf{G}_2} + f^{xc}_{\mathbf{G}_1\mathbf{G}_2}\right]\cdot\chi_{\mathbf{G}_2\mathbf{G'}} \tag{3.41}$$

   The choice of f_{xc} represents the most important approximation of the entire calculation.

4. **The dielectric function** calculated as

$$\varepsilon^{-1}_{\mathbf{GG'}}(\mathbf{q},\omega) = \delta_{\mathbf{GG'}} + v_{\mathbf{G}}(\mathbf{q})\chi_{\mathbf{GG'}}(\mathbf{q},\omega) \tag{3.42}$$

   allows to obtain absorption and EELS spectra via the macroscopic function

$$\varepsilon_M(\omega) = \frac{1}{\varepsilon^{-1}_{00}(\mathbf{q},\omega)} \tag{3.43}$$

4
Computational DFT and TDDFT

The previous chapter introduced the theoretical basis for the calculation of excited states. We have seen that two main steps are needed: the calculation of the ground state via the Density Functional Theory and then the study of dielectric properties within Time Dependent Functional Theory.
In this chapter we want to present the methods of implementation of these theories.

4.1 Ground state calculation

The code used in this work which implements DFT is the ABINIT code [33].
ABINIT is a package *whose main program allows one to find the total energy, charge density and electronic structure of systems made of electrons and nuclei (molecules and periodic solids) within DFT, using pseudopotentials and a planewave basis* [34]. In this first section we want to briefly explain what this definition means [17, 35, 36].

4.1.1 Plane wave basis sets

The main problem of DFT implementation is the computational treatment of the continuity of space.
First, one needs to represent the wavefunctions of the system. For a periodic Hamiltonian, such as in crystals, Bloch's Theorem (§B.1.4) states that the electronic wavefunctions at each $\mathbf{k}$ point can be expanded in terms of a discrete plane-wave basis set and written as

$$\psi_{n\mathbf{k}}(\mathbf{r}) = \frac{1}{\sqrt{\Omega}} \sum_{\mathbf{G}} u_{n\mathbf{k}}(\mathbf{G}) e^{i(\mathbf{k}+\mathbf{G})\cdot\mathbf{r}} = e^{i\mathbf{k}\cdot\mathbf{r}} u_{n\mathbf{k}}(\mathbf{r}) \tag{4.1}$$

where

$$u_{n\mathbf{k}}(\mathbf{r}) = \frac{1}{\sqrt{\Omega}} \sum_{\mathbf{G}} u_{\mathbf{k}}(\mathbf{G}) e^{i\mathbf{G}\cdot\mathbf{r}}$$

is a function periodic over the crystal lattice. Ω is the volume of the system, the vectors $\mathbf{k}$ lie in the first Brillouin zone and the $\mathbf{G}$'s are reciprocal lattice vectors.
ABINIT works in reciprocal space, and each wavefunction is identified by the number of the band n and by the $\mathbf{k}$ that determine the periodic coefficient $u_{n\mathbf{k}}(\mathbf{r})$.

In principle one would need an infinite set of plane waves. However, it can be proved that plane waves with small kinetic energy

$$\frac{|\mathbf{k}+\mathbf{G}|^2}{2}$$

are typically more important than those with large kinetic energy. Then one can introduce a *cutoff energy* E_{cut} to use just a finite number of plane waves that have kinetic energy less than some particular cutoff energy. The "plane wave sphere" used in the calculation will be then defined by the relation

$$\frac{|\mathbf{k}+\mathbf{G}|^2}{2} \leq E_{cut}$$

The truncation of the plane wave basis set at a finite cutoff energy will lead to an error in the computed total energy. However, it is always possible to reduce the importance of this error by increasing the value of the cutoff energy until the total energy has converged.
One of the difficulties associated with the use of planewave basis sets is that the number of basis states changes discontinuosly with cutoff energy, like shown (in two dimensions) in Fig. 4.1. This problem can be reduced by using denser **k** point sets.

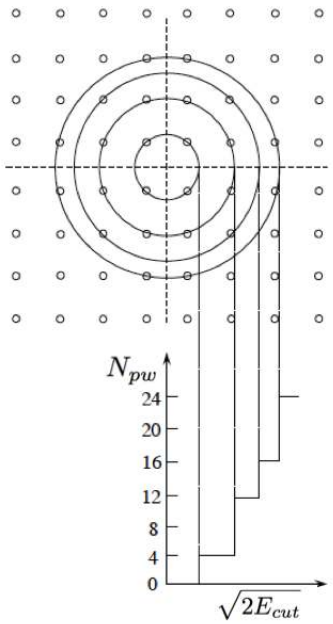

Figure 4.1: Discontinuity in the number of plane waves [36]

The sudden change in the number of plane waves causes discontinuities also in the total energy, as we will see later in our results.

As the code works in reciprocal space, all the quantities, such as the potential and the electronic density, have to be brought in reciprocal space. This means that one needs to perform a discrete Fourier transform over the sets $\{\mathbf{r}_i\}$ and $\{\mathbf{G}\}$. The fast algorithm used to do this is the so-called Fast Fourier Transform (FFT).

4.1.2 Brillouin zone integration

DFT involves discrete summations over states, as in the expression of the total kinetic energy in Eq.(3.15) or in the electronic density in Eq.(3.11). In the periodic case, wavefunctions are labeled by n and $\mathbf{k}$, so that the sum over states is given by the summation over energy bands

and integration over the Brillouin zone. Then we have for example for the density:

$$\begin{aligned}\rho(\mathbf{r}) &= \frac{1}{N_{\mathbf{k}}}\sum_{n}^{occ}\sum_{\mathbf{k}}^{BZ}|\psi_{n\mathbf{k}}(\mathbf{r})|^2 = \\ &= \frac{1}{N_{\mathbf{k}}}\frac{\Omega}{(2\pi)^3}\sum_{n}^{occ}\int_{BZ}\mathrm{d}\mathbf{k}\,|\psi_{n\mathbf{k}}(\mathbf{r})|^2 = \\ &= \frac{\Omega_{cell}}{(2\pi)^3}\sum_{n}^{occ}\int_{BZ}\mathrm{d}\mathbf{k}\,|\psi_{n\mathbf{k}}(\mathbf{r})|^2\end{aligned}$$

where $\dfrac{(2\pi)^3}{\Omega_{cell}}$ is the volume of the Brillouin zone and Eq.(B.1) was used.
For practical purposes the integral is, of course, performed as a summation

$$\rho(\mathbf{r}) = \sum_{n}^{occ}\sum_{i=1}^{N_{\mathbf{k}}} w_i|\psi_{n_i\mathbf{k}_i}(\mathbf{r})|^2$$

where the (lattice dependent) weights w_i and points $\mathbf{k}_i$ are chosen to reproduce the integral as accurately as possible, by using the smallest possible number of **k**-points. If the function to be integrated is periodic and symmetric in the reciprocal coordinates, the so-called *special k-points* can be chosen by exploiting the symmetry properties of the crystal. An often used method for the choice of the special points is that of Monkhorst-Pack grids [37], which have been adopted also in this work.
A Monkhorst-Pack set consists in points equally spaced in the Brillouin zone, which are not related to each other by any symmetry operation. In comparison with an arbitrary grid of points, which does not reflect the symmetries of the Brillouin zone, the Monkhorst-Pack set reduces drastically the number of points necessary to attain a specific precision in calculating integrals.

4.1.3 Pseudopotentials

We have seen that, thanks to Bloch's Theorem, the electronic wavefunctions can be expanded using a discrete set of plane waves. Fourier theory teaches us that, roughly speaking, details in real space are described if their characteristic length is larger that the inverse of the largest wavevector. This means that a very large number of plane waves is needed to expand the tightly bound core orbitals and to follow the rapid oscillations of the wavefunctions of the valence electrons in the core region. An extremely large plane-wave basis set would be required to perform an all-electron calculation, and a lot of computational time would be needed.

The *pseudopotential* approximation [38–40] allows the electronic wavefunctions to be expanded using a much smaller number of plane-wave basis states. It is known that core electrons do not contribute in a significant manner to physical properties. Only valence electrons do, while core electrons are "frozen" in their atomic state. This suggests that one can safely ignore changes in core states (frozen core approximation): the pseudopotential approximation exploits this concept by removing the core electrons and replacing them and the strong potential by a weaker pseudopotential that acts on a set of *pseudo* wavefunctions rather than on the true valence wavefunctions, as schematically illustrated in Fig. 4.2.

The valence wavefunctions oscillate rapidly in the region occupied by the core electrons because of the strong ionic potential in this region. These oscillations mantain the orthogonality

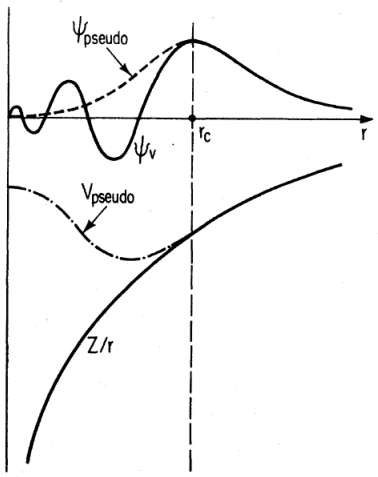

Figure 4.2: Schematic illustration of all-electron (solid lines) and pseudoelectron (dashed lines) potentials and their corresponding wavefunctions. The radius at which all-electron and pseudoelectron values match is designated $\mathbf{r}_c$ [17].

between the core wavefunctions and the valence ones:

$$\int \mathrm{d}\mathbf{r}\, \psi_{c\mathbf{k}}(\mathbf{r})\psi_{v\mathbf{k}}(\mathbf{r}) = 0$$

Since the core is virtually inert to changes in the chemical environment (such as bondings), we can construct a pseudopotential from atomic wavefunctions, even if this is not the method with which modern pseudopotentials are built [41]. The true valence wavefunction ψ is expressed as the sum of a smooth wavefunction φ (the pseudowavefunction) and a sum over occupied core states ψ_c:

$$\psi = \varphi + \sum_c b_c \varphi_c$$

The wavefunction is forced to be orthonormal to the core states $\langle\varphi_c|\psi\rangle = 0$. Solving for b_c:

$$\psi = \varphi - \sum_c \langle\varphi_c|\varphi\rangle\varphi_c$$

Operating on ψ with the Hamiltonian $H = T + V_c$ (where V_c is the attractive core potential) gives the correct energy eigenvalue E.
Substituting $H\psi = E\psi$ yields, after some rearrangement:

$$(H + V_R)\varphi = (T + V_c + V_R)\varphi = E\varphi \tag{4.2}$$

where

$$V_R = \sum_c (E - E_c)|\varphi_c\rangle\langle\varphi_c|$$
$$H\varphi_c = E_c\varphi_c$$

The potential V_R acts like a short-ranged repulsive potential. The pseudopotential is in general spatially nonlocal and depends on $\mathbf{r}$ and $\mathbf{r}'$.

Eq.(4.2) is the new Schrödinger equation for the pseudowavefunction φ, where E is the true energy corresponding to the true wavefunction ψ of the system. The potential $V = V_c + V_R$ is the sum of an attractive long-ranged and a repulsive short-ranged part. Near the core the two parts cancel fairly completely and the whole potential is well behaved and weak over the whole range, like in Fig. 4.2.

In DFT calculations, density is the main variable. If the density is to be calculated accurately, it is necessary that outside the core the pseudo wavefunctions and real wavefunctions are identical, not just in their spatial dependencies but also in their absolute magnitudes, so that the two wavefunctions generate identical charge densities. Pseudopotentials that satisfy this conditions are called *norm conserving* [42]. A widely used type of norm-conserving pseudopotential is the Martins-Troullier [43] one, which has been used in this work.

4.1.4 Application to graphite

Now we want to use ABINIT to calculate ground state properties of the system we want to study within DFT-LDA. The Kohn-Sham structure obtained will allow to calculate dielectric properties.

Graphite structure

Hexagonal graphite consists of an AB stacking of hexagonal planes of carbon (graphene) parallel to the cristallographic c axis, as shown in Fig. 4.3. This layered graphene-based structure and the type of chemical bonding make graphite a very anisotropic solid and a typical example of a quasi-two dimensional system.

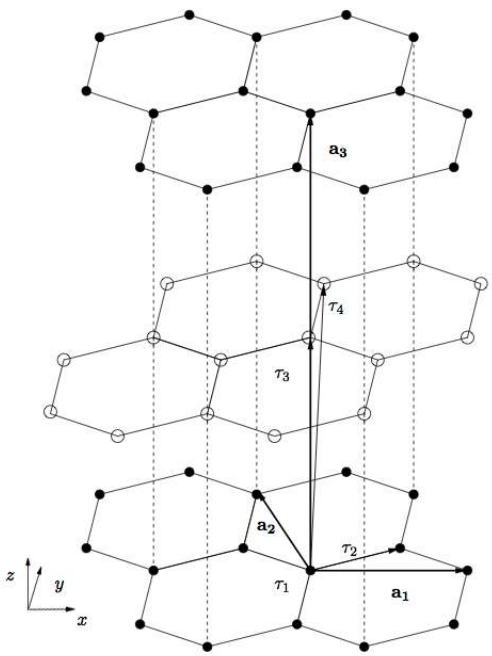

Figure 4.3: 3D structure of graphite

The choice of the primitive vectors is not unique. We take the two primitive vectors lying in the plane with an angle between them of 120°, and the third one perpendicular to the plane. In cartesian coordinates they are:

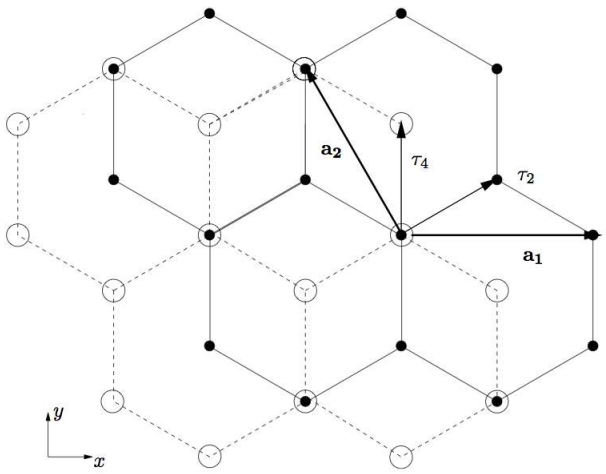

Figure 4.4: Plane structure of graphite

$$\begin{aligned}
\mathbf{a}_1 &= a\,(1,0,0) \\
\mathbf{a}_2 &= a\left(-\cos\frac{\pi}{3}, \sin\frac{\pi}{3}, 0\right) \\
\mathbf{a}_3 &= c\,(0,0,1)
\end{aligned}$$

The basis vectors in reduced coordinates $(\mathbf{a}_1, \mathbf{a}_2, \mathbf{a}_3)$ are

$$\begin{aligned}
\tau_{\mathbf{1}} &= (0,0,0) & \tau_{\mathbf{2}} &= \left(\frac{1}{3}, \frac{2}{3}, 0\right) \\
\tau_{\mathbf{3}} &= \left(0,0,\frac{1}{2}\right) & \tau_{\mathbf{4}} &= \left(\frac{1}{3}, \frac{2}{3}, \frac{1}{2}\right)
\end{aligned}$$

Using the relation $\mathbf{a_i} \cdot \mathbf{b_j} = 2\pi\delta_{ij}$ the reciprocal lattice basis vectors $\mathbf{b_i}$ are found to be

$$\begin{aligned}
\mathbf{b_1} &= \frac{2\pi}{a}\left(1, \frac{1}{\tan\frac{\pi}{3}}, 0\right) \\
\mathbf{b_2} &= \frac{2\pi}{a}\left(0, \frac{1}{\sin(\frac{\pi}{3})}, 0\right) \\
\mathbf{b_3} &= \frac{2\pi}{c}\,(0,0,1)
\end{aligned}$$

From the previous discussion, we already know that there are two parameters whose value must be checked to be sure of the reliability of the final result: the number of plane waves (i.e. E_{cut}) and the $\mathbf{k}$ point grid.
The procedure used to find the most suitable values for the parameters is called convergence, and it implies changing the parameter until results (for example, total energy) are reasonably stable.

We find that the total energy is converged with $E_{cut} = 30$ Ha and a Monkhorst-Pack grid 16x16x6 with 90 **k** points in the irreducible Brillouin zone, from which the total set of **k** points is generated through symmetry operations. The **k** point grid is shifted on the z axis to exclude the Γ point, which is taken into itself by any symmetry operation.

Lattice parameters

The lengths a and c appearing in the primitive vectors are found after a minimization with respect to the total energy of the system: this is actually one of the applications of ground state theories such as DFT.

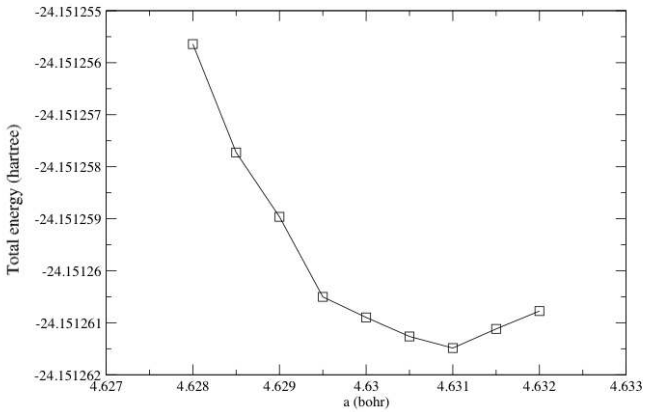

(a) Minimization with respect to a

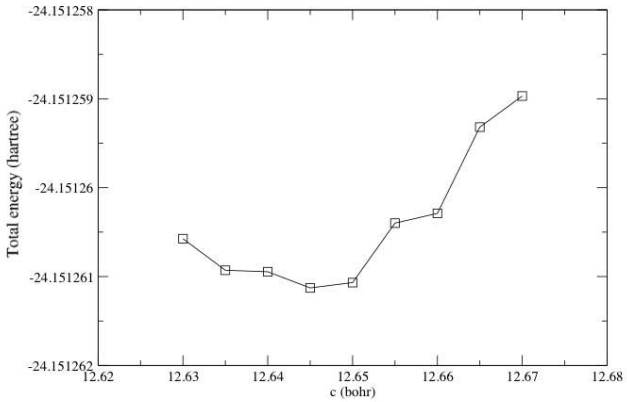

(b) Minimization with respect to c

Figure 4.5: Minimization with respect to lattice parameters of the total energy (in hartree). The strange shape of the curve in (b) is due to the fact that by changing the parameter c also the **G** vector set changes, while E_{cut} remains fixed. A greater c implies a denser **G** grid, and a lower total energy: this means that the curve in (b) is actually made up of different curves for increasing numbers of **G** vectors (see Fig. 4.1)

We find

$$a = 4.6310 \text{ bohr} = 2.4506 \text{ Å}$$
$$c = 12.645 \text{ bohr} = 6.691 \text{ Å}$$

where 1 bohr = 0.5292 Å.
Our values are in good agreement with the experimental values $a = 2.46$ Å and $c = 6.70$ Å and have the correct $\left(\frac{c}{a}\right)_{hex}$ ratio 2.73 [44].

The planes of graphite interact through the weak Van der Waals forces, that cannot be described by a DFT-LDA calculation (see §3.2.5). We would expect that the absence of these attractive forces would lead to an overextimation of the distance c. Anyway, this does not happen because of the overestimation of cohesive forces in LDA, which fictituosly corrects the small error due to the lack of Van der Waals interaction.

KS Band structure

As said in the previous chapter, DFT is not explicitly meant to give a correct calculation of excited states, because the KS eigenvalues have no physical meaning and are not the true quasi-particle energies of the system. Then if we draw the Kohn and Sham band structure along the circuit shown in Fig. 4.6a and 4.6ab we get the band structure of the non-interacting electron system. The band structure obtained is reported in Fig. 4.6c.
Our result is consistent with previous calculations (for example [5]). Actually, as said in the cited article, the major features of this band structure are in qualitative agreement with the experimental measurements by photoemission and very-low energy electron diffraction. There are of course quantitative discrepancies, that can be solved with self-energy corrections within the GW approximation.

We can try to consider also another circuit, the one in Fig. 4.7. If we compare the two band structures, we can see that while in Fig. 4.6c bands are parabolic, in 4.7c they are linear, and the H point is a singular point for the derivative: this is actually the same type of band structure which is observed in graphene [45] and leads to the observation of the so called Dirac fermions. If we remember the expression for the effective mass

$$m^* = \left(\frac{\partial^2 \epsilon}{\partial k^2}\right)^{-1} \tag{4.3}$$

we see that in H m^* is zero, because the derivative is infinite. This fact has consequences for conductivity, and has therefore been object of many studies, in particular for graphene [45, 46] . The phenomenon has later been observed also in graphite [47].

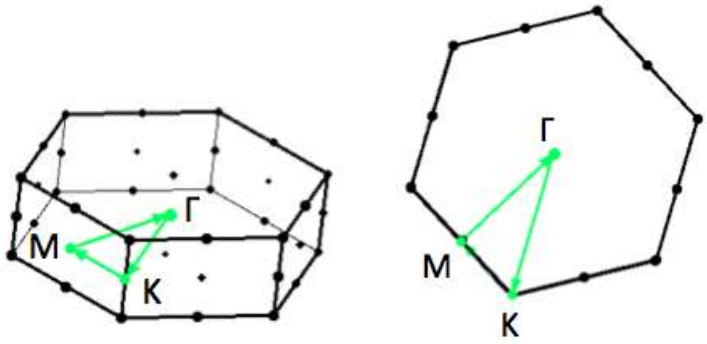

(a) First Brillouin zone in graphite (b) First Brillouin zone seen in 2D with first circuit of integration

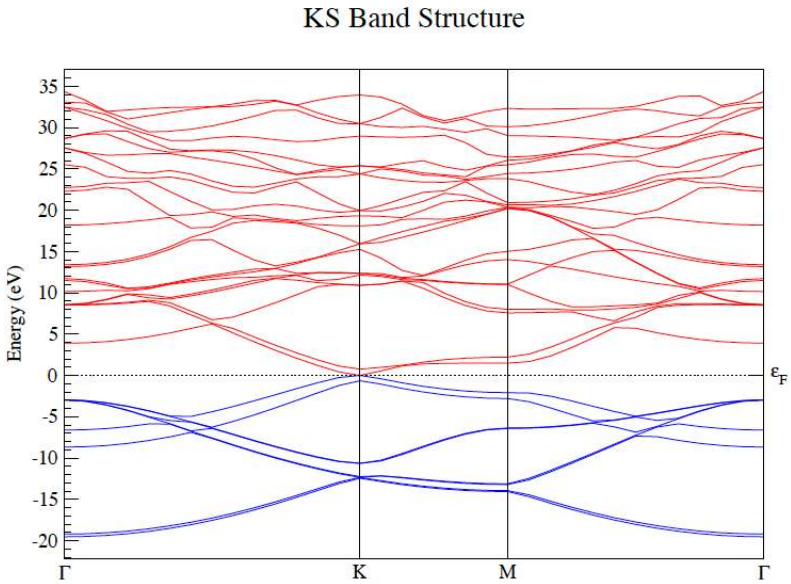

(c) Band Structure obtained from the first circuit

Figure 4.6

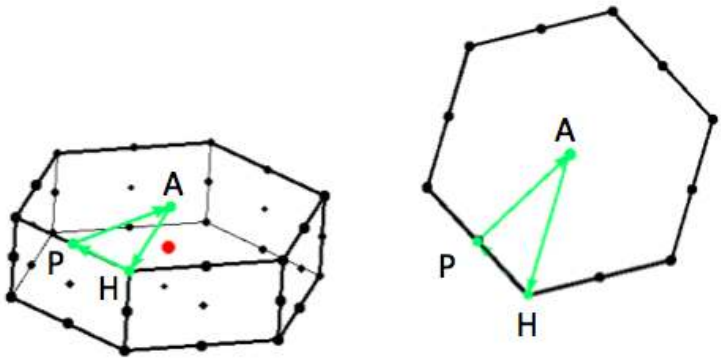

(a) Second circuit to obtain KS band structure (b) First Brillouin zone seen in 2D

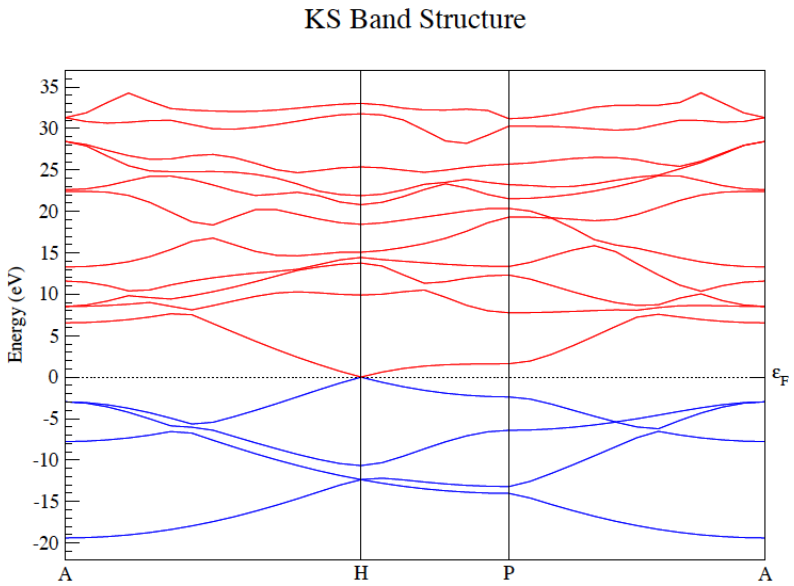

(c) Band Structure obtained from second circuit

Figure 4.7

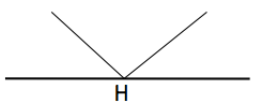

Figure 4.8: Schematic linear bands in the H point

Ground state density

At the end of a DFT calculation one gets the ground state density of the system: we can visualize it in real space and obtain figures such as 4.9.

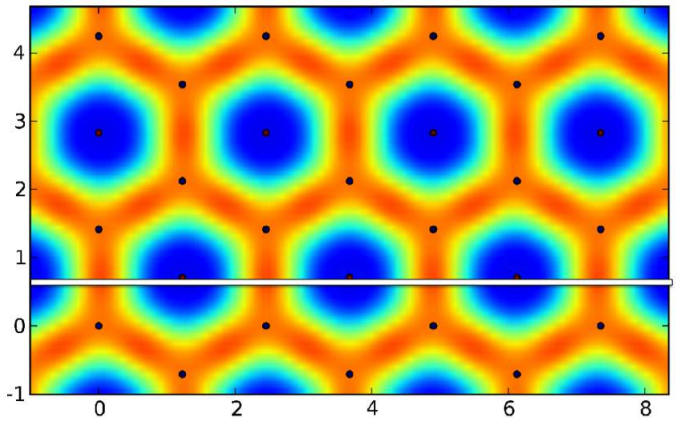

(a) xy vision near the lower plane ($z = 0.26$Å)

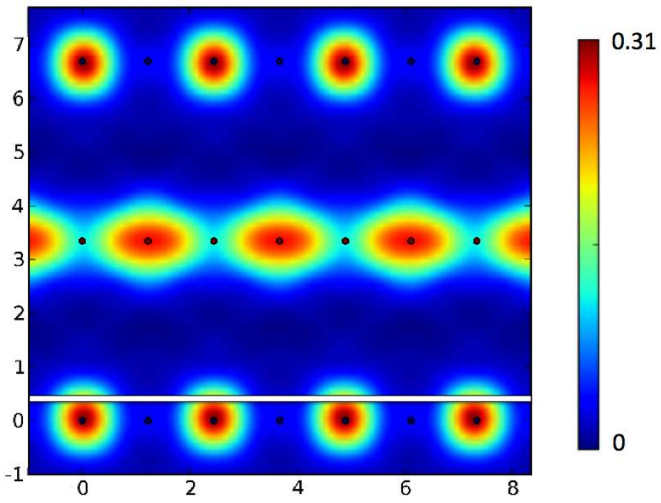

(b) xz vision ($y = 0.73$Å)

Figure 4.9: Calculated ground state electronic density. In a) and b) the cutting lines referring to b) and a) respectively are shown in white. The colour scale is normalized on the maximum of density in the cell (about $0.31 \frac{e}{\text{bohr}^3}$ in the red regions)

4.2 Dielectric properties: excited states

Once the Kohn-Sham structure has been calculated with ABINIT, dielectric properties can be obtained through TDDFT. The code used for this is DP [48], which implements ab initio linear-response TDDFT in frequency-reciprocal space and on a plane wave basis set.
Given the momentum transfer $\mathbf{q}$, DP allows to calculate on an energy range (ω_i, ω_f) both dielectric spectra, such as EELS (electron energy-loss spectroscopy) and IXS (inelastic X-ray scattering spectroscopy) and optical spectra, such as optical absorption. DP allows also to choose the kernel f_{xc}, the kind of approximation used in the TDDFT calculation.

4.2.1 DP parameters

The steps to follow to obtain a spectrum are listed in §3.4.2. The most demanding calculation is that for χ^0 in Eq.(3.40): once one has $\chi^0_{\mathbf{GG'}}(\mathbf{q},\omega)$, the rest is easier and the spectra can be calculated.
So what is important is the convergence of χ^0, which DP calculates as

$$\chi^0_{\mathbf{GG'}}(\mathbf{q},\omega) = \frac{2}{\Omega}\sum_{n,n',\mathbf{k}}^{\text{nbands}} \frac{(f_{n',\mathbf{k+q}} - f_{n,\mathbf{k}})\langle\phi_{n,\mathbf{k}}|e^{-i(\mathbf{q+G})\cdot\mathbf{r}}|\phi_{n',\mathbf{k+q}}\rangle\langle\phi_{n',\mathbf{k+q}}|e^{i(\mathbf{q+G'})\cdot\mathbf{r'}}|\phi_{n,\mathbf{k}}\rangle}{\omega - (\epsilon_{n,\mathbf{k}} - \epsilon_{n',\mathbf{k}}) + i\eta} \quad (4.4)$$

where ϕ are the Kohn-Sham wavefunctions:

$$\phi_{n,\mathbf{k}}(\mathbf{r}) = \frac{1}{\sqrt{\Omega}}\sum_{\mathbf{G}}^{\text{npwwfn}} e^{i(\mathbf{G+k})\cdot\mathbf{r}} u_{n\mathbf{k}}(\mathbf{G})$$

npwmat, npwwfn, nbands

Three important DP parameters contribute mostly to the convergence of results:

- in the exact Eq.(3.40) the sum is over all possible bands, which is not computationally possible: the number of bands actually taken by DP is nbands. The energy range of relevant transition must be covered for the spectra to be reliable;
- the number of plane waves taken to represent KS wavefunctions is also finite and given by the parameter npwwfn;
- the dimension of the matrix $\chi^0_{\mathbf{GG'}}$ needs to be specified: the number of $\mathbf{G}$ components is given by the parameter npwmat. Choosing npwmat$\neq 1$ corresponds to taking into account local field effects.

Choice of the k point grid

In the ground state calculation the sums over $\mathbf{k}$ include all the $\mathbf{k}$ points: symmetry operations are exploited to obtain as much terms as possible. On the other hand, the sum over $\mathbf{k}$ points in Eq.(4.4) is a sum over non equivalent transitions. This implies that in order to do faster calculations the $\mathbf{k}$ points considered need to be non equivalent. High simmetry points are to be excluded from the grid, which can be different from the one used in the calculation of the density from which the KS structure is obtained.

Broadening and $\Delta\omega$

In this brief overview about DP, two more parameters are worth a discussion.
To understand the necessity of the parameter η, let us consider the form of the independent particle polarizability χ^0, for a single resonant transition:

$$\chi^0 \propto \frac{1}{\omega - \omega_0 - i\eta}$$

We do not consider the $\tilde{\rho}$'s because they do not depend on frequency, and we are now interested in the frequency behaviour. If we take the real and imaginary parts of this expression, we get

$$\mathrm{Re}\{\chi^0\} = \frac{\omega - \omega_0}{(\omega - \omega_0)^2 + \eta^2}$$
$$\mathrm{Im}\{\chi^0\} = -\frac{\eta}{(\omega - \omega_0)^2 + \eta^2}$$

As χ^0 is a response function, the two are related by Kramers Kronig relations, and will have a behaviour like that in Fig. 4.10.

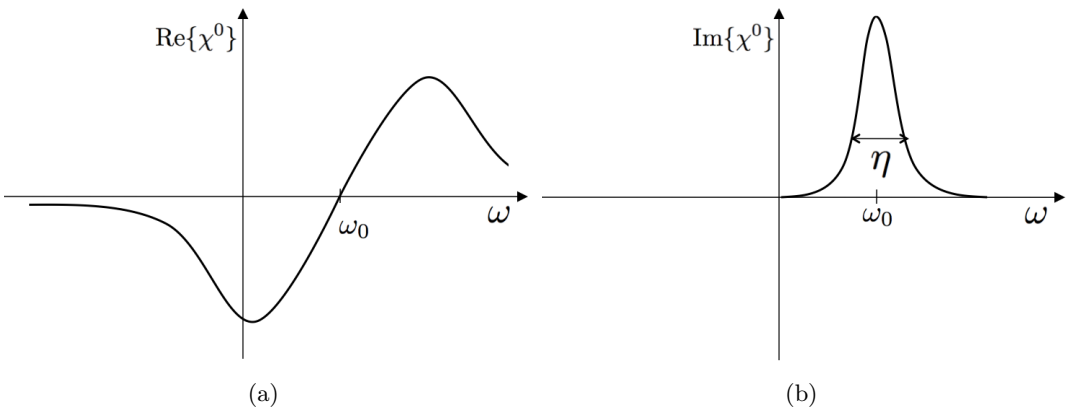

Figure 4.10: Real and imaginary part of χ^0 for a single transition

In particular we know that the imaginary part of χ^0 is the simplest possible approximation of an absorption spectrum. If we look at its analytic form in Fig. 4.10b, we see that it is a Lorentzian curve with a peak in ω_0 whose width is determined by η.
The spectra are not calculated continuosly, but using a sampling $\Delta\omega$. If η is too small with respect to the $\Delta\omega$, the peak could be missed in the sampling. On the other hand, η cannot be too large, because the representation (3.27) of χ^0 is valid in the limit $\eta \to 0$.
Thus, in principle, the ideal situation would be the one in which both $\Delta\omega$ and η are small, but this is obviously time-consuming and one has to find a compromise.

TDDFT in reciprocal space

The TDDFT scheme used in this work and included in DP works in frequency domain and in the reciprocal space, which is the most convenient to deal with solids, and is based on the linear response framework. This is not the only possible choice: there are codes which work with real-space TDDFT, such as Octopus [49].
One of the advantages of the DP scheme is that it allows to decouple the ground state calculation from that one of the response, because it is not necessary that $f_{xc} = \dfrac{\partial V_{xc}}{\partial \rho}$.
Without this costraint, it is possible to choose different kernels for the ground state DFT calculation and the TDDFT calculation.

4.2.2 Application to graphite

Studying the convergence of DP results implies checking the spectra for different values of the above cited parameters. An example is in Fig. 4.11.

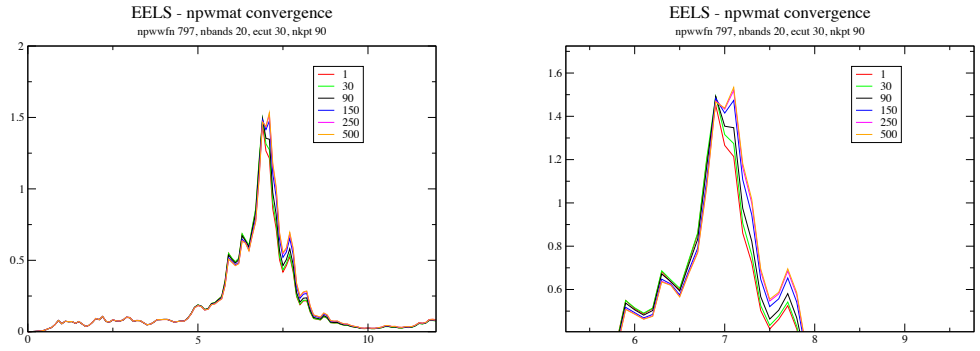

(a) Range 0-12 eV

(b) Zoom over the 7 eV peak

Figure 4.11: Different spectra for RPA EELS, $\mathbf{q}_{red} = (0.00005, 0, 0)$

We follow the scheme of the approximations of the previous chapter (§3.4.1) and calculate the macroscopic dielectric function for $\mathbf{q} \to 0$ and $\mathbf{q} \neq 0$. Our converged values for these calculations are npwmat= 239, npwwfn= 797 and nbands= 60.
We keep the same 90-**k** point grid and 30 Ha cut-off as for the ground state calculation.

ε_1 and ε_2

If we work with $f_{xc} = 0$ and do not consider local field effects, we get the Independent Particle approximation; by considering also LFE, we get RPA; a calculation within the ALDA has been also performed. The results of the calculations are in Fig. 4.12a and b.

We see that LFE are more important for larger values of **q**, as found in literature [4]. This is because a larger **q** corresponds to a smaller wavelength, which is more able to see details of the atomic structure.
We expect LFE to be even more important in the case of a **q** perpendicular to the plane, because it is in z direction that graphite is more inhomogeneous: an example is in Fig. 4.12c.

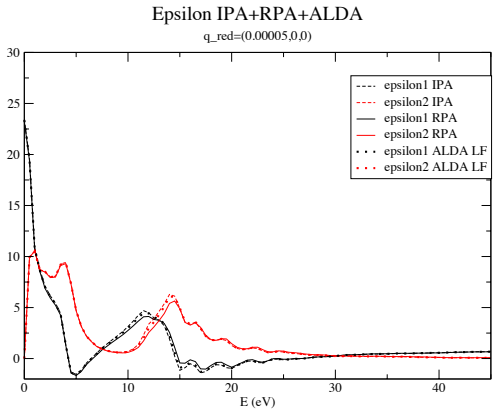

(a) ε_{M1} and ε_{M2} for $\mathbf{q}_{red} = (0.00005, 0, 0)$

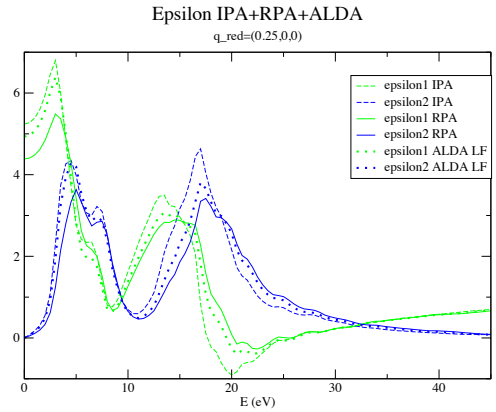

(b) ε_{M1} and ε_{M2} for $\mathbf{q}_{red} = (0.25, 0, 0)$

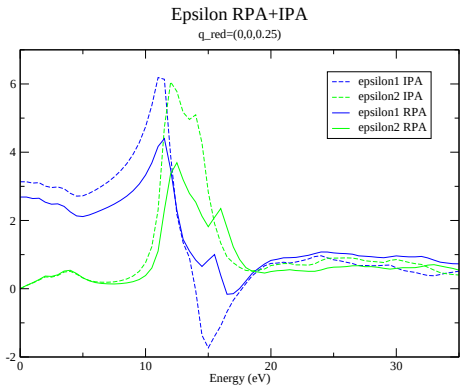

(c) ε_{M1} and ε_{M2} for $\mathbf{q}_{red} = (0, 0, 0.25)$

Figure 4.12: ε_1 and ε_2 in the IPA, RPA and ALDA approximation. a) and b) are for an in-plane $\mathbf{q}$, c) for a $\mathbf{q}$ in z direction.

EELS spectra

From the calculated dielectric functions ε_{M1} and ε_{M2} we can get the Energy Loss spectra as

$$\text{EELS} \propto \text{Im}\left\{\frac{1}{\varepsilon_M}\right\}$$

We consider the same two momentum transfers as before and get for an in-plane $\mathbf{q}$ the spectra in Fig. 4.13.
The two peaks are clearly visible already in the IPA, as well as the dispersion for different values of $\mathbf{q}$. We see that the ALDA kernel does not add significative details to the result, so we decide to keep the RPA approximation, which already proved successful for the case of graphite [4, 5].

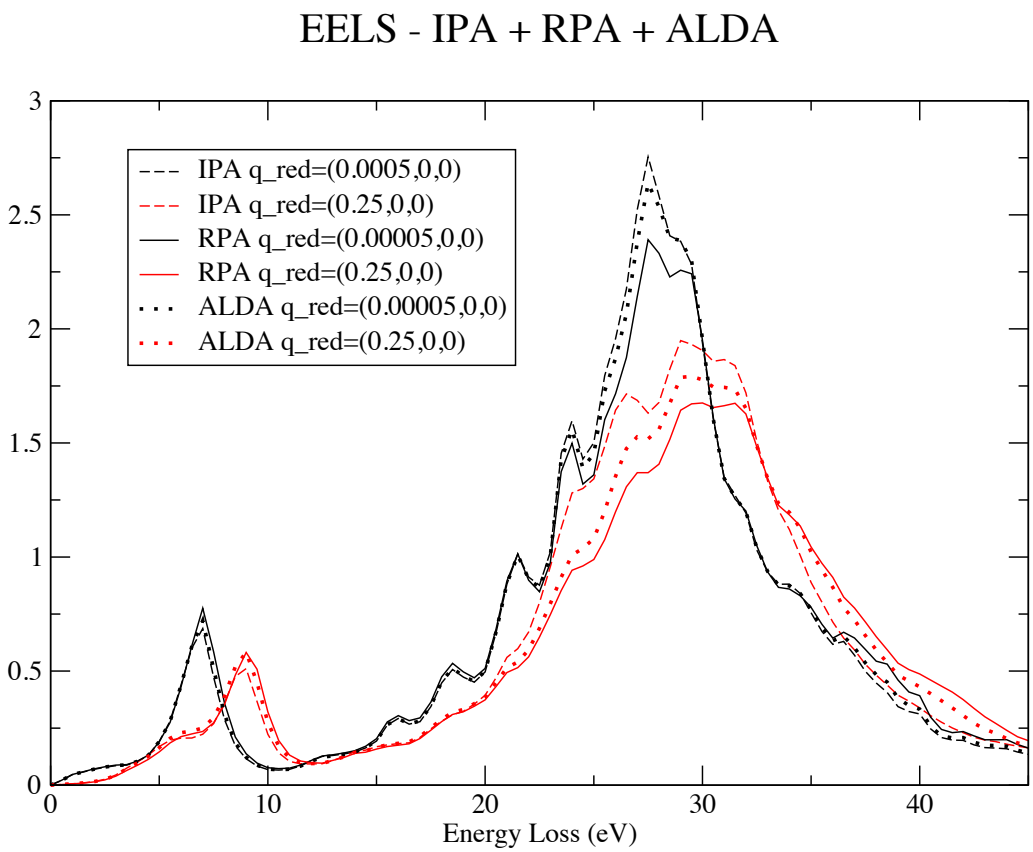

Figure 4.13: EELS spectra of graphite in the three approximations

The first four chapters have given an overview on the theory and the methodology necessary to deal with the problem of electronic excitations, and to obtain spectra. Now we want to apply all this in case of graphite, in particular to the study of the charge induced by an external perturbation.

5
Plasmons in Graphite

5.1 Plasmons

The behaviour of the electrons in a solid presents similarities with the one of a classical plasma. To develop these similarities we start by considering the theory for the interacting electron gas [50–52].

5.1.1 The electron gas as a quantum plasma

Classical plasmas are highly ionized collections of electrons and positive charges at high temperatures and low densities; physical examples are hot gaseous discharges and the ionosphere. The model which is typically used for the study of the electronic behaviour in a plasma is the replacement of the positive ions by a uniform background of positive charge, sometimes called *jellium*. The free-electron gas model for a metal (see for example [53]) differs from that used for a classical plasma only in that we deal with a system in which the electron density is very high and the temperature quite low, so that quantum, rather than classical, statistics for the electrons must be used. It is quite natural to regard the free-electron gas at high densities and low temperatures as a quantum plasma.
Quantum plasmas, like classical ones, display considerable organized, or collective, behaviour of the kind expected from the long range of the Coulomb interaction beteween electrons. Such collective behaviour manifests itself in two ways: *screening* and *collective oscillation*.

Let us consider first what we mean with screening: suppose there exists an imbalance in the charge distribution at some point in the plasma, say an excess of positive charge. The electrons will then tend to concentrate in that region, since they are quite mobile and respond readily to the attractive potential represented by the positive charge excess. In doing so, the electrons will act to screen the influence of the charge imbalance and to restore charge neutrality in the plasma.
On the other hand, the existence of organized oscillations in plasma may be understood in the following way: when the electrons move to screen a charge disturbance in the plasma, they will, in general, pass the equilibrium position, as in the classical harmonic oscillator. They are consequentely pulled back toward that region, pass the equilibrium again, etc, in such a way that an oscillation is set up about the state of charge neutrality. This charge density wave is called *plasmon*, and its nature can be understood in a very simple way.

A *naive* view

A first way to have an idea of this oscillatory behaviour is considering a simple model [7, 53] to obtain the characteristic frequency of oscillation of an electron system.
Consider a system of electrons in a region $L_x \cdot L_y \cdot L_z$, whose concentration is n. The net charge density at equilibrium is zero because of a uniform background density of positive ions.

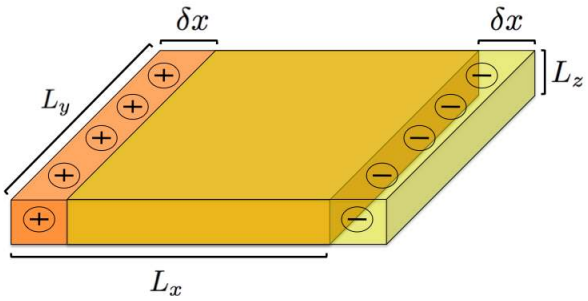

Figure 5.1

At a certain initial time t_0, a region of the electron charge is uniformly translated a distance δx without perturbing the rest of the system, as in Fig. 5.1. This creates two regions of thickness δx with a net charge density, one positive and the other negative, which will be attracted by each other: in absence of damping this will give rise to an harmonic oscillation of the system at a frequency that in this case can be easily obtained.
We write the polarization (dipole moment per unit volume) as[1]

$$\mathbf{P} = \frac{\text{net charge} \cdot L_x}{V} = -\frac{ne\delta x L_y L_z \cdot L_x}{L_x L_y L_z} = -ne\delta x$$

that gives rise to the electric field

$$\mathbf{E} = -4\pi\mathbf{P} = 4\pi ne\delta x$$

The force on an electron in the polarized region is thus

$$m\ddot{x} = -e\mathbf{E} = -4\pi ne^2\delta x$$

We recognize in this last expression the equation for a simple oscillator with characteristic frequency

$$\boxed{\omega_P^2 = \frac{4\pi ne^2}{m}} \tag{5.1}$$

which is usually called *plasma frequency*.

Charge oscillations

This oscillatory behaviour can be seen more sophisticated way in terms of the equation of motion of the density fluctuations in the electron gas [50].
The particle density at the point $\mathbf{r}$ is given by

$$\rho(\mathbf{r}) = \sum_i \delta(\mathbf{r} - \mathbf{r}_i) = \sum_{\mathbf{q}} \rho_{\mathbf{q}} e^{i\mathbf{q}\cdot\mathbf{r}}$$

[1] In this simple model we abandon the atomic units

where $\rho_{\mathbf{q}}$ is the fluctuation about the average electron density $\rho_0 = N$ (we take the volume to be unity). These density fluctuations are given in Fourier space by

$$\rho_{\mathbf{q}} = \sum_i e^{-i\mathbf{q}\cdot\mathbf{r}} \tag{5.2}$$

The equation of motion of the charge oscillations of the electron gas in a uniform positive background can be shown to be that of an harmonic oscillator with the same ω_P frequency found in Eq.(5.1):

$$\ddot{\rho_{\mathbf{q}}} + \omega_P^2 \rho_{\mathbf{q}} \simeq 0$$

under particular conditions that allow one to neglect the driving force terms on the right (see [50] for a detailed treatment). In particular, it is valid in the limit $\mathbf{q} \to 0$, when the wavelength of the oscillation is larger.
What we can expect intuitively is that the condition for a collective oscillation is the exciting wavelenght to be large compared to the average electron spacing. In this case there is a clear distinction between the plasmon excitations and the individual electron excitations; on the other hand, for short wavelenghts we expect the plasmon mode to disappear only individual electron excitation to survive.
This is what is actually quantitatively shown in [50]: In general the quantum plasma behaves collectively for wave vectors smaller than a critical vector $\mathbf{q} \ll \mathbf{q}_c$ and exhibits oscillations at a frequency near ω_P. For short wavelength phenomena, $\mathbf{q} \gg \mathbf{q}_c$, the plasma behaves like a system of individual free particles.

For an electron gas at a typical metallic density, $n = 10^{23} \frac{\mathrm{e}}{\mathrm{cm}^3}$ and the energy in a plasmon is $\hbar\omega_P \sim 12\mathrm{eV}$.
We see then that no thermal excitation of plasmons is possible at normal temperatures. Anyway, as we will see, an excitation is possible if carried out by single electrons.
The plasmon energy $\hbar\omega_P$ is much more large compared to the single particle energy because a plasma oscillation at long wavelengths involves the correlated motion of a very large number of electrons. No single electron is greatly perturbed, but because a large number of electrons move together, the resultant energy is quite substantial.
Plasma oscillations resemble sound waves, in the sense that they both involve oscillation of density, but there is a substantial difference between the two. Ordinary sound waves exist in consequence of collisions between particles, which act to bring local thermodynamic equilibrium. If one tries to change the density of particles at a given point, the collision will act as a restoring force towards equilibrium: the condition for the existence of a sound wave is that there be many collisions between the particles during the period of an oscillation.
For the plasma oscillations, it is the averaged force field of many other particles which acts as a restoring force: collisions, therefore, act to disrupt the influence of the average field, and tend to damp the collective mode.
This picture is someway qualitative: the phenomenon can be furthermore studied with the collective description of the electron gas developed in [51, 52]. In this treatment Bohm and Pines introduce a set of collective variables to describe plasmons, and carry out a series of transformations to a representation in which the plasmons are independent elementary excitations of the interacting electron system. With this more precise method, the qualitative assertions stated above are confirmed.

5.1.2 Dielectric response of an electron system

We now want to briefly present a formulation capable of describing the screening of a longitudinal field which varies in both space and time (longitudinal because the motion of particles gives rise to density fluctuations in the system). What we are interested in is the dielectric response of the electron gas to such a field, which can be expressed in terms of a longitudinal wave vector and frequency dependent $\varepsilon(\mathbf{q},\omega)$. It can be shown [50] that in the case of the electron gas this takes the form

$$\frac{1}{\varepsilon(\mathbf{q},\omega)} - 1 = \frac{4\pi}{q^2}\sum_n |\langle n|\rho^\dagger_{\mathbf{q}}|0\rangle|^2 \left[\frac{1}{\omega-\omega_{n0}+i\delta} - \frac{1}{\omega+\omega_{n0}+i\delta}\right] \tag{5.3}$$

where $\rho^\dagger_{\mathbf{q}}$ refers to the density fluctuation as above and ω_{n0} is a "natural" excitation frequency of the electron gas[2] $\varepsilon(\mathbf{q},\omega)^{-1}$ as it appears in Eq.(5.3) is a complex quantity. Its real part describes the polarization processes which are in phase with the external field; the imaginary part represents the out-of-phase part, and is related to the transfer of energy from the test charge to the system.

Energy loss of a fast electron Let us consider now the way in which a fast electron of momentum $\mathbf{q_0}$, energy ω_0 transfers energy and momentum to the electron gas.

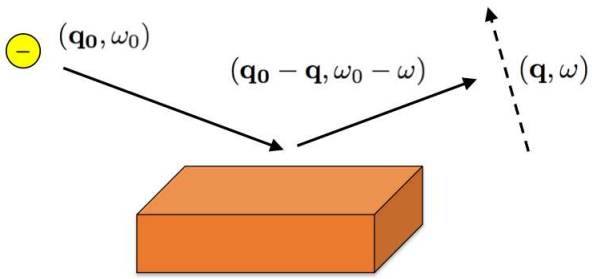

Figure 5.2

The Fermi golden rule may be applied to obtain the probability per unit time $W(\mathbf{q},\omega)$ that the particle transfer momentum $\mathbf{q}$ and energy ω to the electron gas (supposed in its ground state) and this is found to be

$$W(\mathbf{q},\omega) = 2\pi\left(\frac{4\pi}{q^2}\right)^2 \sum_n |\langle n|\rho^\dagger_{\mathbf{q}}|0\rangle|^2 \delta(\omega-\omega_{n0}) \tag{5.4}$$

where we recognize the Coulombian interaction $\dfrac{4\pi}{q^2}$.

If we compare this last expression with the imaginary part of $\dfrac{1}{\varepsilon(\mathbf{q},\omega)}$[3] we can also write

$$W(\mathbf{q},\omega) = -\frac{8\pi}{q^2}\mathrm{Im}\frac{1}{\varepsilon(\mathbf{q},\omega)} \tag{5.5}$$

which clearly recalls the result obtained classically in §1.3.2.

[2] Eq.(5.3) actually corresponds to $\varepsilon = 1 + v\chi$.

[3] Which can be obtained by applying Eq.(3.39) to Eq.(5.3).

5.1.3 The dynamic structure factor

It may be seen from Eq.(5.4) that the term that determines the energy and momentum transfer in the scattering experiment is

$$S(\mathbf{q},\omega) = \sum_n |\langle n|\rho_{\mathbf{q}}^{\dagger}|0\rangle|^2 \delta(\omega - \omega_{n0})$$

which we shall call the dynamic structure factor, and contains the scattering properties of the system [54]. The dynamic structure factor gives a direct measure of the density fluctuation spectrum of the electron gas, and it is the central quantity of interest in an electron scattering experiment, since it represents the maximum information one can hope to gain by measuring the angular distribution of the inelastically scattered electrons.
The relationship between $S(\mathbf{q},\omega)$ and $\dfrac{1}{\varepsilon(\mathbf{q},\omega)}$ can be written explicitly as

$$\mathrm{Im}\frac{1}{\varepsilon(\mathbf{q},\omega)} = -\frac{4\pi^2}{q^2}[S(\mathbf{q},\omega) - S(\mathbf{q},-\omega)]$$

So the measure of S from an inelastical scattering experiment allows to know also ε.
As Van Hove [54] first emphasized, a knowledge of $S(\mathbf{q},\omega)$ allows one to obtain detailed information concerning the space-time correlations for a many-particle system. In fact, the dynamic structure factor is the Fourier transform in space and time of the time-dependent density-density correlation function

$$p(\mathbf{r},t) = \frac{1}{N}\langle\psi_0|\rho_H(\mathbf{r}+\mathbf{r}',t+t')\rho_H(\mathbf{r}',t')|\psi_0\rangle$$

where $\rho_H(\mathbf{r},t)$ is the particle density in the Heisemberg representation and ψ_0 is the exact ground state function. With the assumption of translational invariance of the system it can be shown[50] that

$$p(\mathbf{r},t) = \frac{1}{N}\langle\psi_0|\rho_H(\mathbf{r},t)\rho_H(0)|\psi_0\rangle = \frac{1}{N}\sum_{\mathbf{q}}\int_{-\infty}^{+\infty} S(\mathbf{q},\omega)e^{i(\mathbf{q}\cdot\mathbf{r}-\omega t)}$$

$S(\mathbf{q},\omega)$ is actually the fundamental quantity for the description of longitudinal properties of the electron gas, or, indeed, of any many-particle system. It gives directly the dielectric function ε, which is more easy to calculate theoretically for an electron system.

5.1.4 Plasmons in solids

The behaviour of ε and ε^{-1} in solids is determined by the elementary excitations that are present in the system of interest. For the range of frequencies usually studied in solids these excitations may be generically characterized as individual particle excitations involving interband and intraband[4] transitions, and collective excitations, in particular plasma oscillations, which have the same nature of collective excitations of an electron gas seen so far.
The valence electrons in a solid interact with each other and experience a position-dependent periodic potential due to the ion cores. In the limit of long wavelenghts, the study of collective

[4]In the band approximation, an intraband transition is one in which the initial and final state are both located in the same band, and are possible just in metals, since insulators are charactierized by bads which are either completely full or completely empty. Interband transitions are instead usually thought of as transitions between two bands for which the matrix element of the momentum taken with resoect to the initial and final states does not vanish. See for example [7, 13]

oscillations in solids follows quite easily from the electron gas model, remembering that plane wave matrix elements and excitation frequencies are replaced by Bloch function matrix elements and excitation frequencies appropriate to a single electron moving in the periodic potential $U(\mathbf{r})$.
Also in solids the influence of the Coulomb interaction between the electrons is manifested through screening and collective oscillations.
The first difference betveen plasmons in solids and in the electron gas is that as a consequence of interband transitions one may get a frequency different from ω_P in the limit $\mathbf{q} \to 0$. The existence of interband transitions at the plasmon energy will cause also a damping of plasmons in solids.
Finally, as there is always overlap of the plasmon energies and the individual electron excitation energies, the distinction between the collective plasmon modes and the individual particle modes cannot be as complete in the solid as in the free electron gas.

5.1.5 Experimental observations: EELS experiments

The principal experimental evidence for the existence of plasmons as a well-defined mode of the valence electrons in solids comes from EELS experiments we already mentioned in §1.3.2. As already said, the experiments consist generally in measuring the energy lost by keV-electrons as they emerge from a thin solid film. If one measures the angular distribution of the inelastically scattered electrons, as well as their energy, one actually obtains both the energy and momentum transfer to the electrons in the solid, that is to say, the dynamical form factor $S(\mathbf{q}, \omega)$, or what is equivalent, $\mathrm{Im}\left\{\dfrac{1}{\varepsilon_M(\mathbf{q}, \omega)}\right\}$.
In the next section we consider the information that can be obtained on graphite with this kind of technique.

5.2 Results in Graphite

In this section we want to briefly review some theoretical work that has already been done about graphite, contained in [4, 5, 55]. Experimentally, EELS measurements on graphite for a momenum transfer $\mathbf{q}$ parallel to the basal plane, two characteristic plasmon peaks are observed. They are related to collective excitations of the valence π electrons (π plasmon, $7 - 12$ eV) and of all valence electrons ($\pi + \sigma$ plasmon, $28 - 33$ eV).

5.2.1 Ab initio results in literature

Considering the articles cited above, we can learn a certain number of things about our system that will be useful in the following. In [4], ab-initio calculations on graphite were made in RPA and TDLDA approximations in order to give a theoretical interpretation of the dependence of the loss spectra upon the orientation of the momentum transfer.

Fig. 5.3 shows that TDLDA does not bring significative improvements to the final results, as both RPA and TDLDA are in excellent agreement with the experimental data. It shows also that local field effects (LFE) are more important when the transferred momentum has a z component, as seen also in §4.2.2: this is easily understood if one realizes that LFE are a measure of the inhomogeneity of the system, and it is in z direction that layered materials like graphite show less homogeneity. In fact, layered systems are among those for which LFE have

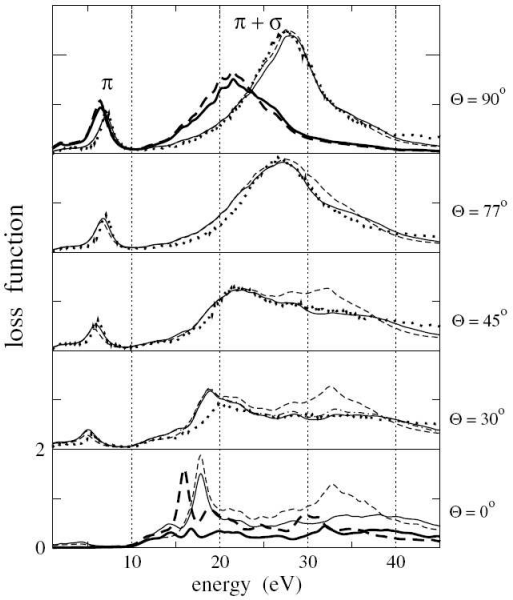

Figure 5.3: From [4]. Calculated and measured loss function for different orientation angles between the momentum transfer $\mathbf{q}$ (for $q = 0.25\text{Å}^{-1}$) and the c axis directions. Dashed lines are obtained without, continuous lines including LFE within the RPA. The dot-dashed curve in the $\Theta = 30$ spectrum (hardly distinguishable from the continuous one) is a TDLDA result (with LFE). A broadening of 0.5 eV was used. The thick lines denot the results with a double interlayer spacing. The experimental results [56] are indicated by the dotted lines.

more influence.
In [5], among other results, the plasmon dispersion is found and compared to experimental data: see Fig. 5.4.

In [55], RPA calculations and IXS measurements are used to reveal and explain a striking discontinuity in the dynamic structure factor $S(\mathbf{q}, \omega)$ of graphite at momentum transfers $\mathbf{q_r} + \mathbf{G_0}$ close to Bragg allowed reciprocal lattice vectors $\mathbf{G_0}$: infinitesimal changes in the momentum transfer induce strong changes in the resulting spectra. This kind of behaviour is deeply different from the predictions that could be made with the homogeneous electron gas model. Thus this anomaly represents an example of the important role played by local field effects in the electronic properties of crystals.

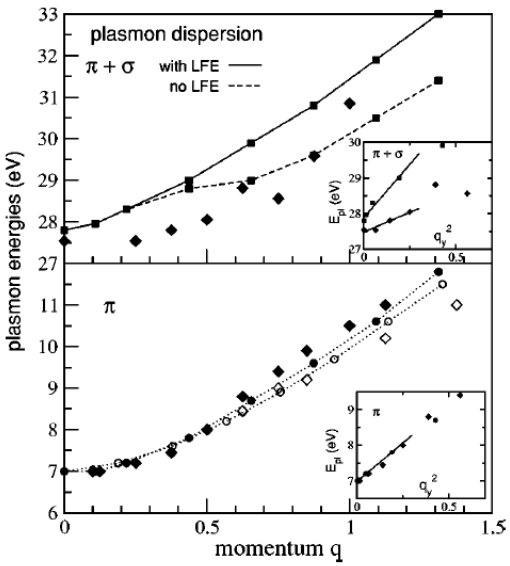

Figure 5.4: From [5]. Plasmon dispersion in graphite. Filled (open) symbols denote plasmon-peak positions for in-plane momentum $q_x(q_y)$. The results of calculations are denoted by squares and circles joined by lines to guide the eye, whereas the diamonds are the experimental data for the π and $\pi + \sigma$ [56] plasmons. q is given in units of Å^{-1}. Insets display plasmon-peak versus q_y^2 and the least-square-fit lines.

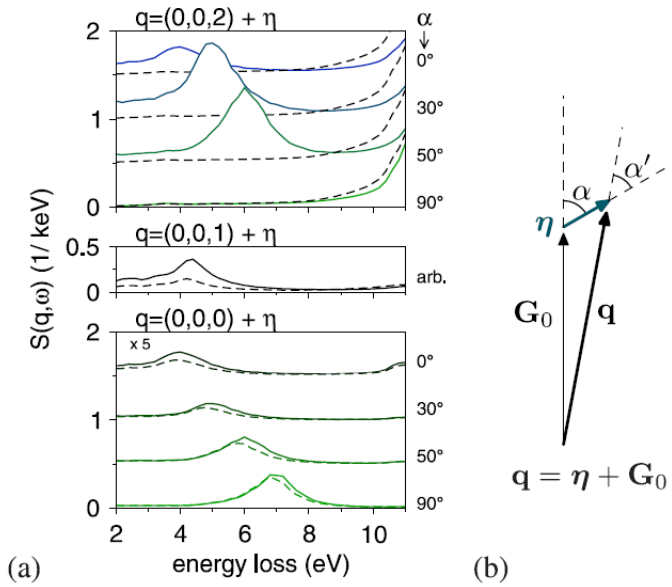

Figure 5.5: From [55] a) Dynamic structure factor $S(\eta + \mathbf{G_0}, \omega)$ for small deviations $|\eta| = 5{\cdot}\text{Å}^{-1}$ from reciprocal lattice vectors $\mathbf{G_0}$ calculated with (solid line) or without (dashed line) LFE. Bottom: for $\mathbf{G_0} = (0,0,0)$, $S(\eta, \omega)$ depends on the direction of η. Middle: for $\mathbf{G_0} = (0,0,1)$, arbitrary η lead to the same spectrum. Top: for$\mathbf{G_0} = (0,0,2)$, $S(\eta + \mathbf{G_0}, \omega)$ again changes with η, but only when LFE are included. b) Definition of the angles α and α'.

6
Microscopic charge fluctuations

Energy-loss techniques experiments (such as inelastic x-ray, electron, or neutron scattering) normally give results in frequency representation.
Anyway, if such measurements truly reflect dynamics, a temporal representation may also be illuminating. A 2004 paper by Abbamonte *et al.* [2] shows that this frequency response can be inverted in time and space, allowing real time imaging of electron dynamics in a medium. This allows the spatial and temporal extent of an excitation to be determined.

6.1 Imaging dynamics from experimental results

In the reference paper, the authors consider the results from a inelastic x-ray scattering experiment on a sample of liquid water.
In IXS, a photon with well defined momentum and energy $(\mathbf{k}_i, \omega_i)$ is impinged on a specimen that scatters it to a final $(\mathbf{k}_f, \omega_f)$. The resulting spectral density of scattered photons is proportional to the dynamic structure factor of the material

$$S(\mathbf{K}, \omega)$$

where $\mathbf{K} = \mathbf{k}_i - \mathbf{k}_f$ and $\omega = \omega_i - \omega_f$ are the transferred momentum and energy.
$S(\mathbf{K}, \omega)$ is related to the imaginary part of a response function by the fluctuation-dissipation theorem, as seen in §5.1.3. $\mathrm{Im}\{\chi(\mathbf{K}, \omega)\}$ can be thereby experimentally determined.

This what is done in the experiment described in [2]; the IXS data set at disposal provides the imaginary part of the response function $\chi(\mathbf{K}, \omega)$. It is important to note that the experimental technique which is usually adopted in IXS provides just the diagonal part of the more general $\chi(\mathbf{K}, \mathbf{K}', \omega)$: this will have great relevance in the following.
The real part can be retrieved by exploiting the causal properties of χ (i.e. using Kramers Kronig relations), if the imaginary part is known for a large number of frequencies[1].
With $\mathrm{Re}\{\chi(\mathbf{K}, \omega)\}$ and $\mathrm{Im}\{\chi(\mathbf{K}, \omega)\}$, the reconstruction of $\chi(\mathbf{r}, t)$ is in principle possible.
In the paper this procedure is used to image the disturbance generated by a point perturbation in liquid water:

$$V_{ext} = \delta_{\mathbf{r}\mathbf{r}0}\delta(t - t_0) \tag{6.1}$$

The resulting time frames are in Fig. 6.1.

[1] To obtain the real part, one should in principle know the imaginary part at all frequencies (see Eq.A.5 in Appendix A)

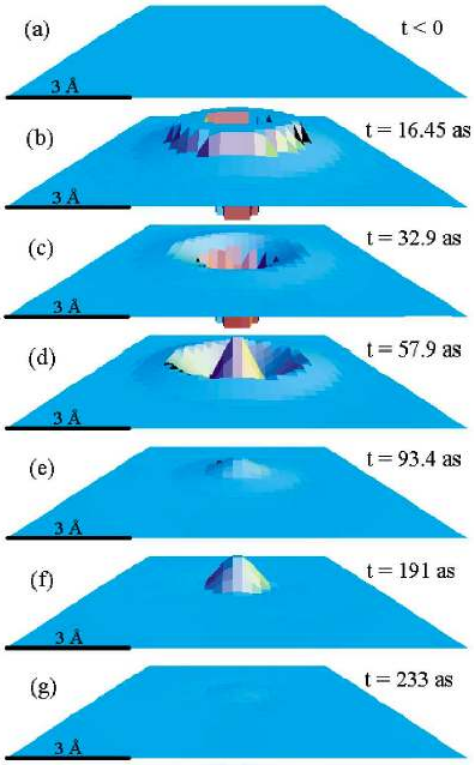

Figure 6.1: Time frames of $\chi(\mathbf{r}, t)$ in units of Å^{-6} [2]

As the medium is isotropic, the disturbance is spherically symmetric, and each image is a section of this sphere with $\chi(\mathbf{r}, t)$ plotted in units of Å^{-6} on the vertical axis.
At negative times $\chi(\mathbf{r}, t)$ vanishes and the system is "placid". At $t = 0$ the system is struck with a positive perturbation, generating a negative recoil at the origin surrounded by a positive buildup at $|x| = 1.3$ Å as current flows away from the source point. An anharmonic oscillation occurs, with a time scale of order of the plasma frequency

$$T = \frac{2\pi}{\omega_p} = 180\text{as}$$

We see then that $\chi(\mathbf{r}, t)$ provides then a means to visualize electron dynamics.

6.1.1 Diagonal and off-diagonal response

The frames in Fig. 6.1 represent an area of 10 Å, and the space resolution obtained from the experimental momentum range is $\mathrm{d}x = 1.27$Å. Nevertheless, individual atoms are not visible. This is because the polarizability is actually a function of two spatial variables $\chi(\mathbf{r}, \mathbf{r}', t)$ with a Fourier transform of the form $\chi(\mathbf{q}, \mathbf{q}', \omega)$. This is an expression of non-locality: the response function in a point of the system depends also on the other points of the system.
With only one momentum transfer in scattering, the experiment can only give the diagonal response $\chi(\mathbf{q}, \mathbf{q}, \omega)$. Translated in real space, this means considering an homogeneous medium: this can be seen from the definition of the Fourier Transform of the two point function

$$\chi(\mathbf{r}, \mathbf{r}') = \int \mathrm{d}\mathbf{q}\mathrm{d}\mathbf{q}'\, e^{i\mathbf{q}\cdot\mathbf{r}} \chi(\mathbf{q}, \mathbf{q}') e^{-i\mathbf{q}'\cdot\mathbf{r}'}$$

which if $\mathbf{q} = \mathbf{q}'$ becomes

$$\chi(\mathbf{r}, \mathbf{r}') = \int \mathrm{d}\mathbf{q}\mathrm{d}\mathbf{q}'\, \delta(\mathbf{q} - \mathbf{q}')\chi(\mathbf{q}, \mathbf{q}')e^{i(\mathbf{q}'\cdot\mathbf{r} - \mathbf{q}\cdot\mathbf{r}')} =$$
$$= \int \mathrm{d}\mathbf{q}\, \chi(\mathbf{q})e^{i\mathbf{q}\cdot(\mathbf{r}-\mathbf{r}')} = \chi(\mathbf{r} - \mathbf{r}')$$

where only the distance dependence $(\mathbf{r} - \mathbf{r}')$ is left.
What is obtained in the experimental paper are thus only spatial averages, the result of the mean of many events at different locations in the specimen.

The cited paper considers the case of inelastic x-ray scattering. With the techniques described in the previous chapters, we are able to simulate the results of energy loss experiments, such as IXS or EELS. There will be a major difference between our results and the ones used in the paper: we can calculate also off-diagonal elements of the matrix

$$\underline{\underline{\chi}}(\mathbf{q}, \omega) = \begin{bmatrix} \chi_{\mathbf{G_0}\mathbf{G_0}}(\mathbf{q}, \omega) & \chi_{\mathbf{G_0}\mathbf{G_1}}(\mathbf{q}, \omega) & \cdots & \chi_{\mathbf{G_0}\mathbf{G_N}}(\mathbf{q}, \omega) \\ \chi_{\mathbf{G_1}\mathbf{G_0}}(\mathbf{q}, \omega) & \chi_{\mathbf{G_1}\mathbf{G_1}}(\mathbf{q}, \omega) & \cdots & \chi_{\mathbf{G_1}\mathbf{G_N}}(\mathbf{q}, \omega) \\ \vdots & & & \\ \chi_{\mathbf{G_N}\mathbf{G_0}}(\mathbf{q}, \omega) & \chi_{\mathbf{G_N}\mathbf{G_1}}(\mathbf{q}, \omega) & \cdots & \chi_{\mathbf{G_N}\mathbf{G_N}}(\mathbf{q}, \omega) \end{bmatrix}$$

and so we expect to obtain a better resolution than the one in the reference article, because we will not be making hypothesis of the homogeneity of the system.
We choose to visualize the oscillations of charge in our system, so we are interested in the quantity ρ_{ind} appearing in Eq.(B.13).
In our case, the response function is the polarizability χ, that we can obtain from our TDDFT calculation with DP. The idea is to develop a program able of post-processing data given by DP to study electronic dynamics in graphite.

We want to use the tools at our disposal to investigate the importance of the off-diagonal elements in the response of our system, in order to point out which experimental measures would be needed to achieve a better spatial resolution in this kind of technique.

6.2 Plane wave as external perturbation

We want to apply the general formula Eq.(B.13) found in §B.3

$$\boxed{\rho_{ind}(\mathbf{r}, t) = \frac{1}{\Omega}\sum_{\mathbf{q_r}}\sum_{\mathbf{G}\mathbf{G}'}\int \mathrm{d}\omega\, \chi_{\mathbf{G}\mathbf{G}'}(\mathbf{q_r}, \omega)V_{ext}(\mathbf{q_r} + \mathbf{G}', \omega)e^{i(\mathbf{q_r}+\mathbf{G})\cdot\mathbf{r}}e^{-i\omega t}} \tag{6.2}$$

to find the induced charge density in real space and time. We will use this general formula for different V_{ext}.

First, consider a plane wave of given frequency ω_0 and wavelength $\dfrac{2\pi}{q_0}$:

$$\widehat{V}_{ext}(\mathbf{r}, t) = e^{i(\mathbf{q_0}\cdot\mathbf{r} - \omega_0 t)} \tag{6.3}$$

Note that now $\widehat{V}_{ext}$ is a complex quantity, introduced for mathematical reasons. In Fourier space this becomes:

$$\widehat{V}_{ext}(\mathbf{q}, \omega) = \delta_{\mathbf{q},\mathbf{q_0}}\delta(\omega - \omega_0)$$

Using the notation

$$\mathbf{q} = \mathbf{q_r} + \mathbf{G}$$
$$\mathbf{q_0} = \mathbf{q_{0r}} + \mathbf{G_0}$$

we obtain

$$\widehat{V}_{ext}(\mathbf{q}) = \delta_{\mathbf{q_r}+\mathbf{G},\mathbf{q_0}}\delta(\omega-\omega_0) = \delta_{\mathbf{q_r},\mathbf{q_{0r}}}\delta_{\mathbf{G},\mathbf{G_0}}\delta(\omega-\omega_0)$$

In Fourier space the induces charge reads (using Eq.(B.12))

$$\begin{aligned}\widehat{\rho}_{ind}(\mathbf{q_r}+\mathbf{G},\omega) &= \sum_{\mathbf{G'}}\chi_{\mathbf{GG'}}(\mathbf{q_r},\omega)\widehat{V}_{ext}(\mathbf{q_r}+\mathbf{G'},\omega)\\ &= \sum_{\mathbf{G'}}\chi_{\mathbf{GG'}}(\mathbf{q_r},\omega)\delta_{\mathbf{q_r},\mathbf{q_{0r}}}\delta_{\mathbf{G'},\mathbf{G_0}}\delta(\omega-\omega_0) =\\ &= \chi_{\mathbf{GG_0}}(\mathbf{q_r},\omega)\delta_{\mathbf{q_r},\mathbf{q_{0r}}}\delta(\omega-\omega_0) \qquad (6.4)\end{aligned}$$

The induced charge density in real space can be obtained either Fourier transforming Eq.(6.4) or using the expression (6.2). As we used a complex form of potential, ρ_{ind} results complex. In this particular case, the integrals over the first Brillouin zone and over ω are killed by the two δ functions.

$$\begin{aligned}\widehat{\rho}_{ind}(\mathbf{r},t) &= \frac{1}{\Omega}\sum_{\mathbf{q_r}}\sum_{\mathbf{G}}\int \mathrm{d}\omega\hat{\rho}_{ind}(\mathbf{q_r}+\mathbf{G},\omega)e^{i(\mathbf{q_r}+\mathbf{G})\cdot\mathbf{r}}e^{-i\omega t}\\ &= \frac{1}{\Omega}\sum_{\mathbf{G}}\chi_{\mathbf{GG_0}}(\mathbf{q_{0r}},\omega_0)e^{i(\mathbf{q_{0r}}+\mathbf{G})\cdot\mathbf{r}}e^{-i\omega_0 t} \qquad (6.5)\end{aligned}$$

Eq.(6.5) yields then the charge density induced by a plane wave in a crystal. As one could expect, the plane wave perturbation selects only the ω_0 frequency in the response (this corresponds mathematically to the δ). One sum on $\mathbf{G}$ vectors remains: this accounts for the off-diagonal elements which improve the spatial resolution of our results.
As our potential was a plane wave written in the complex exponential notation, the resulting quantity for the induced charge is still complex. To achieve a physical meaning, we have to take either the real or the imaginary part of this quantity $\hat{\rho}_{ind}$, that is to say, the response to the real or imaginary part of the potential: we choose the real one, which corresponds to the response to a cosinus potential.

If we take a "snapshot" of our perturbation at $t = 0$, we are left only with the spatial part of Eq. (6.4)

$$\rho_{ind}(\mathbf{q_r}+\mathbf{G}) = \chi_{\mathbf{GG_0}}(\mathbf{q_r})\delta_{\mathbf{q_r},\mathbf{q_{0r}}}(\mathbf{q_r}) \qquad (6.6)$$

When the external perturbation is a plane wave, in the reciprocal space it is a spike, and the response is a series of spikes a $\mathbf{G}$ away one from the other.
This discreteness derives from the fact that $\chi_{\mathbf{GG_0}}$ is a matrix because our system is a crystal: this can be physically interpreted as Bragg scattering of internal fields.

Now that the analytical solution is clear, it is necessary to implement it in a code.
An important part of the work has been dedicated to the preparation of a code that could allow to visualize the real space and time dynamics related to the chosen perturbation; the program has been written with the Python [57] coding language. It works with the $\chi_{\mathbf{GG'}}(\mathbf{q},\omega)$ given in input and produces as output the induced charge $\widehat{\rho}(\mathbf{r},t)$ in the simulation cell.

6.2.1 Results

We start with visualizing the induced charge ρ_{ind} in a plane. We can fix both the energy and the momentum of the external plane wave: as previously said, we would like to investigate the nature of collective oscillations, so we will focus on energies corresponding to plasmon peaks in the EELS spectra of graphite (Fig. 4.13).

Snapshot in energy range 0-45 eV

We begin by looking at $t = 0$, using thus Eq.(6.6). We look at the induced charge near one plane for different energies ω_0 of the plane wave, for which we choose an in-plane transferred momentum $\mathbf{q}_x$. The x actually refers to reciprocal space and means that $\mathbf{q}$ is in the direction of $\mathbf{b}_1$ (see §4.1.4).
The kind of image we obtain is reproduced in Fig. 6.2 for an in-plane $\mathbf{q} \to 0$ and $\omega_0 = 7$eV.

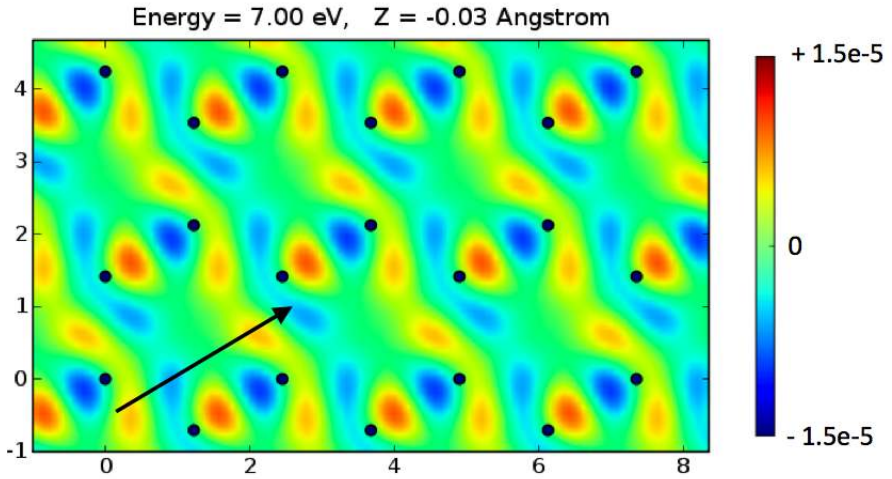

Figure 6.2: Induced charge density in a plane of graphite by a plane wave at $t = 0$. $\omega_0 = 7$ eV, $\mathbf{q} = 0.00005 \cdot \mathbf{b}_1$. The black arrow shows the direction of $\mathbf{q}$, the unit of charge density is $\frac{\mathrm{e}}{\mathrm{bohr}^3}$

In Fig. 6.2, the red regions are the ones where there is more charge than equilibrium, and the blue ones where there is less. The dark spots are the atoms of the plane: what we see is the polarization induced around them by V_{ext} .
We are considering a plane wave as external perturbation, which is different from the delta perturbation used in [2] to obtain Fig. 6.1. Anyway, it is possible to compare the spatial resolution of the results in Fig. 6.1 and Fig. 6.2. With our technique, details in the atomic scale are visible; this is an improvement with respect to Fig. 6.1, where what was seen was only a spatial average.
What is obtained by considering the energy range between 0 and 45 eV is summarized in Fig. 6.3. The colorscale is the same shown in Fig. 6.2.

With a look at these images one can notice that the greater values of induced charge (resonances) occur for energies near to plasmon peaks. So we can reasonably say that there is a connection between what we are looking at and plasmons.

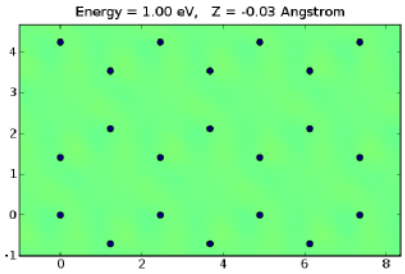
Energy = 1.00 eV, Z = -0.03 Angstrom

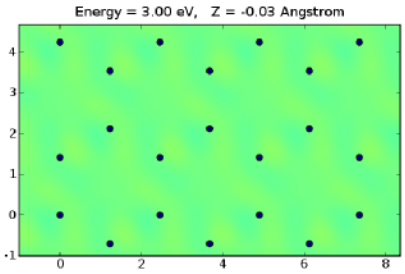
Energy = 3.00 eV, Z = -0.03 Angstrom

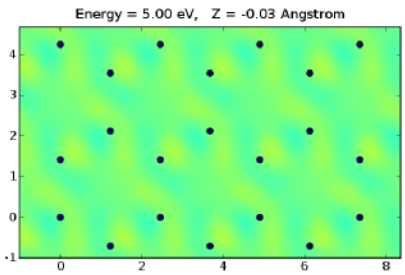
Energy = 5.00 eV, Z = -0.03 Angstrom

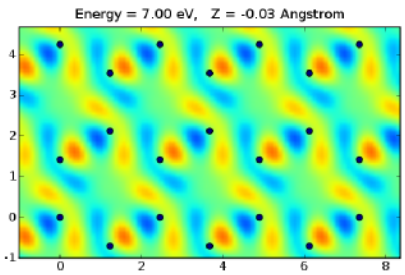
Energy = 7.00 eV, Z = -0.03 Angstrom

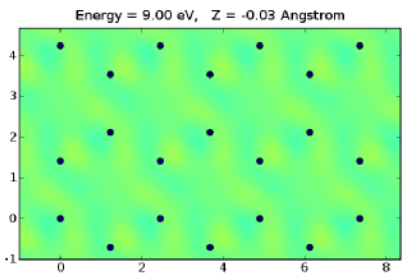
Energy = 9.00 eV, Z = -0.03 Angstrom

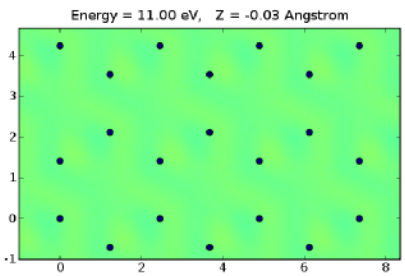
Energy = 11.00 eV, Z = -0.03 Angstrom

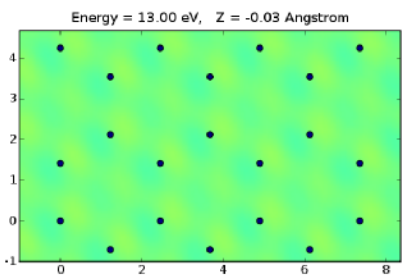
Energy = 13.00 eV, Z = -0.03 Angstrom

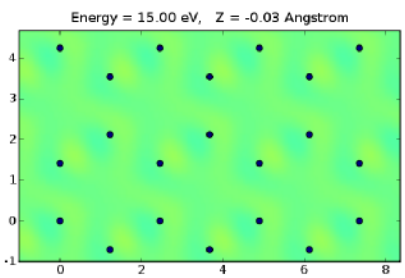
Energy = 15.00 eV, Z = -0.03 Angstrom

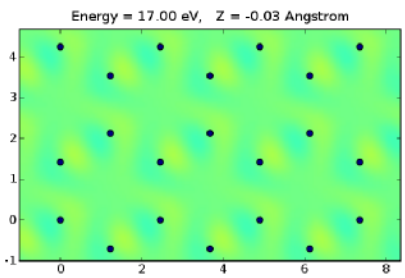
Energy = 17.00 eV, Z = -0.03 Angstrom

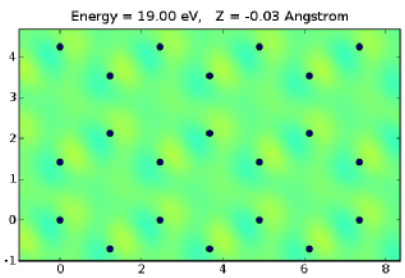
Energy = 19.00 eV, Z = -0.03 Angstrom

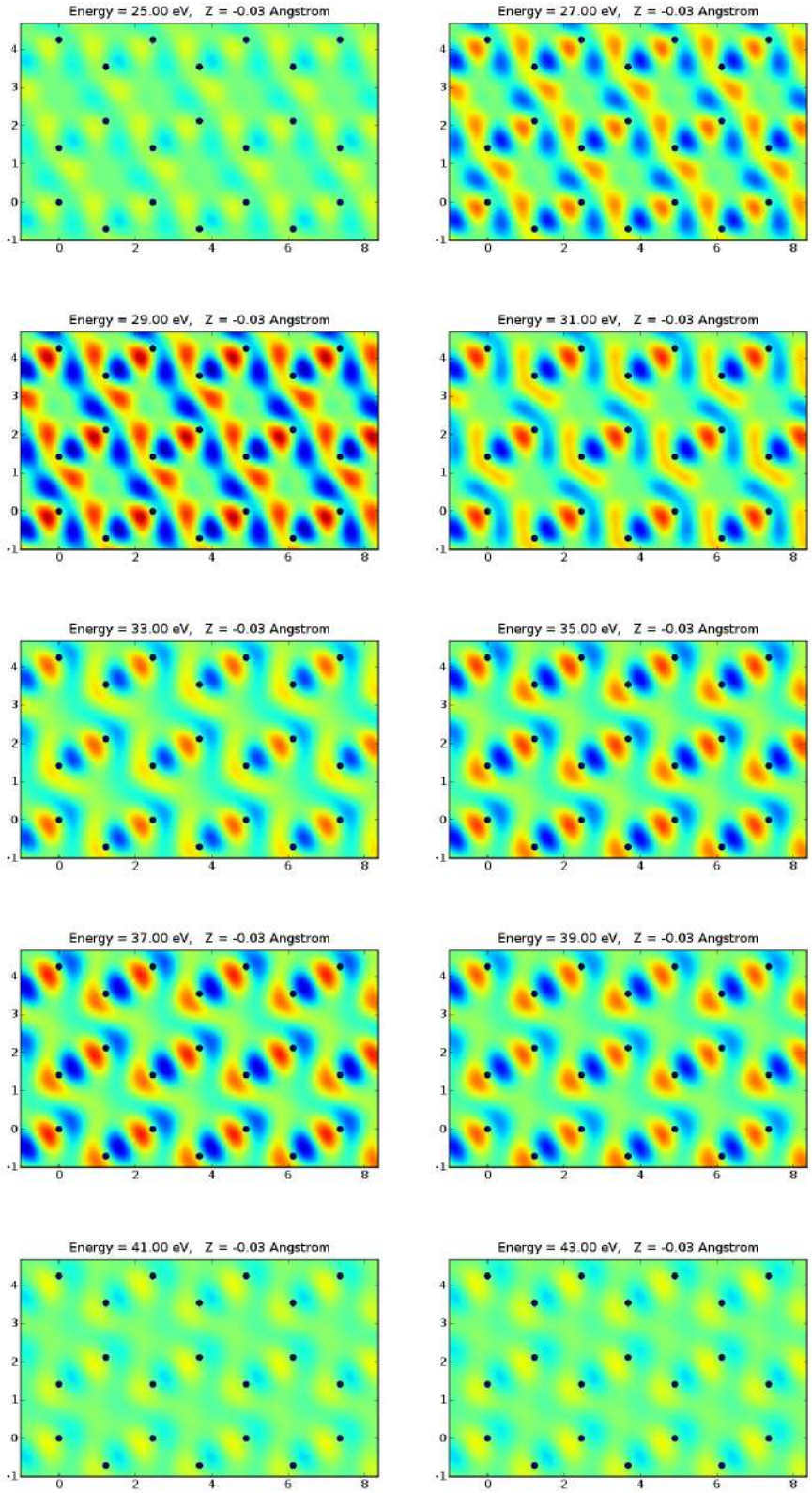

Figure 6.3: ρ_{ind} at different energies, $t = 0$

Real and Imaginary part

In order to make this connection less qualitative, we need a quantity which could be representative of the amount of induced charge in the simulation cell. A resonable guess could be the maximum amplitude of the oscillation induced by the external potential; however, we cannot simply take the maximum of the induced charge in our simulation cell, because we cannot be sure that the maximum of the long-wavelength perturbation actually occurs in the cell. In order to overcome this difficulty, we can exploit the complex nature of the calculated induced charge. We started with a complex potential $\widehat{V}_{ext}$ to simplify calculations, and this brought to a complex induced charge $\widehat{\rho}_{ind}$. We said previously that the physical meaning should be given just to the real or imaginary part of both $\widehat{V}_{ext}$ and $\widehat{\rho}_{ind}$; more generally speaking, the need is to choose a phase φ of $\widehat{V}_{ext}$ and consider the same phase of $\widehat{\rho}_{ind}$ to obtain the physically relevant V_{ext} and ρ_{ind}, as shown in Fig. 6.4.

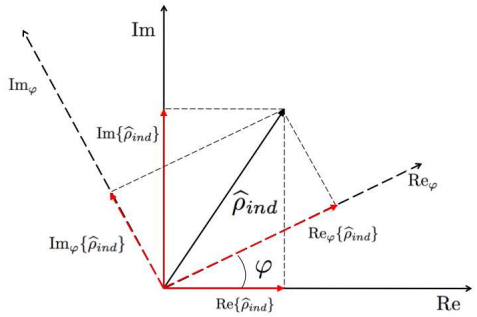

Figure 6.4: Choice of the phase for ρ_{ind}

This can be mathematically expressed as

$$\begin{aligned}\rho_{ind} = \mathrm{Re}_\varphi\{\widehat{\rho}_{ind}\} = \mathrm{Re}\{\widehat{\rho}_{ind}\}\cos\varphi + \mathrm{Im}\{\widehat{\rho}_{ind}\}\sin\varphi = \\ = \mathrm{Re}\{\widehat{\rho}_{ind}e^{-i\varphi}\}\end{aligned}$$

where with Re_φ we mean the real part with respect to the axes rotated by φ.
The real and imaginary part are particular cases of this more general definition:

$$\begin{aligned}\varphi = 0 \qquad & \rho_{ind} = \mathrm{Re}_0\{\widehat{\rho}_{ind}\} = \mathrm{Re}\{\widehat{\rho}_{ind}\} \\ \varphi = \frac{\pi}{2} \qquad & \rho_{ind} = \mathrm{Re}_{\frac{\pi}{2}}\{\widehat{\rho}_{ind}\} = \mathrm{Re}\{-i\widehat{\rho}_{ind}\} = \mathrm{Im}\{\widehat{\rho}_{ind}\}\end{aligned}$$

The arbitrariness of the choice is then contained in the phase $e^{-i\varphi}$.
Consider again the form taken by the induced charge in real space:

$$\widehat{\rho}_{ind}(\mathbf{r},t) = \frac{1}{\Omega}\sum_{\mathbf{G}}\chi_{\mathbf{GG_0}}(\mathbf{q_{0r}},\omega_0)e^{i(\mathbf{q_{0r}}+\mathbf{G})\cdot\mathbf{r}}e^{-i\omega_0 t}$$

It can be seen that both the spatial and temporal dependence are given by a complex exponential. Thus, the choice of φ is equivalent to a translation in space or time: this implies that the complex nature of our variables allows us to explore how the amplitude of ρ_{ind} varies in space and time. In particular, if we want to calculate the maximum amplitude of the induced charge for a given

perturbation, we can use the relations

$$\max_{\mathbf{r},\mathbf{R}} \rho_{ind}(\mathbf{r}+\mathbf{R},t) = \max_{\mathbf{r}} |\widehat{\rho}_{ind}(\mathbf{r},t)|$$
$$\max_{\mathbf{r},t} \rho_{ind}(\mathbf{r}+\mathbf{R},t) = \max_{\mathbf{r}} |\widehat{\rho}_{ind}(\mathbf{r},t_0)| \qquad \forall t_0 \tag{6.7}$$

where $\mathbf{R}$ is a vector of the Bravais lattice and $\mathbf{r}$ is a coordinate in the unit cell, so that the dishomogeneity of the material is taken in account. The meaning of Eqs.(6.7) is that finding the maximum induced charge in space (or time) corresponds to finding the maximum response among those to at all possible phases of $\widehat{V}_{ext}$, that is, the maximum of the absolute value, which takes the phase into account.

The absolute value $\max|\hat{\rho}_{ind}|_{\mathbf{r}}$ is then a physically relevant quantity, and we can plot it for the range of energies previously considered, for $\mathbf{q} \to 0$ and $\mathbf{q_0} \neq 0$ (Fig. 6.5).

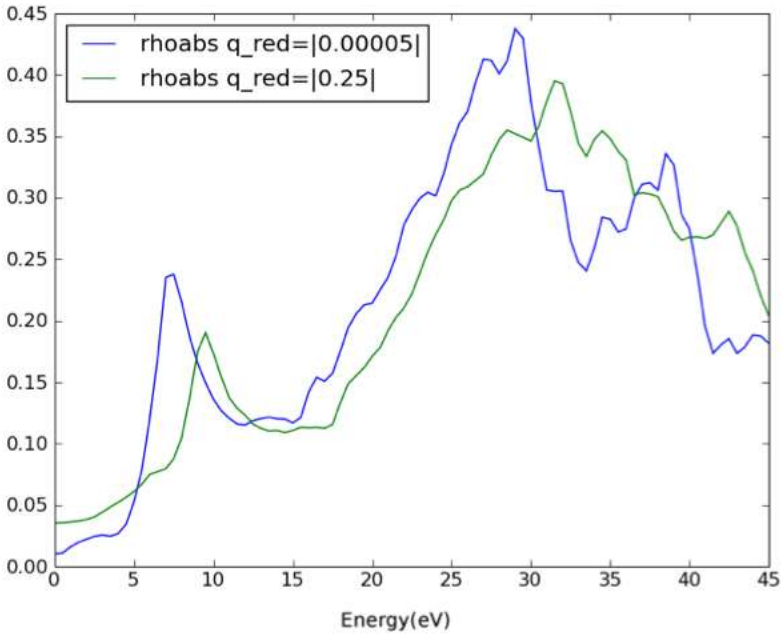

Figure 6.5: Maximum of induced charge density in the simulation cell for different $\mathbf{q}_0$. The charges are normalized by the factor $\dfrac{1}{|\mathbf{q_0}+\mathbf{G_0}|}$

The peaks have the same positions as in the spectra seen in §4.2.2, and this confirms the impression given by Fig. 6.3 and the connection with plasmons. We also observe the same peak dispersion as expected on the basis of theory [5].
As pointed out in the caption of Fig. 6.5, there is a big difference between the magnitudes of the charge for $\mathbf{q} \to 0$ and $\mathbf{q} \neq 0$. This can be understood from the mathematical point of view if we look at the expression for the force resulting from the potential 6.3:

$$\widehat{F}_{ext} = -\frac{\mathrm{d}\widehat{V}_{ext}}{\mathrm{d}\mathbf{r}} = -i(\mathbf{q_0}+\mathbf{G_0})e^{i(\mathbf{q_0}+\mathbf{G_0})\cdot\mathbf{r}}e^{-i\omega t}$$

from which it is evident that $\widehat{F}_{ext} \propto \mathbf{q_0}$. Then a smaller $\mathbf{q_0}$ induces a smaller charge, as one could reasonably expect by thinking that a smaller transferred momentum is actually a lighter "kick" on the electronic system.

3D visualization

A different and effective visualization is possible if a value for ρ_{ind} is fixed and isosurfaces of induced charge drawn.
Fig. 6.6 contains the isosurfaces for the two plasmon energies $\omega_0 = 7$ eV (a) and $\omega_0 = 29.5$ eV (b) at vanishing in-plane momentum. It is visible that the polarization is in the direction of $\mathbf{q_0}$, along the bonds between carbon atoms.

The same images for $\mathbf{q} \neq 0$ are much more illuminating. Fig. 6.7a corresponds to a $\omega_0 = 9$eV plane wave, thus corresponding to the first plasmon excitation (see Fig.4.13), the so called π plasmon. Actually the shape of isosurfaces in Fig. 6.7a ressembles very closely the shape of π orbitals, the ones supposed to be involved.
In Fig. 6.7b, whose energy correspond to the $\pi + \sigma$ plasmon, a contribution from sigma bonds can be seen, even if this is less clear than in the previous case.

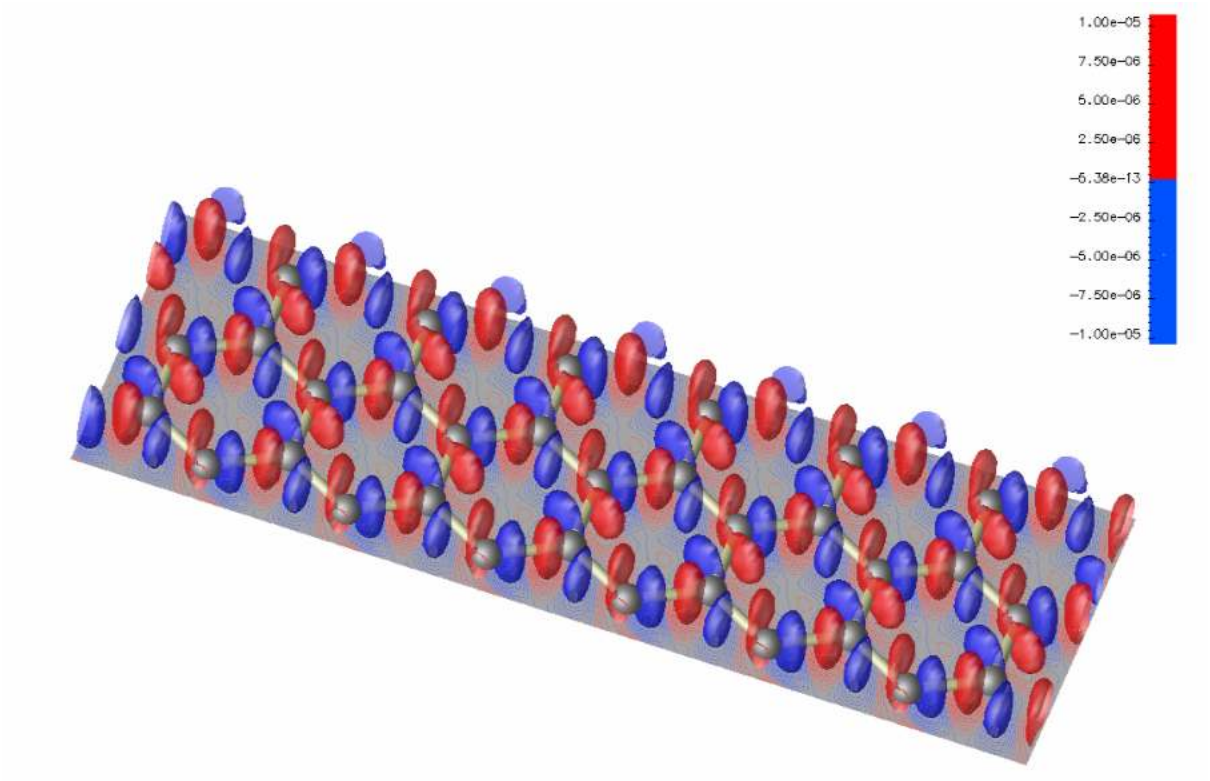

(a) $\omega_0 = 7\text{eV}$

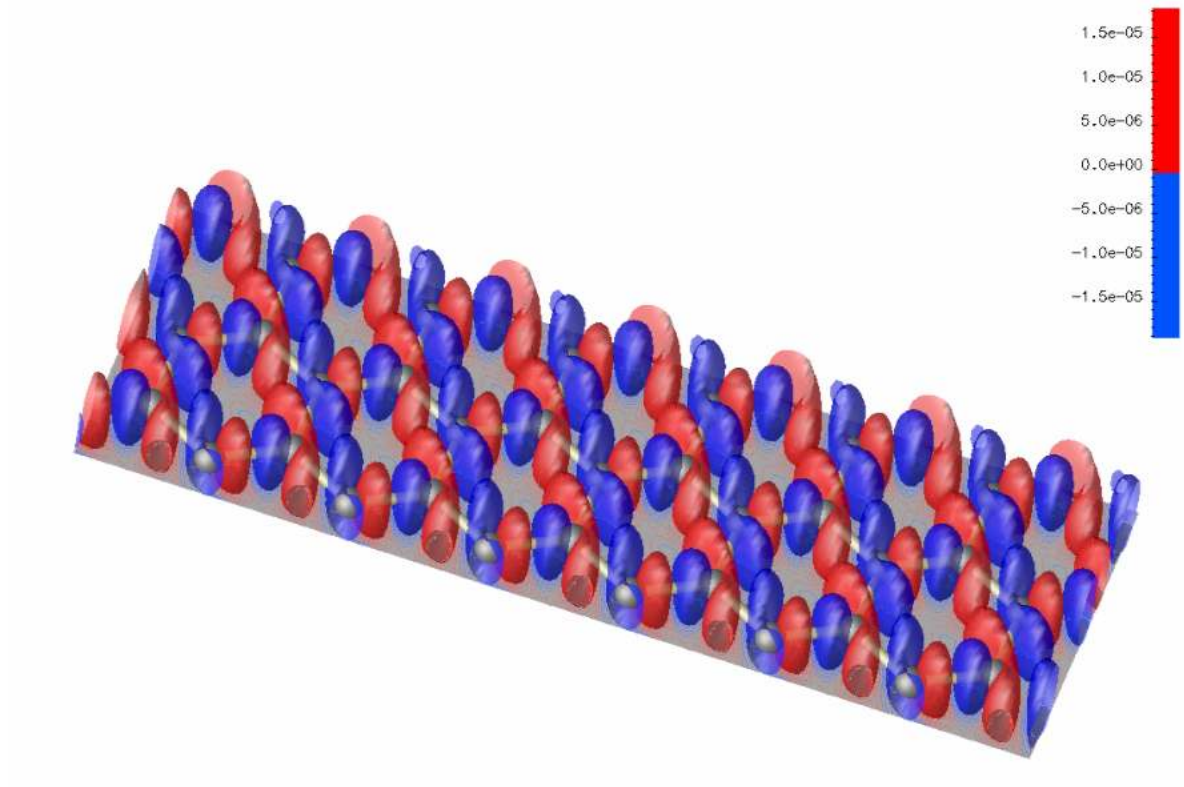

(b) $\omega_0 = 29.5\text{eV}$

Figure 6.6: 3D visualization for $\mathbf{q} \to 0$, $|\rho(\mathbf{r}, 0)| = 0.00001 \frac{e}{\text{bohr}^3}$.

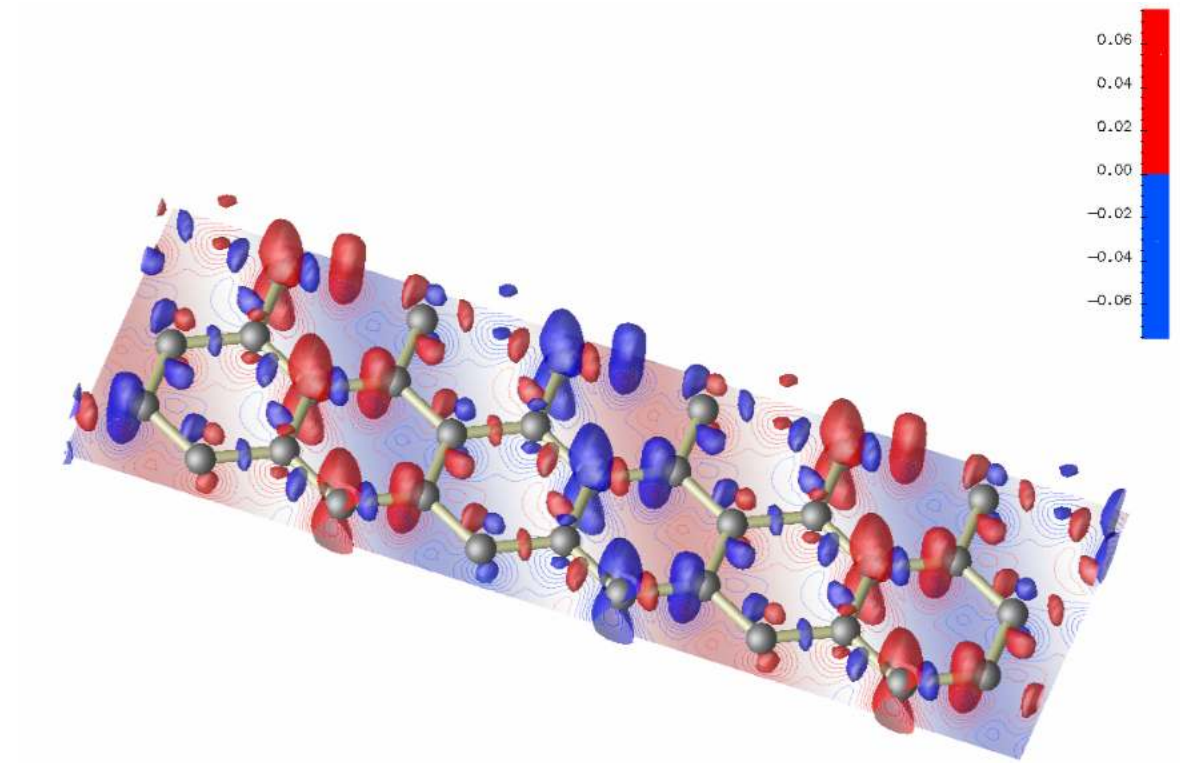

(a) $\omega_0 = 9\text{eV}$

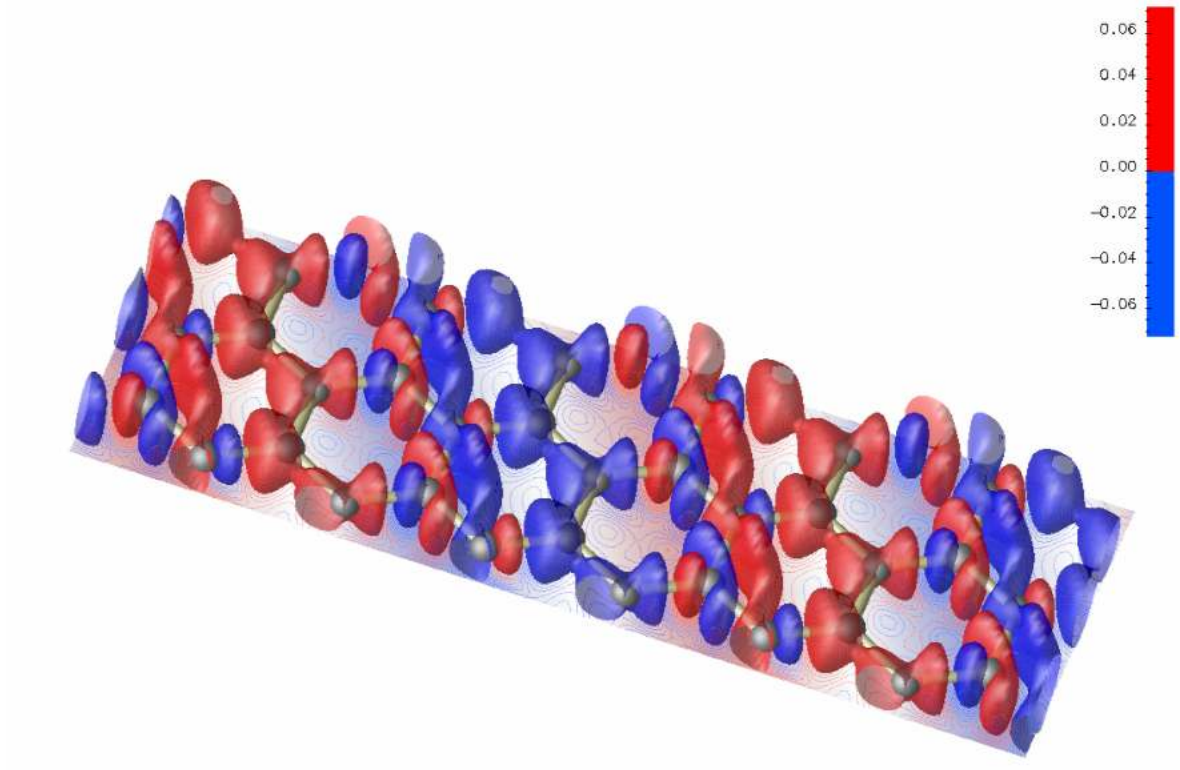

(b) $\omega_0 = 32\text{eV}$

Figure 6.7: 3D visualization for $\mathbf{q} = 0.25 \cdot \mathbf{b_1}$, $|\rho(\mathbf{r}, 0)| = 0.044 \frac{e}{\text{bohr}^3}$.

Time dependence

Now we add time dependence to study the evolution of oscillations at the energies we are interested in.

7 eV, vanishing transferred momentum At $\omega_0 = 7$eV, we expect to find something related to the π plasmon. We choose a small q in x direction in reciprocal space. What we obtain for $\rho_{ind}(\mathbf{r}, t)$ is in Fig. 6.8.

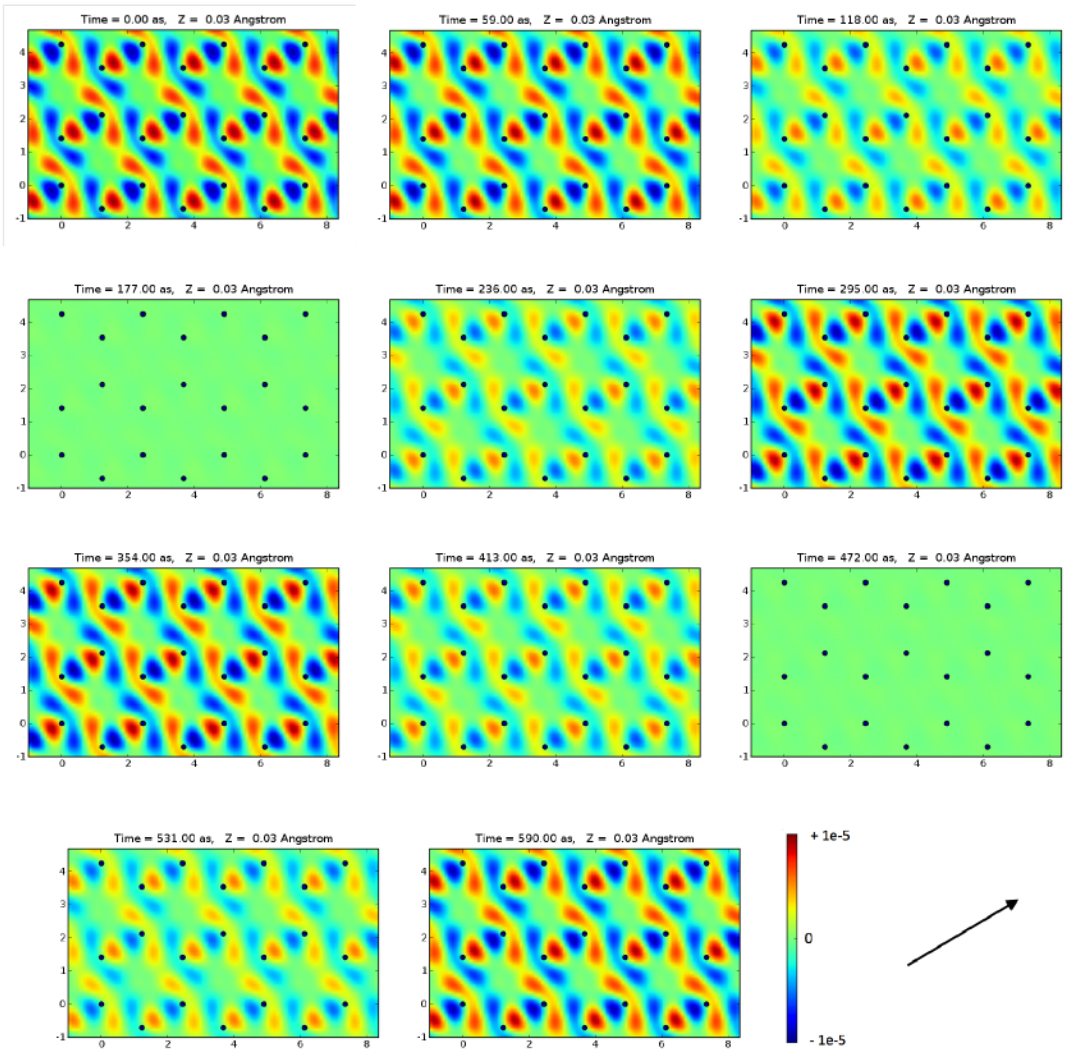

Figure 6.8: Temporal evolution of ρ_{ind} for $E_0 = 7$ eV between 0 and 590 as (corresponding to a period T). The direction of $\mathbf{q}$ is also shown.

The temporal evolution shows a stationary oscillation with the same period as the incident wave. The fact that there is no spatial change in time was expected, because we know that $\mathbf{q} \to 0$ corresponds to a long-wavelength perturbation which then is nearly constant in our simulation cell, but varies in time.

9 eV, finite transferred momentum If we consider a $\mathbf{q} \neq 0$, we have to look at another energy because of plasmon dispersion, $\omega_0 = 9\text{eV}$. In this case, we do get a spatial dependence: the resulting induced charge structure has a wavelength and a period equal to the ones of the external plane wave.

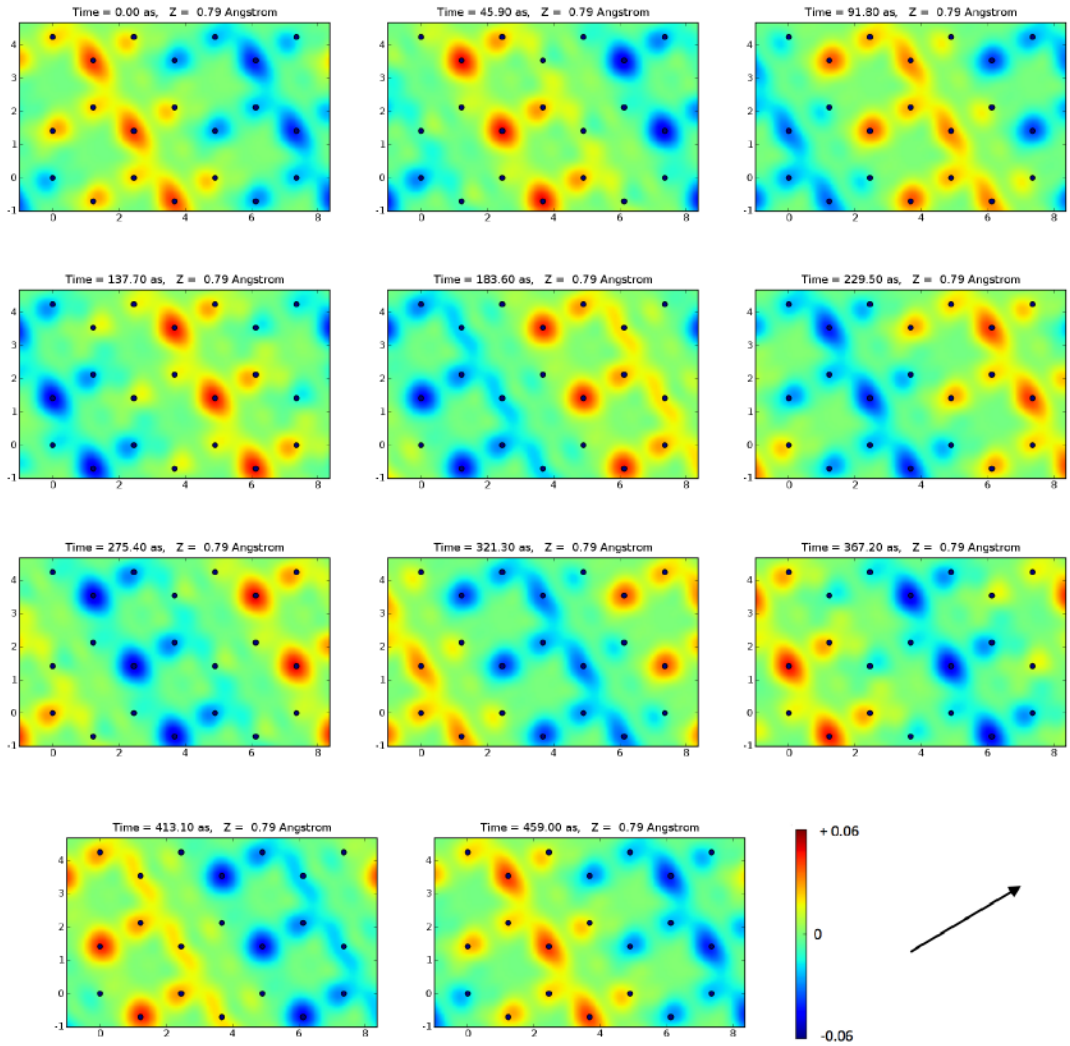

Figure 6.9: Temporal evolution of ρ_{ind} for $E_0 = 9$ eV between 0 and 459 as (corresponding to a period T). The direction of $\mathbf{q}$ is also shown.

An interesting point in Fig.6.9 is that a different kind of polarization can be seen for A type atoms and B type atoms, those who are stacked or not. This inequivalence is a sign of an interaction between different planes. In the equilibrium condition (without any external perturbation) the interaction between planes is very weak because of the long range Coulomb interaction.

6.2.2 Study of the influence of off-diagonal elements

Let us consider once again Eq.(6.5).

$$\hat{\rho}_{ind}(\mathbf{r},t) = \frac{1}{\Omega}\sum_{\mathbf{G}} \chi_{\mathbf{G}\mathbf{G_0}}(\mathbf{q_{0r}},\omega_0) e^{i(\mathbf{q_{0r}}+\mathbf{G})\cdot\mathbf{r}} e^{-i\omega_0 t} \tag{6.8}$$

With respect to the general expression Eq.(6.2), the external perturbation has selected a frequency ω_0 and the component $\mathbf{G_0}$ of the tensor $\chi_{\mathbf{GG}}$, but a sum on $\mathbf{G}$ vector is left. We want to study how the result changes if we include a different number of shells among those at our disposal. The measurement of off-diagonal elements $\chi_{\mathbf{GG'}}$ is very difficult from the experimental point of view, so our theoretical study could provide interesting complementary information.

Vanishing momentum We begin once again with the case of $\mathbf{q} \to 0$ and the first plasmon energy.

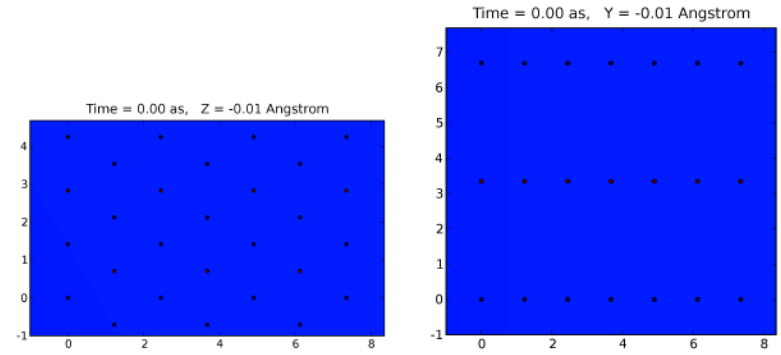

(a) 1 shell included, xy plane $z = 0.01$Å

(b) xz plane $y = 0.65$Å

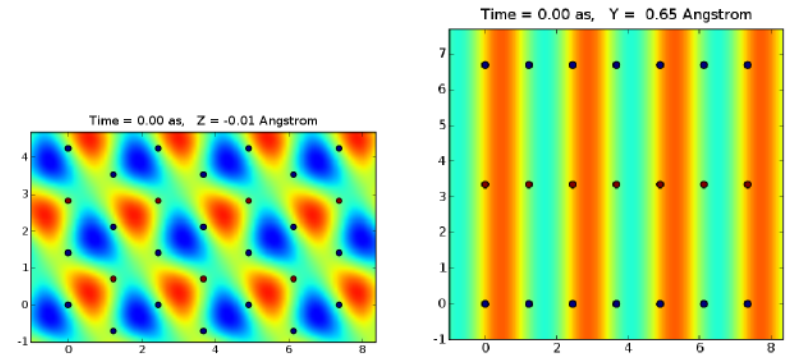

(c) 5 shells included, xy plane $z = 0.01$Å

(d) xz plane $y = 0.65$Å

Figure 6.10: Resolution achieved with the first shells in the case $\mathbf{q} \to 0$, $\omega_0 = 7$ eV

If less than 5 shells (13 $\mathbf{G}$ vectors) are included in the calculations, no details are seen and the medium appears homogenous. With 5 shells, a resolution in the horizontal plane is achieved (6.10c), but not yet in the z direction (6.10d).
This can be understood by considering the form of off-diagonal elements [55, 58, 59]

$$\chi_{\mathbf{G}0} \propto (\mathbf{q}+\mathbf{G})\cdot(\mathbf{q}+0)$$

As it can be seen in the list in Appendix C, the first **G** vectors have no in -plane component, so the projection of $\mathbf{q}+\mathbf{G}$ on $\mathbf{q}$ is very small. From the 5th shell, an in-plane component is present and the projection is bigger (see Fig. 6.11). If more shells are included, more details appear: two examples are in Fig. 6.12.

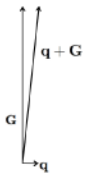

(a) $(\mathbf{q}+\mathbf{G})\cdot\mathbf{q}$ in the first 4 shells

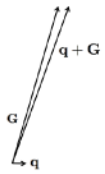

(b) $(\mathbf{q}+\mathbf{G})\cdot\mathbf{q}$ in other shells

Figure 6.11: Difference in the scalar product for $\mathbf{q}\to 0$

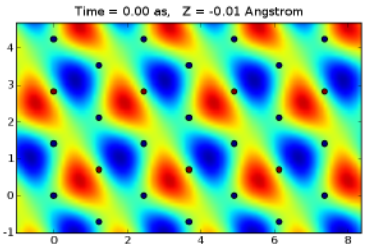

(a) 9 shells included, xy plane $z = 0.01$Å

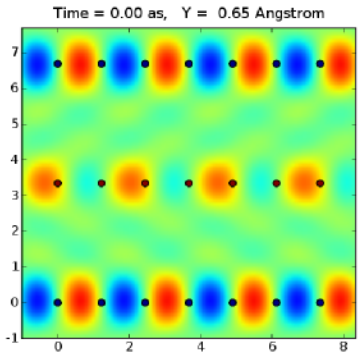

(b) xz plane $y = 0.65$Å

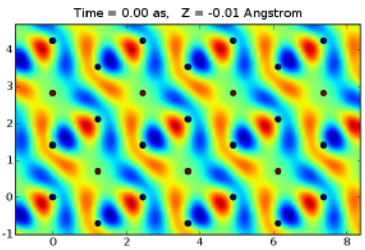

(c) 23 shells included, xy plane $z = 0.01$Å

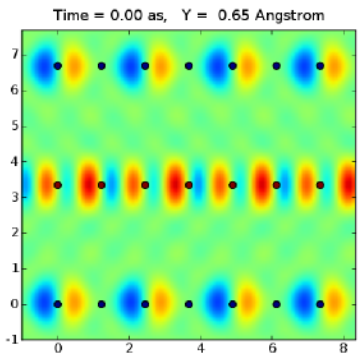

(d) xz plane $y = 0.65$Å

Figure 6.12: Examples of resolution with a different number of shells included in the case $\mathbf{q}\to 0$, $\omega_0 = 7$ eV

Non-vanishing momentum In this case, the first 4 shells do not contribute to the xy resolution, but they allow to obtain some z resolution. The reason of this lies again in the form shown in Eq.(6.8). When $\mathbf{q}$ is finite, the projection of $\mathbf{G}+\mathbf{q}$ over it is nonzero also if $\mathbf{G}$ has no in-plane components.

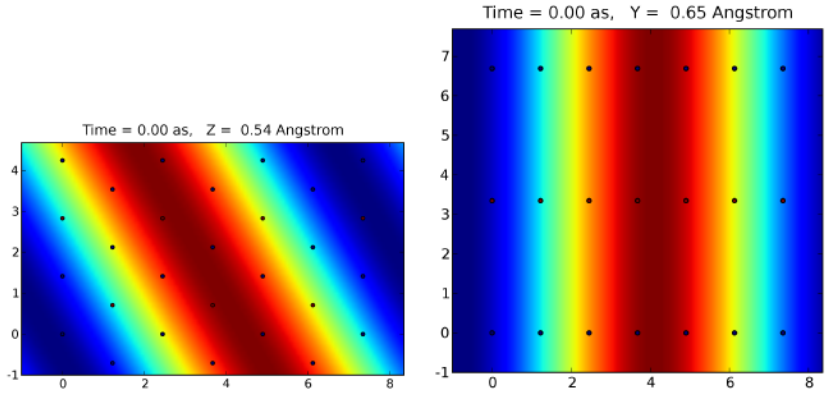

(a) 1 shell included, xy plane $z = 0.01$Å (b) xz plane $y = 0.65$Å

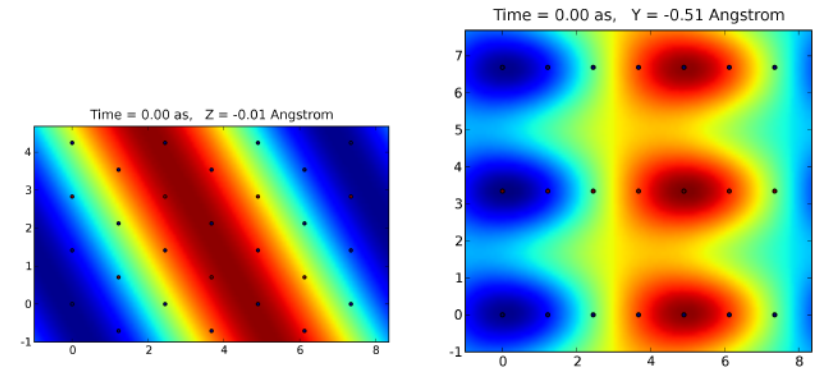

(c) 3 shells included, xy plane $z = 0.01$Å (d) xz plane $y = 0.65$Å

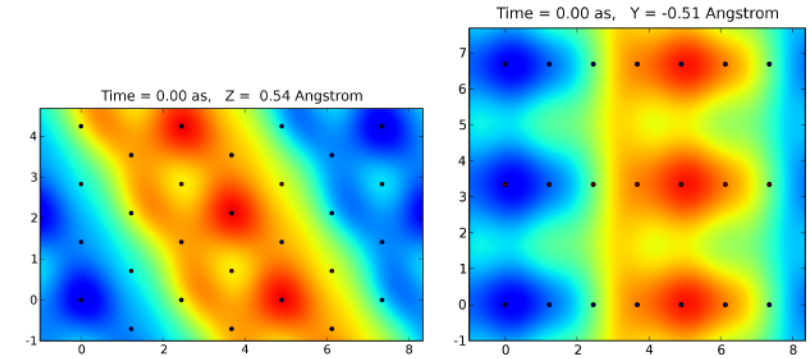

(e) 5 shells included, xy plane $z = 0.01$Å (f) xz plane $y = 0.65$Å

Figure 6.13: Resolution achieved with the first shells in the case $\mathbf{q} \neq 0$, $\omega_0 = 9$ eV

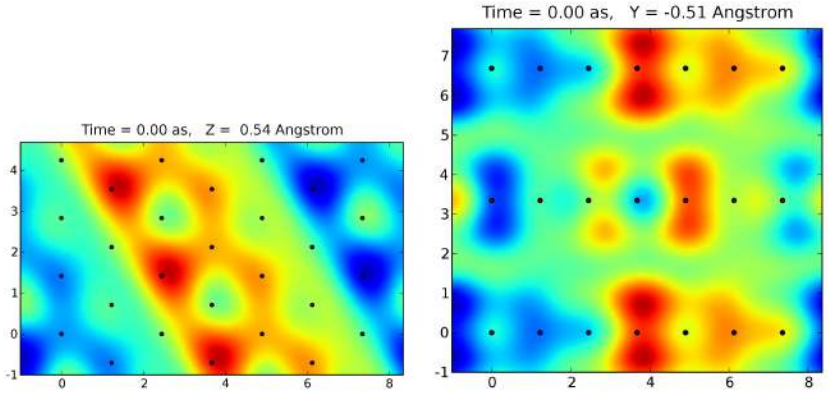

(a) 8 shells included, xy plane $z = 0.01$Å

(b) xz plane $y = 0.65$Å

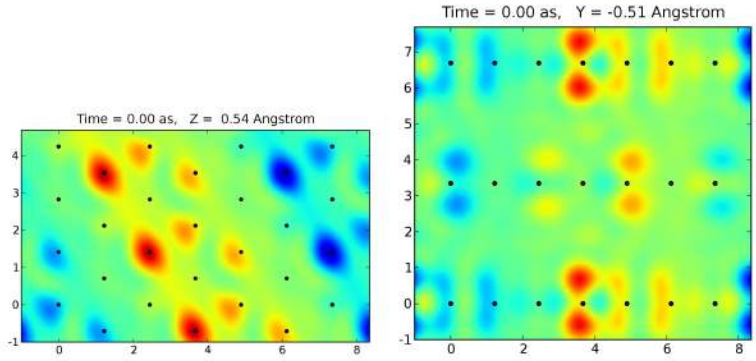

(c) 19 shells included, xy plane $z = 0.01$Å

(d) xz plane $y = 0.65$Å

Figure 6.14: Examples of resolution with a different number of shells included in the case $\mathbf{q} \neq 0$, $\omega_0 = 9$ eV

These results show that it is possible to predict which shells are more important for resolution by considering the angle θ between $\mathbf{G} + \mathbf{q}$ and $\mathbf{q}$, as Eq.(6.8) is equivalent to

$$\chi_{\mathbf{G}0} \propto \cos\theta$$

This concept can be useful also for experimental measures.

We are considering an in-plane $\mathbf{q}$: we know from the literature cited in §5.2 [4, 5] and from our results reported in §4.2.2 that LFE, which are related to off diagonal elements, are not important for the EELS spectra. Now we have seen that for visualizing the induced charge off diagonal elements play instead a key role. This because the EELS spectrum is an integral quantity, while our way of visualizing the charge takes fully into account the microscopic nature of electron dynamics.

6.3 A delta perturbation in time

Consider now a different external perturbation, localized in time:

$$\widehat{V}_{ext}(\mathbf{r},t) = e^{i\mathbf{q_0}\cdot\mathbf{r}}\delta(t-t_0)$$

This potential is nearer to the delta perturbation in space and time in Abbamonte's paper [2]. In reciprocal space this corresponds to

$$\begin{aligned}\widehat{V}_{ext}(\mathbf{q},\omega) &= \frac{1}{2\pi}\delta_{\mathbf{qq_0}}\int \mathrm{d}t\, e^{i\omega t}\delta(t-t_0)\\ &= \frac{1}{2\pi}\delta_{\mathbf{qq_0}}e^{i\omega t_0}\end{aligned}$$

As previously, we consider first the induced charge density in reciprocal space

$$\begin{aligned}\hat{\rho}^{ind}(\mathbf{q_r}+\mathbf{G},\omega) &= \sum_{\mathbf{G'}}\widehat{\chi}(\mathbf{q_r}+\mathbf{G},\mathbf{q_r}+\mathbf{G'},\omega)\widehat{V}_{ext}(\mathbf{q_r}+\mathbf{G'},\omega) =\\ &= \frac{1}{2\pi}\widehat{\chi}(\mathbf{q_r}+\mathbf{G},\mathbf{q_r}+\mathbf{G_0},\omega)\delta_{\mathbf{q_r}\mathbf{q}_{\mathbf{r}0}}e^{i\omega t_0}\end{aligned}$$

and then we finally find the induced charge in real space and time:

$$\begin{aligned}\hat{\rho}_{ind}(\mathbf{r},t) &= \frac{1}{\Omega}\sum_{\mathbf{q_r}}\sum_{\mathbf{G}}\int_{-\infty}^{+\infty}\mathrm{d}\omega\hat{\rho}^{ind}(\mathbf{q_r}+\mathbf{G},\omega)e^{i(\mathbf{q_r}+\mathbf{G})\cdot\mathbf{r}}e^{-i\omega t}\\ &= \frac{1}{2\pi\Omega}\sum_{\mathbf{G}}e^{i(\mathbf{q}_{\mathbf{r}0}+\mathbf{G})\cdot\mathbf{r}}\int_{-\infty}^{+\infty}\mathrm{d}\omega\,\chi_{\mathbf{GG_0}}(\mathbf{q}_{\mathbf{r}0},\omega)e^{-i\omega(t-t_0)}\end{aligned} \tag{6.9}$$

Comparing Eqs.(6.5) and (6.9) we see that in the latter a sum on frequencies is involved, which is more complicated also from the computational point of view.

Actually, we do not know the value of χ at all frequencies, but only at those for which we calculated the spectra, that is to say a finite and discrete set of frequencies.
A first problem is that the integration in Eq.(6.9) is performed on frequencies going from $-\infty$ to $+\infty$.
We decide to calculate χ also for negative frequencies, which is not normally done, and to choose a reasonable value of energy to end the calculation.
A possible way to consider just positive frequencies is shown in §B.5, and a method to extend the integral to high frequencies is in §D.2.

The second problem is the fact that our $\chi(\omega)$ is discrete. Fourier theory implies that $\chi(t)$ is periodic, a property incompatible with the costraint that $\chi(t)$ vanish for all $t<0$ required by causality. The periodical repetition of $\chi(t)$ is the so-called aliasing, which implies a repetition of $\chi(t)$ after a $t_a = \dfrac{2\pi}{\Delta\omega}$.
What can be tried to reduce this problem is to take a small $\Delta\omega$ so that the repetition appear out of the temporal interval we are interested to. With $\Delta\omega = 0.5$ eV we get $t_a \simeq 8300$ as, which is over the timescale we expect electron dynamics to be.

If we substitute the integral in Eq.(6.9) with a finite sum over discrete frequencies, we get something different from the ideal δ we would like to have as V_{ext}.

If we consider only the time-frequency dependence of the induced charge and the fact that we have a finite range of discrete frequencies, we can find the effective potential acting in our calculation:

$$\rho_{ind}(\omega) = \chi(\omega)V_{eff}(\omega)$$
$$\rho_{ind}(t) = \int \mathrm{d}\,\omega\chi(\omega)V_{eff}(\omega)e^{-i\omega t} \rightarrow \frac{1}{2\pi}\sum_{\omega_i}\chi(\omega_i)e^{-i\omega_i t}\Delta\omega$$

by comparison of these two expressions we find that the form of our effective potential must be

$$V_{eff}(\omega) = \frac{1}{2\pi}\sum_{\omega_i}\delta(\omega-\omega_i)\Delta\omega$$
$$V_{eff}(t) = \frac{1}{2\pi}\int \mathrm{d}\omega\, e^{i\omega t}\sum_{\omega_i}\delta(\omega-\omega_i) \rightarrow \sum_{\omega_i} e^{i\omega_i t}\Delta\omega$$

Thus the effective potential V_{eff} we are considering is not a delta in time, but rather a function like $\dfrac{\sin t}{t}$, which is a better approximation of a delta the more ω_i are considered.

6.3.1 Results

We have to choose our approximation for the infinite integral of Eq.(6.9). This should be satisfactory if the range of relevant electronic transitions is included in the integral: we take the range $(-150\mathrm{eV}, 150\mathrm{eV})$ as a reasonable approximation. The energy dependence of the $\chi_{\mathbf{GG'}}$ elements is investigated in Appendix D.

Vanishing momentum

We begin with a perturbation with small momentum transfer. The result we obtain is exemplified in Fig. 6.15, where the induced charge in the origin is represented along with the (scaled) external potential: note the different order of magnitude between the real and imaginary part.

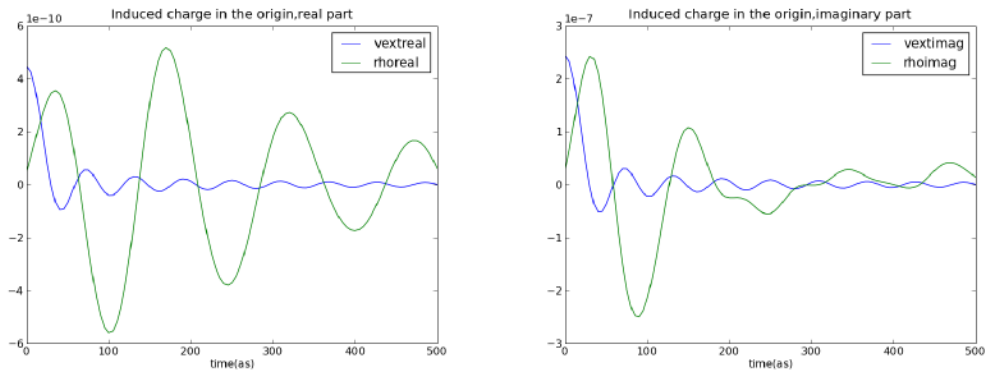

(a) $\mathrm{Re}\{V_{ext}\}\cdot 10^{-11}$, $\mathrm{Re}\{\widehat{\rho}_{ind}\}$ (b) $\mathrm{Im}\{V_{ext}\}\cdot 10^{-3}$, $\mathrm{Im}\{\widehat{\rho}_{ind}\}$

Figure 6.15: Induced charge in the origin in the case $\mathbf{q_0} \rightarrow 0$

The real part of the charge, which we have considered so far, is three orders of magnitude smaller than the imaginary one, and substantially zero, even if the real part of the potential is the dominant one.

Non-vanishing momentum

In the case of non-vanishing momentum we obtain the results in Fig. 6.16. The real part images are not zero in this case: see 6.17.

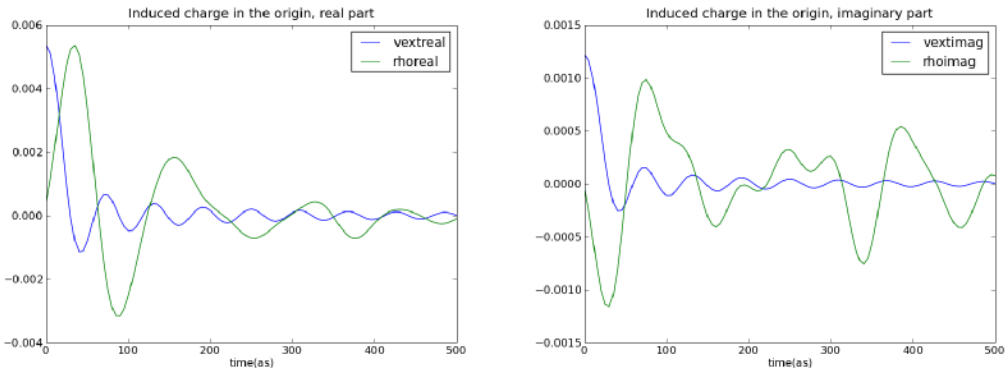

(a) $\mathrm{Re}\{V_{ext}\} \cdot 10^{-4}$, $\mathrm{Re}\{\widehat{\rho}_{ind}\}$ (b) $\mathrm{Im}\{V_{ext}\} \cdot 10^{-5}$, $\mathrm{Im}\{\widehat{\rho}_{ind}\}$

Figure 6.16: Induced charge in the origin in the case $\mathbf{q_0} \neq 0$

There are two interesting features in the previous results: the disappearing of the real part in the $\mathbf{q_0} \to 0$ case and the delay in the response.
The origin of these two phenomena is not immedeately clear.
In particular, it is puzzling to find an imaginary part larger than the real one, because $\widehat{\rho}_{ind}(\mathbf{r}, t)$ comes from the convolution between a real response function $\chi(\mathbf{r}, \mathbf{r}', t)$ and a nearly-real potential $\widehat{V}(\mathbf{r}, t)$:

$$\widehat{\rho}_{ind}(\mathbf{r}, t) = \int \mathrm{d}\mathbf{r}'\mathrm{d}t' \, \chi(\mathbf{r}, \mathbf{r}', t)\widehat{V}(\mathbf{r}', t')$$

We are dealing with a very complex physical problem that includes a lot of transitions, and local field effects. In order to understand it, we reduce it to its simplest form and then add complications, as long as it is analytically possible.

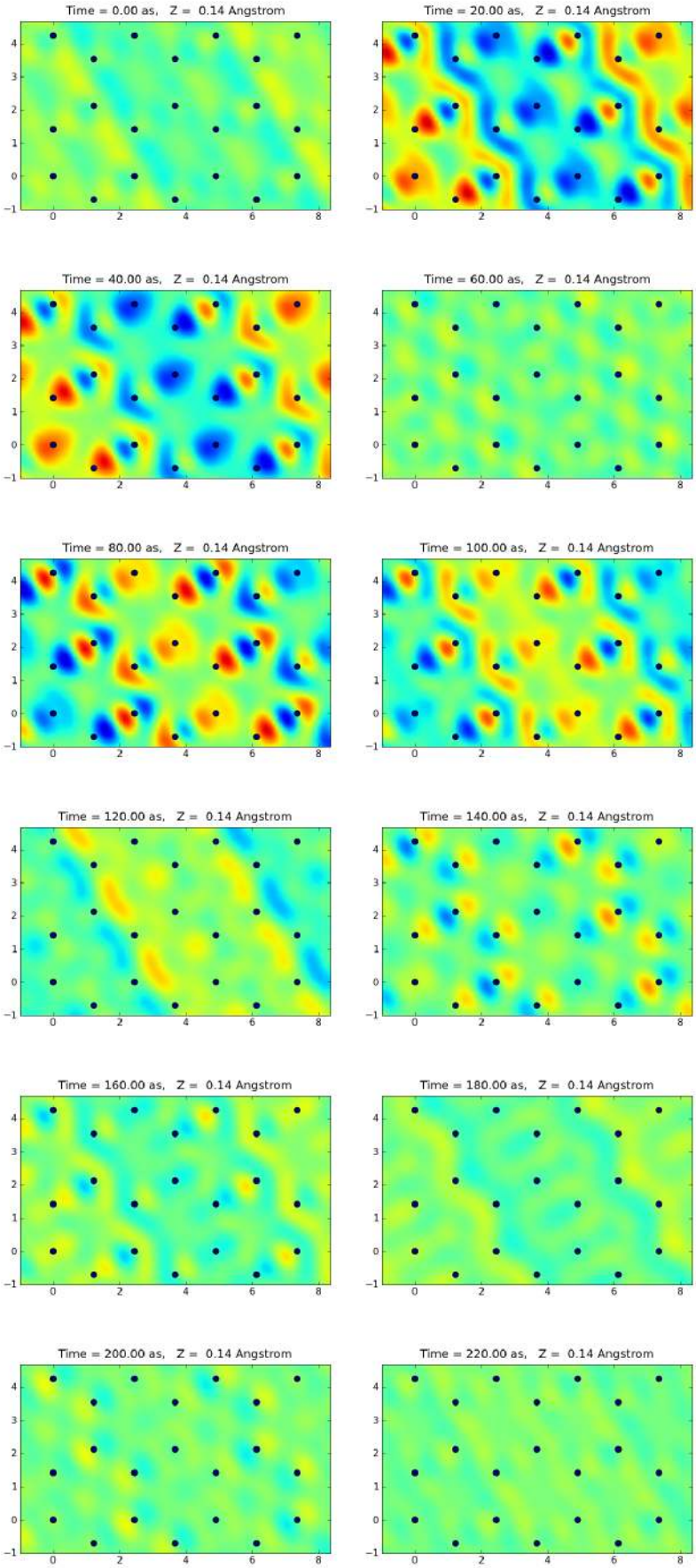

Figure 6.17: Temporal evolution of ρ_{ind}, $\mathbf{q_0} \neq 0$

6.3.2 Analytical solution for simple cases

The calculation we made in the previous section includes millions of transitions and LFE. The greatest simplification from which we can start is considering a non-interacting system, taking just one transition and excluding off-diagonal elements.
We consider the case $\mathbf{q} \to 0$; our procedure will be to obtain an analytical solution for the problem, and then compare it with the resuts given by our program for that particular problem.

χ^0 for one transition

The general formula

$$\chi^0(\mathbf{q},\mathbf{G},\mathbf{G}',\omega) = \frac{2}{\Omega}\sum_{i,j,\mathbf{k}} \frac{(f_{j,\mathbf{k+q}} - f_{i,\mathbf{k}})\langle i,\mathbf{k}|e^{i(\mathbf{q}+\mathbf{G}')\cdot\mathbf{r}'}|j,\mathbf{k}+\mathbf{q}\rangle\langle j,\mathbf{k}+\mathbf{q}|e^{-i(\mathbf{q}+\mathbf{G})\cdot\mathbf{r}}|i,\mathbf{k}\rangle}{\omega - (\epsilon_{j,\mathbf{k}} - \epsilon_{i,\mathbf{k}}) + i\eta}$$
$$= \frac{2}{N_{\mathbf{k}}\cdot\Omega_{cell}}\sum_{i,j,\mathbf{k}} \frac{(f_{j,\mathbf{k+q}} - f_{i,\mathbf{k}})\tilde{\rho}_{ij\mathbf{k}}(\mathbf{q},\mathbf{G})\tilde{\rho}^*_{ij\mathbf{k}}(\mathbf{q},\mathbf{G}')}{\omega - (\epsilon_{j,\mathbf{k+q}} - \epsilon_{i,\mathbf{k}}) + i\eta}$$

becomes in the simple case $\mathbf{G} = \mathbf{G}' = 0$, just one transition (one $\mathbf{k}$ vector):

$$\chi^0(\mathbf{q},0,0,\omega) = \frac{2}{\Omega_{cell}}\left[\frac{\tilde{\rho}_{12\mathbf{k}}(\mathbf{q},0)\tilde{\rho}^*_{12\mathbf{k}}(\mathbf{q},0)}{\omega - (\epsilon_{2,\mathbf{k+q}} - \epsilon_{1,\mathbf{k}}) + i\eta} - \frac{\tilde{\rho}_{21\mathbf{k}}(\mathbf{q},0)\tilde{\rho}^*_{21\mathbf{k}}(\mathbf{q},0)}{\omega + (\epsilon_{2,\mathbf{k+q}} - \epsilon_{1,\mathbf{k}}) + i\eta}\right] =$$
$$= \frac{2}{\Omega_{cell}}\left[\frac{|\tilde{\rho}_{12\mathbf{k}}(\mathbf{q})|^2}{\omega - \Delta\epsilon + i\eta} - \frac{|\tilde{\rho}_{21\mathbf{k}}(\mathbf{q})|^2}{\omega + \Delta\epsilon + i\eta}\right]$$

Considering time reversal symmetry we see that $|\tilde{\rho}_{21}|^2 = |\tilde{\rho}_{12}|^2 = |\tilde{\rho}|^2$ (see §B.4).
So the formula becomes[2]

$$\chi^0_{00}(\mathbf{q},\omega) = \frac{2}{\Omega_{cell}}\left[\frac{|\tilde{\rho}(\mathbf{q})|^2}{\omega - \Delta\epsilon + i\eta} - \frac{|\tilde{\rho}(\mathbf{q})|^2}{\omega + \Delta\epsilon + i\eta}\right] \tag{6.10}$$

We want to use this simple χ^0 to approximate χ in the formula for the induced charge density (6.9)

$$\hat{\rho}_{ind}(\mathbf{r},t) = \frac{1}{2\pi}\sum_{\mathbf{G}} e^{i(\mathbf{q}_{\mathbf{r}0}+\mathbf{G})\cdot\mathbf{r}}\int_{-\infty}^{+\infty} \mathrm{d}\omega\, \chi_{\mathbf{GG_0}}(\mathbf{q}_{\mathbf{r}0},\omega)e^{-i\omega(t-t_0)} =$$
$$\simeq \frac{1}{2\pi}e^{i\mathbf{q}_{\mathbf{r}0}\cdot\mathbf{r}}\int_{-\infty}^{+\infty} \mathrm{d}\omega\, \chi^0_{00}(\mathbf{q}_{\mathbf{r}0},\omega)e^{-i\omega(t-t_0)} \tag{6.11}$$

To calculate the integrals of the two complex terms in Eq.(6.10) we use the Residue Theorem and Jordan's Lemma[60]. We start with the first term (resonant):

$$\int_{-\infty}^{+\infty} \frac{e^{-i\omega(t-t_0)}}{\omega - \Delta\epsilon + i\eta}$$

We have to distinguish the two cases for $t > t_0$ and $t < t_0$:

[2]From this expression it is visible that the first non zero term in the expansion is the $\frac{1}{\omega^2}$ one.

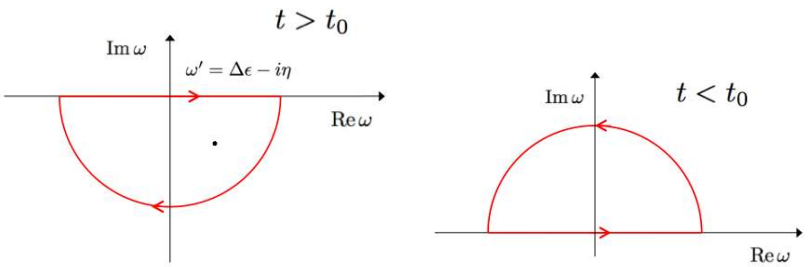

(a) (b)

Figure 6.18: Contours of integration for the first term of Eq.(6.10)

- $\boxed{t > t_0}$ We choose as circuit for integration the semicircle in the lower half plane shown in Fig. 6.18a, which contains a pole in $\omega' = \Delta\epsilon - i\eta$. Following the Residue theorem, we know the integral over the circuit is

$$\oint \frac{e^{-i\omega(t-t_0)}}{\omega - \Delta\epsilon + i\eta} = (-1)2\pi i \,\mathrm{Res}(f, \omega')$$

where the minus sign is due to the direction of integration (clockwise). This integral can be divided in two parts:

$$\oint \frac{e^{-i\omega(t-t_0)}}{\omega - \Delta\epsilon + i\eta} = \int_{-\infty}^{+\infty} \frac{e^{-i\omega(t-t_0)}}{\omega - \Delta\epsilon + i\eta} + \int_C \frac{e^{-i\omega(t-t_0)}}{\omega - \Delta\epsilon + i\eta}$$

and the $\int_C$ tends to 0 thanks to Jordan's Lemma. The pole in ω' is of the first order, so the residue is given by

$$\frac{\text{Numerator(pole)}}{\frac{d}{d\omega}\text{Denominator}|_{\text{pole}}}$$

Then we finally get

$$\int_{-\infty}^{+\infty} \frac{e^{-i\omega(t-t_0)}}{\omega - \Delta\epsilon + i\eta} = -2\pi i \, e^{-i\Delta\epsilon(t-t_0)} e^{-\eta(t-t_0)} \qquad \text{for } t > t_0$$

- $\boxed{t < t_0}$ The integration circuit is the upper half plane (Fig. 6.18b), which contains no poles. So the integration gives zero in this case.

The result of the integration of the first term in Eq.(6.10) is then

$$\int_{-\infty}^{+\infty} \frac{e^{-i\omega(t-t_0)}}{\omega - \Delta\epsilon + i\eta} = -2\,\Theta(t-t_0)\pi i \, e^{-i\Delta\epsilon(t-t_0)} e^{-\eta(t-t_0)}$$

A similar reasoning leads to the result for the integration of the anti-resonant term[3]

$$\int_{-\infty}^{+\infty} \frac{e^{-i\omega(t-t_0)}}{\omega + \Delta\epsilon + i\eta} = -2\,\Theta(t-t_0)\pi i \, e^{i\Delta\epsilon(t-t_0)} e^{-\eta(t-t_0)}$$

[3]From these explicit calculations we see that in order to have a response function for the electronic character, which has to be causal, the sign of the imaginary part $i\eta$ is important: mathematically, it "puts" the poles in the right part of the complex plane.

If we put these results in Eq.(6.11) we get

$$\begin{aligned}\hat{\rho}_{ind}(\mathbf{r},t) &= \frac{2}{\Omega_{cell}} i\, e^{i\mathbf{q}\cdot\mathbf{r}}\,\Theta(t-t_0)\,e^{-\eta(t-t_0)}\,|\tilde{\rho}|^2\,(e^{i\Delta\epsilon(t-t_0)} - e^{-i\Delta\epsilon(t-t_0)}) = \\ &= \frac{2i}{\Omega_{cell}}[\cos(\mathbf{q}\cdot\mathbf{r}) + i\sin(\mathbf{q}\cdot\mathbf{r})]\Theta(t-t_0)e^{-\eta(t-t_0)}\cdot 2i\sin(\Delta\epsilon(t-t_0))\cdot 2|\tilde{\rho}|^2 = \\ &= -\frac{4}{\Omega_{cell}}\Theta(t-t_0)e^{-\eta(t-t_0)}[\cos(\mathbf{q}\cdot\mathbf{r}) + i\sin(\mathbf{q}\cdot\mathbf{r})]\sin(\Delta\epsilon(t-t_0))\cdot|\tilde{\rho}|^2\end{aligned}$$

So the real and imaginary parts are

$$\mathrm{Re}\,\hat{\rho}_{ind}(\mathbf{r},t) = -\frac{4}{\Omega_{cell}}\Theta(t-t_0)e^{-\eta(t-t_0)}\cos(\mathbf{q}\cdot\mathbf{r})\sin(\Delta\epsilon(t-t_0))\cdot|\tilde{\rho}|^2 \tag{6.12}$$

$$\mathrm{Im}\,\hat{\rho}_{ind}(\mathbf{r},t) = -\frac{4}{\Omega_{cell}}\Theta(t-t_0)e^{-\eta(t-t_0)}\sin(\mathbf{q}\cdot\mathbf{r})\sin(\Delta\epsilon(t-t_0))\cdot|\tilde{\rho}|^2 \tag{6.13}$$

Notice that the maximum of the response is delayed with respect to t_0, just like in the results of the previous section. This is typical behaviour one finds in simple quantum mechanical systems, and has an analogous even in the classical harmonic oscillator, which needs a characteristic time to reach the maximum of oscillation. The behaviour we get in Fig. 6.19 is that of a simple damped oscillation[4], led by the sin term as we are considering the case $\mathbf{q} = 0$.

χ^0 for two transitions

The next step is to consider two transitions instead of just one. If we add another transition with energy $\Delta\epsilon_2$ the polarizability in Eq. (6.10) becomes

$$\chi^0_{00}(\mathbf{q},\omega) = \frac{2}{\Omega_{cell}}\left[\frac{|\tilde{\rho}_1(\mathbf{q})|^2}{\omega-\Delta\epsilon_1+i\eta} - \frac{|\tilde{\rho}_1(\mathbf{q})|^2}{\omega+\Delta\epsilon_1+i\eta} + \frac{|\tilde{\rho}_2(\mathbf{q})|^2}{\omega-\Delta\epsilon_2+i\eta} - \frac{|\tilde{\rho}_2(\mathbf{q})|^2}{\omega+\Delta\epsilon_2+i\eta}\right]$$

This yields an induced charge density

$$\hat{\rho}_{ind}(\mathbf{r},t) = -\frac{4}{\Omega_{cell}}\Theta(t-t_0)e^{-\eta(t-t_0)}\,e^{i\mathbf{q}\cdot\mathbf{r}}\left(|\tilde{\rho}_1|^2\sin(\Delta\epsilon_1(t-t_0)) + |\tilde{\rho}_2|^2\sin(\Delta\epsilon_2(t-t_0))\right)$$

We get as real and imaginary parts

$$\mathrm{Re}\,\hat{\rho}_{ind}(\mathbf{r},t) = -\frac{4}{\Omega_{cell}}\Theta(t-t_0)e^{-\eta(t-t_0)}\cos(\mathbf{q}\cdot\mathbf{r})\left(|\tilde{\rho}_1|^2\sin(\Delta\epsilon_1(t-t_0)) + |\tilde{\rho}_2|^2\sin(\Delta\epsilon_2(t-t_0))\right)$$

$$\mathrm{Im}\,\hat{\rho}_{ind}(\mathbf{r},t) = -\frac{4}{\Omega_{cell}}\Theta(t-t_0)e^{-\eta(t-t_0)}\sin(\mathbf{q}\cdot\mathbf{r})\left(|\tilde{\rho}_1|^2\sin(\Delta\epsilon_1(t-t_0)) + |\tilde{\rho}_2|^2\sin(\Delta\epsilon_2(t-t_0))\right)$$

In the two transitions case the resulting induced charge is the combination of the characteristic oscillations corresponding to the two characteristic energies E_1 and E_2, weighted by the probabilities $\tilde{\rho}$. These same coefficients determine the contribution of each characteristic time to the total delay, which will be influenced by the most relevant transition. This reasonement can be easily extended to an arbitrary number of independent transitions.

[4] Actually the damping is given by η, which in the practical calculation should be as small as possible

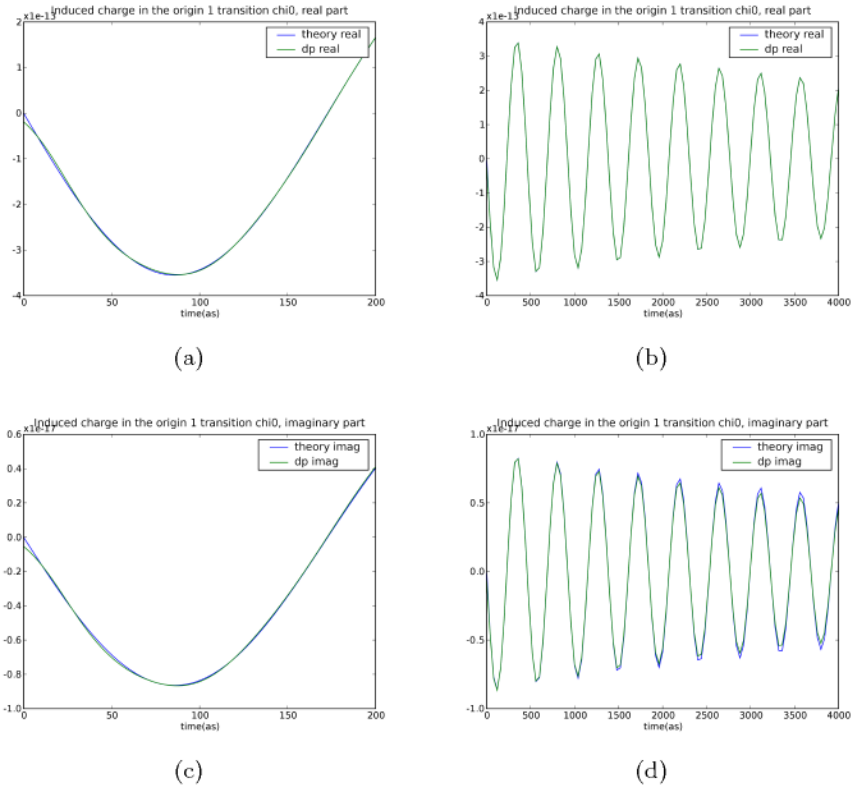

Figure 6.19: One transition χ^0. Comparison between the induced charge near the origin as obtained by numerical integration of the χ^0 obtained from DP and by the analytical formulas (6.12). The agreement is nearly perfect, except for the difference near $t = t_0$ and the damping for big t's in the imaginary part. Notice that there are four orders of magnitude between the real and the imaginary part: the reason for this can be understood by putting $\mathbf{r} = 0$ in Eqs.(6.12)

χ for one transition

Let us now come back to the one-transition case, and rewrite Eq.(6.10) as

$$\chi^0 = \frac{1}{\Omega_{cell}} \cdot \frac{4|\tilde{\rho}(\mathbf{q})|^2 \Delta\epsilon}{(\omega + i\eta)^2 - \Delta\epsilon^2} \tag{6.14}$$

We want to find the expression for the full polarizability χ, neglecting local field effects. This implies that the Dyson equation in the RPA approximation

$$\chi = \chi^0 + \chi^0 v \chi$$

is a simple algebrical equation (and not a matricial one, which would involve the problem of inversion) and is resolved by the relation

$$\chi = \frac{\chi^0}{1 - v\chi^0}$$

By substituting Eq.(6.10) in this last equation we get

$$\begin{aligned}\chi &= \frac{1}{\Omega_{cell}} \cdot \frac{4|\tilde{\rho}(\mathbf{q})|^2\Delta\epsilon}{(\omega+i\eta)^2-\Delta\epsilon^2} \cdot \left[1 - \frac{v}{\Omega_{cell}} \cdot \frac{4|\tilde{\rho}(\mathbf{q})|^2\Delta\epsilon}{(\omega+i\eta)^2-\Delta\epsilon^2}\right]^{-1} = \\ &= \frac{1}{\Omega_{cell}} \cdot \frac{4|\tilde{\rho}(\mathbf{q})|^2\Delta\epsilon}{(\omega+i\eta)^2-\Delta\epsilon^2} \cdot \frac{\Omega_{cell}[(\omega+i\eta)^2-\Delta\epsilon^2]}{\Omega_{cell}[(\omega+i\eta)^2-\Delta\epsilon^2]-4v|\tilde{\rho}(\mathbf{q})|^2\Delta\epsilon} = \\ &= \frac{4|\tilde{\rho}(\mathbf{q})|^2\Delta\epsilon}{\Omega_{cell}[(\omega+i\eta)^2-\Delta\epsilon^2]-4v|\tilde{\rho}(\mathbf{q})|^2\Delta\epsilon} \end{aligned} \tag{6.15}$$

We define

$$\widehat{\Delta\epsilon}^2 = \Delta\epsilon^2 + \frac{4v|\tilde{\rho}(\mathbf{q})|^2\Delta\epsilon}{\Omega_{cell}}$$

so that we can rewrite Eq.(6.15) as

$$\chi = \frac{1}{\Omega_{cell}} \cdot \frac{4|\tilde{\rho}(\mathbf{q})|^2\Delta\epsilon}{(\omega+i\eta)^2-\Delta\epsilon^2-\frac{4v|\tilde{\rho}(\mathbf{q})|^2\Delta\epsilon}{\Omega_{cell}}} = \frac{1}{\Omega_{cell}} \cdot \frac{\Delta\epsilon}{\widehat{\Delta\epsilon}} \cdot \frac{4|\tilde{\rho}(\mathbf{q})|^2\widehat{\Delta\epsilon}}{(\omega+i\eta)^2-\widehat{\Delta\epsilon^2}}$$

We notice that the last factor of this last expression has the same form as Eq.(6.14), and we can deduce the result of the integration in analogy with before:

$$\int_{-\infty}^{+\infty} \mathrm{d}\omega\, \chi(\mathbf{q},\omega)e^{-i\omega(t-t_0)} = \frac{4}{\Omega_{cell}} \cdot \frac{\Delta\epsilon}{\widehat{\Delta\epsilon}}\Theta(t-t_0)e^{-\eta(t-t_0)}\pi i \left[e^{i\widehat{\Delta\epsilon}(t-t_0)} - e^{-i\widehat{\Delta\epsilon}(t-t_0)}\right]|\tilde{\rho}(\mathbf{q})|^2$$

The induced charge density is then

$$\begin{aligned}\rho_{ind}(\mathbf{r},t) &= \frac{1}{2\pi}e^{i\mathbf{q_0}\cdot\mathbf{r}}\int_{-\infty}^{+\infty}\mathrm{d}\omega\,\chi(\mathbf{q},\omega)e^{-i\omega(t-t_0)} = \\ &= -\frac{4}{\Omega_{cell}}\Theta(t-t_0)\frac{\Delta\epsilon}{\widehat{\Delta\epsilon}}e^{-\eta(t-t_0)}e^{i\mathbf{q_0}\cdot\mathbf{r}}\sin(\widehat{\Delta\epsilon}(t-t_0))\end{aligned}$$

We can write more explicitly the real and imaginary parts as

$$\begin{aligned}\mathrm{Re}\rho_{ind}(\mathbf{r},t) &= -\frac{4}{\Omega_{cell}}\Theta(t-t_0)e^{-\eta(t-t_0)}\frac{\Delta\epsilon}{\sqrt{\Delta\epsilon^2+4v|\tilde{\rho}(\mathbf{q})|^2\Delta\epsilon}}\cos(\mathbf{q_0}\cdot\mathbf{r})\sin(\widehat{\Delta\epsilon}(t-t_0)) \\ \mathrm{Im}\rho_{ind}(\mathbf{r},t) &= -\frac{4}{\Omega_{cell}}\Theta(t-t_0)e^{-\eta(t-t_0)}\frac{\Delta\epsilon}{\sqrt{\Delta\epsilon^2+4v|\tilde{\rho}(\mathbf{q})|^2\Delta\epsilon}}\sin(\mathbf{q_0}\cdot\mathbf{r})\sin(\widehat{\Delta\epsilon}(t-t_0))\end{aligned}$$

From these relations it is visible that the introduction of the Coulomb interaction increases the oscillation frequency (as $\widehat{\Delta\epsilon} > \Delta\epsilon$) and slightly decrease the amplitude of a factor $\frac{\Delta\epsilon}{\widehat{\Delta\epsilon}}$.
While χ^0 stands for independent interband transitions, in χ the interaction between electrons is taken into account: this is the first step to describe collective phenomena, like plasmons.

χ^0 as a two dimensional matrix

In order to model the inclusion of local field effects, let us consider now the case of χ^0 for one transition with energy ΔE, but besides $\mathbf{G}_0 = (0,0,0)$ let us take also other diagonal elements, let us name it with a generic $\mathbf{G}_x$. Our χ^0 has then the form

$$\chi^0_{\mathbf{GG}}(\mathbf{q_r},\omega) = \begin{bmatrix} \chi^0_{\mathbf{G}_0\mathbf{G}_0}(\mathbf{q_r},\omega) & \chi^0_{\mathbf{G}_0\mathbf{G}_x}(\mathbf{q_r},\omega) \\ \\ \chi^0_{\mathbf{G}_x\mathbf{G}_0}(\mathbf{q_r},\omega) & \chi^0_{\mathbf{G}_x\mathbf{G}_x}(\mathbf{q_r},\omega) \end{bmatrix}.$$

where the four elements are

$$\begin{aligned}
\chi^0_{\mathbf{G}_0\mathbf{G}_0}(\mathbf{q_r},\omega) &= \frac{2}{\Omega_{cell}}\left[\frac{|\rho_{12}(\mathbf{q_r},\mathbf{G_0})|^2}{\omega-\Delta\epsilon+i\eta} - \frac{|\rho_{21}(\mathbf{q_r},\mathbf{G_0})|^2}{\omega+\Delta\epsilon+i\eta}\right] \\
\chi^0_{\mathbf{G}_x\mathbf{G}_x}(\mathbf{q_r},\omega) &= \frac{2}{\Omega_{cell}}\left[\frac{|\rho_{12}(\mathbf{q_r},\mathbf{G}_x)|^2}{\omega-\Delta\epsilon+i\eta} - \frac{|\rho_{21}(\mathbf{q_r},\mathbf{G}_x)|^2}{\omega+\Delta\epsilon+i\eta}\right] \\
\chi^0_{\mathbf{G}_0\mathbf{G}_x}(\mathbf{q_r},\omega) &= \frac{2}{\Omega_{cell}}\left[\frac{\tilde\rho_{12}(\mathbf{q_r},\mathbf{G_0})\tilde\rho^*_{12}(\mathbf{q_r},\mathbf{G}_x)}{\omega-\Delta\epsilon+i\eta} - \frac{\tilde\rho_{21}(\mathbf{q_r},\mathbf{G_0})\tilde\rho^*_{21}(\mathbf{q_r},\mathbf{G}_x)}{\omega+\Delta\epsilon+i\eta}\right] \\
\chi^0_{\mathbf{G}_x\mathbf{G}_0}(\mathbf{q_r},\omega) &= \frac{2}{\Omega_{cell}}\left[\frac{\tilde\rho_{12}(\mathbf{q_r},\mathbf{G}_x)\tilde\rho^*_{12}(\mathbf{q_r},\mathbf{G_0})}{\omega-\Delta\epsilon+i\eta} - \frac{\tilde\rho_{21}(\mathbf{q_r},\mathbf{G_0})\tilde\rho^*_{21}(\mathbf{q_r},\mathbf{G_0})}{\omega+\Delta\epsilon+i\eta}\right]
\end{aligned}$$

From Eq.(6.11) we see that we just need to sum over the left wing, that is $\chi_{\mathbf{G_0G_0}}$ and $\chi_{\mathbf{G}_x\mathbf{G_0}}$. From the previous paragraphs we know the general formula

$$\int_{-\infty}^{+\infty} \mathrm{d}\omega \left[\frac{A}{\omega-\Delta\epsilon+i\eta} - \frac{B}{\omega+\Delta\epsilon+i\eta}\right] e^{i\omega(t-t_0)} = 2\Theta(t-t_0)\pi i e^{-\eta(t-t_0)}\left[Be^{i\Delta\epsilon(t-t_0)} - Ae^{-i\Delta\epsilon(t-t_0)}\right]$$

Then in this case we find for the induced charge density, using Eq.(6.11) and dropping the dependence of $\tilde\rho$'s on $\mathbf{q_r}$ for simplicity:

$$\begin{aligned}
\widehat{\rho}_{ind}(\mathbf{r},t) &= \frac{1}{2\pi}\cdot\frac{2}{\Omega_{cell}}\cdot 2\Theta(t-t_0)\pi i e^{-\eta(t-t_0)}\cdot \\
&\cdot\Bigg[e^{i(\mathbf{q_r}+\mathbf{G_0})\cdot\mathbf{r}}\Big(2i|\tilde\rho(\mathbf{G_0})|^2\sin(\Delta\epsilon(t-t_0)\Big) + \\
&+ e^{i(\mathbf{q_r}+\mathbf{G}_x)\cdot\mathbf{r}}\Big(\tilde\rho_{21}(\mathbf{G}_0)\tilde\rho^*_{21}(\mathbf{G}_x)e^{i\Delta\epsilon(t-t_0)} - \tilde\rho_{12}(\mathbf{G}_x)\tilde\rho^*_{12}(\mathbf{G_0})e^{-i\Delta\epsilon(t-t_0)}\Big)\Bigg] = \\
&= \frac{2i}{\Omega_{cell}}\Theta(t-t_0)e^{-\eta(t-t_0)}e^{i\mathbf{q_r}\cdot\mathbf{r}}\cdot \\
&\cdot\Bigg[2ie^{i\mathbf{G_0}\cdot\mathbf{r}}|\tilde\rho(\mathbf{G_0})|^2\sin(\Delta\epsilon(t-t_0)) + \\
&+ e^{i\mathbf{G}_x\cdot\mathbf{r}}\Big(\tilde\rho_{21}(\mathbf{G}_0)\tilde\rho^*_{21}(\mathbf{G}_x)e^{i\Delta\epsilon(t-t_0)} - \tilde\rho_{12}(\mathbf{G}_x)\tilde\rho^*_{12}(\mathbf{G_0})e^{-i\Delta\epsilon(t-t_0)}\Big)\Bigg]
\end{aligned}$$

This formula can be easily extended to an arbitary number of off-diagonal elements:

$$\begin{aligned}
\widehat{\rho}_{ind}(\mathbf{r},t) &= \frac{2i}{\Omega_{cell}}\Theta(t-t_0)e^{-\eta(t-t_0)}e^{i\mathbf{q_r}\cdot\mathbf{r}}\cdot \\
&\cdot\left[\sum_{\mathbf{G}_i} e^{i\mathbf{G}_i\cdot\mathbf{r}}\Big(\tilde\rho_{21}(\mathbf{G}_0)\tilde\rho^*_{21}(\mathbf{G}_i)e^{i\Delta\epsilon(t-t_0)} - \tilde\rho_{12}(\mathbf{G}_i)\tilde\rho^*_{12}(\mathbf{G_0})e^{-i\Delta\epsilon(t-t_0)}\Big)\right] \qquad (6.16)
\end{aligned}$$

The real and imaginary part are no more easy to recognize, because the off-diagonal elements mix all up. This is related to the reason why the real and imaginary part behave so strangely in our results, and will be later analyzed more in detail.

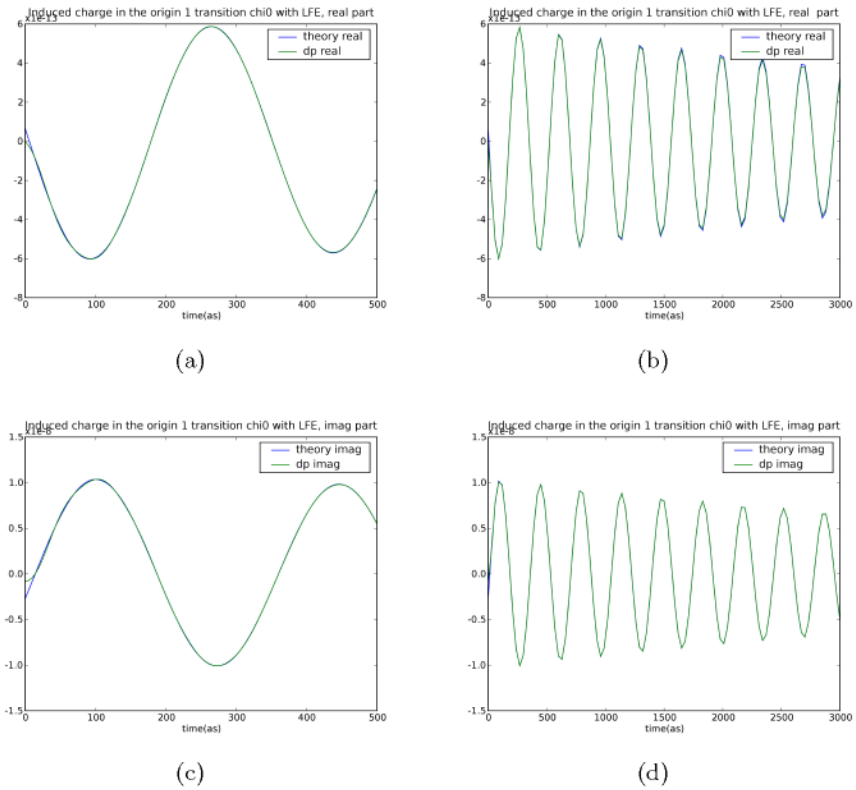

Figure 6.20: Inclusion of local field effects. Comparison between the induced charge near the origin as obtained by numerical integration of the χ^0 obtained from DP and by the analytical formula (6.16) with the inclusion of the first 5 shells of $\mathbf{G}$ vectors. Now the difference of orders of magnitude is reversed, and the imaginary part is bigger.

What we have understood

In our analytical approach we have found both the features that we were not able to explain starting from the results in the not-simplified case. This both ensures about the reliabilty of our program and, which is more important, allows us to understand something more about the physical meaning of what we are observing.

The delay in the maximum of the response appears since the very beginning, in the one-transition case: it represents the time needed by the system to reach its maximum reaction, just like it happens in a classical harmonic oscillator system when it is struck by an external "kick". When more transitions and complications are added, the delay is still present and its value changes with the weight of the other transitions included; in this sense, this quantity can be seen as a characteristic time of the response of the electronic system.

The disappearing of the real part in the $\mathbf{q_0} \to 0$ case seems to be due to the inclusion of local field effects, as shown in the last paragraph. We can see this more explicitly in an alternative way:

Importance of Local Field Effects

Now that we have understood something of the physics with the analytical solutions, we can rely on mathematics to find out more about the nature of $\widehat{\rho}_{ind}$.
We start once again from the external potential

$$\widehat{V}_{ext}(\mathbf{r},t) = e^{i\mathbf{q_0}\cdot\mathbf{r}}\delta(t-t_0)$$

In the limit of small $\mathbf{q_0}$, we have $\mathbf{q_0}\cdot\mathbf{r} \ll 1$ and it is possible to consider the Taylor expansion of the previous expression:

$$\begin{aligned}\widehat{V}_{ext}(\mathbf{r},t) &= \Big[\cos(\mathbf{q_0}\cdot\mathbf{r}) + i\sin(\mathbf{q_0}\cdot\mathbf{r})\Big]\delta(t-t_0) = \\ &\simeq \Big[1-(\mathbf{q_0}\cdot\mathbf{r})^2\Big]\delta(t-t_0) + i\mathbf{q_0}\cdot\mathbf{r}\delta(t-t_0)\end{aligned}$$

The real part of the external potential seems to be dominant with $1 > \mathbf{q_0}\cdot\mathbf{r}$.
We know that the expression for the induced charge in real space is (see Eq.(B.10))

$$\rho_{ind}(\mathbf{r},t) = \int \mathrm{d}\mathbf{r}' \int \mathrm{d}t' \chi(\mathbf{r},\mathbf{r}',t-t')V_{ext}(\mathbf{r}',t')$$

$\chi(\mathbf{r},t)$ is real, and we have just seen V_{ext} to be nearly real: so we would expect ρ_{ind} to be real too, which would mean $\widehat{\rho}_{ind} = \widehat{\rho}^*_{ind}$.
For this perturbation we have

$$\widehat{\rho}_{ind}(\mathbf{r},t) = \frac{1}{2\pi\Omega}\sum_{\mathbf{G}} e^{i(\mathbf{q_{r0}}+\mathbf{G})\cdot\mathbf{r}} \int_{-\infty}^{+\infty} \mathrm{d}\omega\, \chi_{\mathbf{GG_0}}(\mathbf{q_{r0}},\omega)e^{-i\omega(t-t_0)} \tag{6.17}$$

$$\begin{aligned}\widehat{\rho}^*_{ind}(\mathbf{r},t) &= \frac{1}{2\pi\Omega}\sum_{\mathbf{G}} e^{-i(\mathbf{q_{r0}}+\mathbf{G})\cdot\mathbf{r}} \int_{-\infty}^{+\infty} \mathrm{d}\omega\, \chi^*_{\mathbf{GG_0}}(\mathbf{q_{r0}},\omega)e^{i\omega(t-t_0)} = \\ &= \frac{1}{2\pi\Omega}\sum_{-\mathbf{G}} e^{i(-\mathbf{q_{r0}}+\mathbf{G})\cdot\mathbf{r}} \int_{-\infty}^{+\infty} \mathrm{d}\omega\, \chi^*_{-\mathbf{GG_0}}(\mathbf{q_{r0}},-\omega)e^{-i\omega(t-t_0)}\end{aligned}$$

where we have used the change of variables $\mathbf{G} \to -\mathbf{G}$ and $\omega \to -\omega$ [5].
To compare the two and test the reality of $\widehat{\rho}$, we use the symmetry property

$$\chi(\mathbf{q},\mathbf{q}',\omega) = \chi^*(-\mathbf{q},-\mathbf{q}',-\omega)$$

related to the fact that $\chi(\mathbf{r},t)$ is real. We get

$$\widehat{\rho}^*_{ind}(\mathbf{r},t) = \frac{1}{2\pi\Omega}\sum_{-\mathbf{G}} e^{i(-\mathbf{q_{r0}}+\mathbf{G})\cdot\mathbf{r}} \int_{-\infty}^{+\infty} \mathrm{d}\omega\, \chi_{\mathbf{G}-\mathbf{G_0}}(-\mathbf{q_{r0}},\omega)e^{-i\omega(t-t_0)} \tag{6.18}$$

By comparing Eqs.(6.17) and (6.18) we deduce the conditions for $\widehat{\rho}_{ind}(\mathbf{r},t)$ to be real:

[5] $\displaystyle\int_{-\infty}^{+\infty} \mathrm{d}\omega\, f(\omega) = \int_{+\infty}^{-\infty} \mathrm{d}(-\omega)\, f(-\omega) = \int_{-\infty}^{+\infty} \mathrm{d}\omega\, f(-\omega)$

- the sum must contain $\mathbf{G}$ and $-\mathbf{G}$;
- $\mathbf{q_0} \to 0$;
- $\mathbf{G_0} = 0$

Our calculation satisfies the first two conditions, but the inclusion of off-diagonal elements makes the third condition not always fulfilled.
Let us name

$$C(\mathbf{G},\omega) = \frac{1}{2\pi\Omega}\, e^{i\mathbf{G}\cdot\mathbf{r}} e^{-i\omega(t-t_0)}$$

Then we can write

$$\widehat{\rho}_{ind}(\mathbf{r},t) = \sum_{\mathbf{G}} \int_{-\infty}^{+\infty} \mathrm{d}\omega\, C(\mathbf{G},\omega) e^{i\mathbf{q_0}\cdot\mathbf{r}} \chi_{\mathbf{G}0}(\mathbf{q_0},\omega)$$

$$\widehat{\rho}^{*}_{ind}(\mathbf{r},t) = \sum_{\mathbf{G}} \int_{-\infty}^{+\infty} \mathrm{d}\omega\, C(\mathbf{G},\omega) e^{-i\mathbf{q_0}\cdot\mathbf{r}} \chi_{\mathbf{G}0}(-\mathbf{q_0},\omega)$$

With the condition $\mathbf{q_0} \to 0$ we can simplify by taking the Taylor expansion:

$$\widehat{\rho}_{ind}(\mathbf{r},t) = \sum_{\mathbf{G}} \int_{-\infty}^{+\infty} \mathrm{d}\omega\, C(\mathbf{G},\omega)(1 + i\mathbf{q_0}\cdot\mathbf{r}) \chi_{\mathbf{G}0}(\mathbf{q_0},\omega)$$

$$\widehat{\rho}^{*}_{ind}(\mathbf{r},t) = \sum_{\mathbf{G}} \int_{-\infty}^{+\infty} \mathrm{d}\omega\, C(\mathbf{G},\omega)(1 - i\mathbf{q_0}\cdot\mathbf{r}) \lambda_{\mathbf{G}}\, \chi_{\mathbf{G}0}(\mathbf{q_0},\omega)$$

where the value taken by $\lambda_{\mathbf{G}}$

$$\lambda_{\mathbf{G}} = \begin{cases} +1 & \text{if } \mathbf{G} = 0 \\ -1 & \text{else} \end{cases}$$

derives from the symmetry relations that are valid in the case $\mathbf{q} \to 0$[61]:

$$\chi_{00}(\mathbf{q},\omega) = \chi_{00}(-\mathbf{q},\omega)$$
$$\chi_{\mathbf{G}0}(\mathbf{q},\omega) = \chi_{\mathbf{G}0}(-\mathbf{q},\omega)$$

Hence we find for the real and imaginary parts of $\widehat{\rho}_{ind}(\mathbf{r},t)$:

$$\begin{aligned}
\mathrm{Re}\{\widehat{\rho}_{ind}(\mathbf{r},t)\} &= \frac{1}{2}\Big[\widehat{\rho}_{ind}(\mathbf{r},t) + \widehat{\rho}^{*}_{ind}(\mathbf{r},t)\Big] = \\
&= \frac{1}{2}\sum_{\mathbf{G}} \int_{-\infty}^{+\infty} \mathrm{d}\omega\, C(\mathbf{G},\omega)\, \chi_{\mathbf{G}0}(\mathbf{q_0},\omega)\Big[(1 + i\mathbf{q_0}\cdot\mathbf{r}) + (1 - i\mathbf{q_0}\cdot\mathbf{r})\lambda_{\mathbf{G}}\Big] = \\
&= \int_{-\infty}^{+\infty} \mathrm{d}\omega \Big[\underbrace{1\cdot C(0,\omega)\, \chi_{00}(\mathbf{q_0},\omega)}_{\text{head}} + \underbrace{i(\mathbf{q_0}\cdot\mathbf{r}) \sum_{\mathbf{G}\neq 0} C(\mathbf{G},\omega)\, \chi_{\mathbf{G}0}(\mathbf{q_0},\omega)}_{\text{off-diagonal}} \Big]
\end{aligned}$$

$$\begin{aligned}
\mathrm{Im}\{\widehat{\rho}_{ind}(\mathbf{r},t)\} &= \frac{1}{2i}\Big[\widehat{\rho}_{ind}(\mathbf{r},t) - \widehat{\rho}^{*}_{ind}(\mathbf{r},t)\Big] = \\
&= \frac{1}{2i}\sum_{\mathbf{G}} \int_{-\infty}^{+\infty} \mathrm{d}\omega\, C(\mathbf{G},\omega)\, \chi_{\mathbf{G}0}(\mathbf{q_0},\omega)\Big[(1 + i\mathbf{q_0}\cdot\mathbf{r}) - (1 - i\mathbf{q_0}\cdot\mathbf{r})\lambda_{\mathbf{G}}\Big] = \\
&= \int_{-\infty}^{+\infty} \mathrm{d}\omega \Big[\underbrace{(\mathbf{q_0}\cdot\mathbf{r})\, C(0,\omega)\, \chi_{00}(\mathbf{q_0},\omega)}_{\text{head}} + \underbrace{i(-1) \sum_{\mathbf{G}\neq 0} C(\mathbf{G},\omega)\, \chi_{\mathbf{G}0}(\mathbf{q_0},\omega)}_{\text{off-diagonal}} \Big]
\end{aligned}$$

where the contribution of the head of the matrix and of the off-diagonal elements have been clearly separated.
Thus we see that if the medium is considered as homogeneous, and just the component $\mathbf{G} = 0$ is taken into account, the real part is actually dominant over the imaginary part, because the same kind of term $C(0, \omega)\, \chi_{00}(\mathbf{q_0}, \omega)$ is weighted by 1 and by $(\mathbf{q_0} \cdot \mathbf{r})$, respectively.

Things are completely changed by the inclusion of the local field components, because they give a greater contribution to the imaginary part. The final result is actually reversed with respect to what we were expecting for, and the real part of the charge becomes nearly zero.
Even if the problem we have analyzed this is an ideal case, it clearly shows that local field effects are absolutely necessary to the comprehension of microscopic dynamics.

Conclusions

The aim of this theoretical work has been the implementation of a method to calculate the charge density induced in a system by an external perturbation in real space and time, following an idea suggested by the experimental paper [2].
The key quantity needed by this technique is the polarizability in frequency and momentum space $\chi(\mathbf{q}, \mathbf{q}', \omega)$ (a matrix $\chi_{\mathbf{G}\mathbf{G}'}(\mathbf{q}, \omega)$ in the case of crystals), which can be experimentally measured through Energy Loss experiments and to which two Fourier Transforms can be applied in order to obtain the response in real space and time. In this work, this general technique has been applied to graphite.

A particular emphasis has been given to the study of the off-diagonal elements of $\chi_{\mathbf{G}\mathbf{G}'}(\mathbf{q}, \omega)$, which are not considered in the reference article [2] because of the difficulty in their experimental determination.
The calculation of χ has been carried out by using the techniques of Theoretical Spectroscopy, and then postprocessed with a newly implemented Python code. We have performed calculations of the response of our system to two test external perturbations, a plane wave potential and a delta perturbation in time. Thanks to these applications, it has been possible to explicitly show that the inclusion of off-diagonal elements allows to reach an atomic resolution, and a study was carried out about which elements contribute the most to this resolution.
The time development of the system response was investigated through both numerical calculations and simple analytical models. The relation between the observed charge oscillations and plasmon excitations was also studied, allowing thus an analysis of their nature, by discovering which electrons contribute to the excitations.
The high-frequency behaviour of the off-diagonal elements has also been studied in detail and compared with simple analytical models.

Possible perspectives of this work could be the implementation of other perturbations, for example a delta perturbation in space and time. This would allow the study of the different behaviour of localized and delocalized excitations, their behaviour in an anisotropic medium and their time evolution. This would represent a further step in order to give theoretical support to experimental works on the subject of electronic dynamics.

A

Linear Response Functions and Kramers Kronig Relations

Under the action of an external perturbation, a system responds in its own characteristic way [7]. If we consider a measurable property X whose unperturbed value is X_0, we can write his perturbed value in the linear approximation as

$$X = X_0 + \delta X$$

In general, the induced response to an external stimulus f (usually an electromagnetic wave) can be written in the linear approximation as

$$\delta X(\mathbf{r}, t) = \iint_{-\infty}^{+\infty} \mathrm{d}\mathbf{r}'\mathrm{d}t'\, G(\mathbf{r}, \mathbf{r}', t, t') f(\mathbf{r}', t') \tag{A.1}$$

Equation (A.1) describes the response $\delta X(\mathbf{r}, t)$ of the system in the point $\mathbf{r}$ at a time t to the perturbation $f(\mathbf{r}', t')$. The function $G(\mathbf{r}, \mathbf{r}', t, t')$ is called the response function.
If we assume that the time is uniform, we can write

$$G(\mathbf{r}, \mathbf{r}', t, t') = G(\mathbf{r}, \mathbf{r}', t - t')$$

The complicated dependence on $\mathbf{r}$ and $\mathbf{r}'$ in the spatial part can be simplified only in a local approximation, i.e. if one assumes that what happens at a particular place depends only on the fields existing at that place; in this case one would have:

$$G(\mathbf{r}, \mathbf{r}', t, t') = \delta(\mathbf{r} - \mathbf{r}')G(\mathbf{r}, t - t')$$

However, this dependence cannot be neglected in the phenomena we are considering in this work (such as collective oscillations). However, here we are interested in properties concerning the temporal dependence, so we will focus on this one.
We have to include the requirement that the system is causal:

$$G(\mathbf{r}, \mathbf{r}', t - t') = 0 \qquad t < t' \tag{A.2}$$

If one passes in frequency domain, an easier expression in obtained for the temporal part:

$$\delta X(\omega) = G(\omega) f(\omega) \tag{A.3}$$

In terms of Fourier transforms, a monochromatic stimulus $f(\omega)$ is just multiplied by $G(\omega)$ to give the response $\delta X(\omega)$.

If $G(\omega)$ has a pole at $\omega = \omega_0$, i.e. the denominator of $G(\omega)$ vanishes at $\omega = \omega_0$, then there can be a finite response in the absemce of a stimulus. This means that ω_0 corresponds to the eigenfrequency of a normal mode of the system. For example, in plasma oscillations we have the condition

$$\mathbf{D} = \mathbf{E}^{ext} = \varepsilon \mathbf{E} = 0 \tag{A.4}$$

for the plasma oscillation to sustain itself in the absence of an external field. If we write Eq.(A.4) in a form analogous to (A.3)

$$\mathbf{E} = \varepsilon^{-1} \mathbf{E}^{ext} \neq 0$$

we see that ε^{-1} is the response function. Since the poles of the response function give the normal modes or elementary excitations of the system, it is the zeros of the dielectric function that give these natural frequencies.

A.1 Kramers-Kronig Relations

Response functions have some very important properties. In particular their real and imaginary parts are connected by an interesting relationship.
Let ω be complex, $\hat{\omega} = \omega_1 + i\omega_2$. Then

$$G(\omega) = \int \mathrm{d}t\, G(t-t') e^{i\hat{\omega}(t-t')} = \int \mathrm{d}t\, G(t-t') e^{i\omega_1(t-t')} e^{-\omega_2(t-t')}$$

The factor $e^{i\omega_1(t-t')}$ is bounded at all frequencies, while $e^{-\omega_2(t-t')}$ is bounded only in the upper half-plane for $t - t' > 0$ and in the lower half-plane for $t - t' < 0$. Then the requirement of causality (A.2) requires the integral to be evaluated in the upper-half plane.
Now, let ω be on the real axis. From Cauchy's theorem one can obtain

$$G(\omega) = \frac{1}{i\pi} \mathrm{pv} \int_{-\infty}^{+\infty} \frac{\mathrm{d}\omega' G(\omega')}{\omega' - \omega}$$

where pv stands for principal value. If we now split $G(\omega)$ into its real and imaginary parts, we get

$$\mathrm{Re}G(\omega) = \frac{1}{\pi} \mathrm{pv} \int_{-\infty}^{+\infty} \frac{\mathrm{d}\omega' \mathrm{Im}G(\omega')}{\omega' - \omega} \tag{A.5}$$

$$\mathrm{Im}G(\omega) = -\frac{1}{\pi} \mathrm{pv} \int_{-\infty}^{+\infty} \frac{\mathrm{d}\omega' \mathrm{Re}G(\omega')}{\omega' - \omega} \tag{A.6}$$

We see that the real and imaginary parts of the response function are not independent: they are connected by means of formulas called dispersion relations. Eqs.(A.5) are the so-called Kramers-Kronig relations, and imply that one can reconstruct one part if he knows the other, but at all frequencies!
Kramers-Kronig relations can also say something about real and imaginary parts of ε, for which they are usually written in terms of integrals over positive frequencies by exploiting the symmetry properties:

$$\varepsilon_1(\omega) - 1 = \frac{2}{\pi} \mathrm{pv} \int_0^{+\infty} \frac{\mathrm{d}\omega' \varepsilon_2(\omega')}{\omega' - \omega} \tag{A.7}$$

$$\varepsilon_2(\omega) = \frac{2\omega}{\pi} \mathrm{pv} \int_0^{+\infty} \frac{\mathrm{d}\omega' [\varepsilon_1(\omega') - 1]}{\omega' - \omega} \tag{A.8}$$

A.1.1 Physical interpretation

We have seen that the condition of causality imposes some general relationships between the real and imaginary parts of any causal functions in a purely mathematical treatment. We can also see that some kind of relationships must exist between real and imaginary parts with a simple picture.
Consider a single pulse of radiation incident on a system at time $t = 0$, and suppose that the system can absorb only a narrow band of frequencies, only one in the most simplified limit. This monochromatic component has an infinite time extension. To get the response of the system we substract this component to the incident pulse: we get something which is clearly nonsense, because no physical system can have an output before the arrival of the input signal. This means that the response function of the system cannot simply describe the absorption, it must also describe the way in which all other frequency components are shifted in phase so that they cancel the absorbed component for times $t < 0$.
Thus the response function must have a real and imaginary part to describe both absorption and phase shift, and the real part at a single frequency must be related to the imaginary part at all other frequency and vice versa: there must be dispersion relations to satisfy causality.

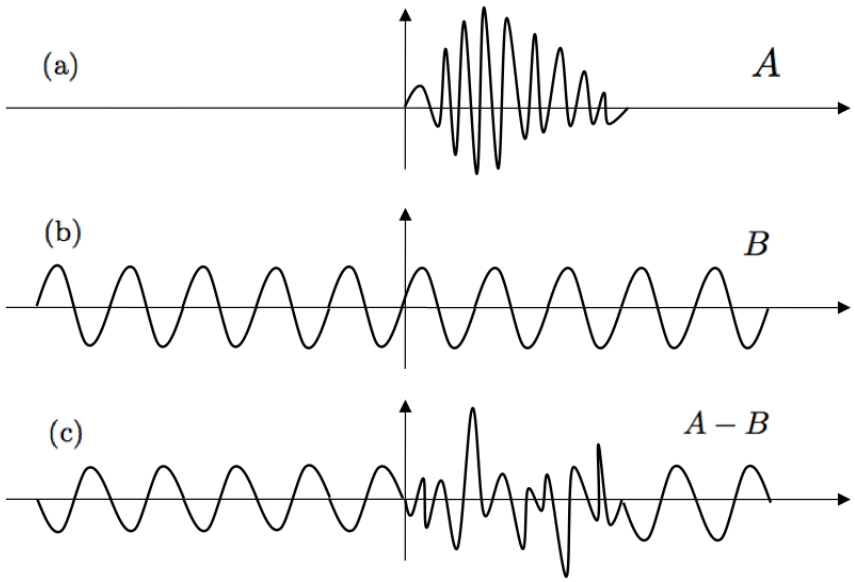

Figure A.1: This figure illustrates schematically the basic reason for the logical connection of causality and dispersion. a) An input A which is zero for times t less than zero is formed as a superposition of many Fourier components b) such as B, each of which extends from $t = -\infty$ to $t = \infty$. These components produce the zero-input signal by destructive interference for $t < 0$. It is impossible to design a system which absorbs just the component B without affecting other components, for in this case, the output (c) would contain the complement of B during times before the onset of the input wave, in contradictions with causality. Thus causality implies that absorption of one frequency must be accompanied by a compensating shift pf phase of other frequencies; the required phase shifts are described by the dispersion relation [62].

A.2 Polarizability

What we want to calculate in this work is the response of the electronic system to an external perturbation. The quantity that expresses this is a response function called polarizability, for which we want to find a general expression [9].
If we consider an external perturbation $F(\mathbf{r},t)$, the perturbation to the system Hamiltonian H_0 is

$$H_1(t) = \int \mathrm{d}\mathbf{r} g(\mathbf{r}) F(\mathbf{r},t)$$

where $g(\mathbf{r})$ is the coupling variable between the perturbation and the system and H_1 is expressed in the interaction picture. It is possible to derive the linear response function in terms of ground state quantities (the many body ground state $N = |\varphi_0\rangle$) and obtain the Kubo formula for the response function, which is valid for an observable g:

$$\chi(\mathbf{r},\mathbf{r}',t-t') = -i\langle N|[g(\mathbf{r},t), g(\mathbf{r}',t')]|N\rangle\Theta(t-t') \tag{A.9}$$

A.2.1 The full polarizability

Let us consider an electronic system subject to an external perturbation V_{ext}: the potential will induce a charge density ρ_{ind}, which in the linear approximation is given by

$$\rho_{ind}(\mathbf{r},t) = \int \mathrm{d}t\mathrm{d}\mathbf{r}'\chi(\mathbf{r},\mathbf{r}',t-t')V_{ext}(\mathbf{r}',t') \tag{A.10}$$

where χ is the polarizability of the electronic system. Here the coupling variable is $\rho(\mathbf{r},t)$ and the perturbative Hamiltonian is

$$H_1(t) = \int \mathrm{d}\mathbf{r}\rho(\mathbf{r},t)V_{ext}$$

It can be shown [9] that in this case

$$\chi(\mathbf{r},\mathbf{r}',\tau) = -i\Theta(\tau)\sum_j \left[f_j(\mathbf{r})f_j^*(\mathbf{r}')e^{i(E_0^N - E_j^N)\tau} - c.c.\right]$$

where $f_j(\mathbf{r}) = \langle N|\rho(\mathbf{r},0)|j_N\rangle$ and E_j^N is the energy of the j^{th} N-particle excited state. In the frequency space

$$\chi(\mathbf{r},\mathbf{r}',\omega) = \sum_j \left[\frac{f_j(\mathbf{r})f_j^*(\mathbf{r}')}{\omega - \Omega_j + i\eta} + \frac{f_j(\mathbf{r})f_j^*(\mathbf{r}')}{\omega + \Omega_j + i\eta}\right] \tag{A.11}$$

From Eq. (A.11) we can see that the full polarizability of the electronic system has poles at the excitation energies of the N-particle system

$$\Omega_j = \pm(E_0^N - E_j^N)$$

which include both resonant and anti-resonant transitions (first and second term in Eq. (A.11).

A.2.2 The Independent-Particle Polarizability

An important case in condensed matter theory is that of an indipendent-particle electronic system subject to an external perturbation. In this case the independent-particle polarizability is [9]

$$\chi^0(\mathbf{r},\mathbf{r}',\omega) = \sum_{\mathbf{k},\mathbf{k}'} \frac{f_{\mathbf{k}}(1-f_{\mathbf{k}'})\phi^*_{\mathbf{k}}(\mathbf{r})\phi_{\mathbf{k}'}(\mathbf{r})\phi^*_{\mathbf{k}'}(\mathbf{r}')\phi_{\mathbf{k}}(\mathbf{r}')}{\omega-\omega_{\mathbf{k}\mathbf{k}'}+i\eta} + \text{anti-resonant term} \tag{A.12}$$

where $\omega_{\mathbf{k}\mathbf{k}'} = \epsilon_{\mathbf{k}} - \epsilon_{\mathbf{k}'}$ is the energy difference of two single-particle levels and $f_{\mathbf{k}}$ is the occupation number of the single-particle orbital.
We can see that the independent particle polarizability has poles at the independent-particle excitation energies. With the anti-resonant term explicitly taken into account, Eq. (A.12) becomes the important result

$$\chi^0(\mathbf{r},\mathbf{r}',\omega) = \sum_{\mathbf{k},\mathbf{k}'} \frac{(f_{\mathbf{k}}-f_{\mathbf{k}'})\phi^*_{\mathbf{k}}(\mathbf{r})\phi_{\mathbf{k}'}(\mathbf{r})\phi^*_{\mathbf{k}'}(\mathbf{r}')\phi_{\mathbf{k}}(\mathbf{r}')}{\omega-\omega_{\mathbf{k}\mathbf{k}'}+i\eta} \tag{A.13}$$

B

Some mathematical implications of symmetry properties in crystals

This chapter is not intended to treat extensively the symmetry properties of crystals, but rather to present some concepts and relations useful for the understanding of the work.

B.1 Direct and Reciprocal Lattice

B.1.1 Bravais Lattice

A fundamental concept in the description of crystalline systems is that of the *Bravais Lattice*, which specifies the periodic array in which the repeated units of the crystal are arranged. It consists of all points in space tith position vectors $\mathbf{R}$ of the form

$$\mathbf{R} = n_1\mathbf{a}_1 + n_2\mathbf{a}_2 + n_3\mathbf{a}_3 \qquad n_1, n_2, n_3 \in \mathbb{Z}$$

where $\mathbf{a}_1$,$\mathbf{a}_2$ and $\mathbf{a}_3$ are the three *primitive vectors* that generate the lattice.
The region of space spanned by the three primitive vectors is one of the possible choices of *primitive unit cell*, a volume of space that when translated through all the vectors in the lattice, just fills all of space without overlapping itself or leaving voids. One important kind of primitive cell is the *Wigner-Seitz* cell: the WS cell about a lattice point is the region of space that is closer to that point than to any other lattice point, and presents the same symmetry properties of the Bravais lattice.

B.1.2 Lattice with a basis

A physical crystal can be described by giving its underlying Bravais lattice, together with a description of the arrangement of atoms within a particular primitive cell. A *crystal structure* consists of identical copies of the same physical unit, called the *basis*, located at all the points of a Bravais lattice. This is the case of important structures like the one of diamond, and is precisely the case of graphite (see §4.1.4).

B.1.3 Reciprocal Lattice

Consider a set of points $\{\mathbf{R}\}$ constituting a Bravais lattice and a plane wave $e^{i\mathbf{k}\cdot\mathbf{r}}$. For general $\mathbf{k}$, such a plane wave will not have the periodicity of the Bravais lattice. The set of all wave vectors $\mathbf{G}$ that yield plane waves with the periodicity of a given Bravais lattice is known as

reciprocal lattice. Analytically $\mathbf{G}$ belongs to the reciprocal lattice of a Bravais lattice of points $\mathbf{R}$ provided that the relation

$$e^{i\mathbf{G}\cdot\mathbf{R}} = 1$$

holds for all the vectors of the Bravais lattice. As a reciprocal lattice is always defined with reference to a Bravais lattice, the latter is often referred to as *direct lattice*.
The $\mathbf{G}$ vectors are spanned by the primitive vectors $\mathbf{b}_1$, $\mathbf{b}_2$ and $\mathbf{b}_3$:

$$\mathbf{G} = n_1\mathbf{b}_1 + n_2\mathbf{b}_2 + n_3\mathbf{b}_3 \qquad n_1, n_2, n_3 \in \mathbb{Z}$$

The $\mathbf{b}_i$ vectors are related to the direct lattice primitive vectors by the relation

$$\mathbf{a_i} \cdot \mathbf{b_j} = 2\pi\delta_{ij}$$

The reciprocal lattice plays a fundamental role in the study of many properties of crystals, like the electronic structure or the diffraction properties.

The Wigner Seitz primitive cell of the reciprocal lattice is known as the *first Brillouin zone* (BZ): this has a great importance, because the symmetry of the systems allows one to describe properties just in the first BZ and from this deducing those of the entire crystal.

B.1.4 Bloch's Theorem

The ions in a perfect crystal are arranged in a regular periodic array. The study of the electrons in the solid corresponds then to the problem of an electron in a potential with the periodicity of the Bravais lattice. This is in principle a many-electron problem, but in the independent electron approximation the electron-electron interactions can be included into an effective periodic potential $U(\mathbf{r})$. Independent electrons, each of which obeys a one electron Schrödinger equation with a periodic potential, are known as *Bloch electrons* and their stationary states have a very important property as a general consequence of the periodicity of the potential:

Bloch's Theorem *The eigenstates of the one-electron Hamiltonian* $H = -\frac{\nabla^2}{2} + U(\mathbf{r})$ *where* $U(\mathbf{r}) = U(\mathbf{R} + \mathbf{r})$ *can be chosen to have the form of plane waves times a function with the periodicity of the Bravais lattice*:

$$\psi_{n\mathbf{k}}(\mathbf{r}) = e^{i\mathbf{k}\cdot\mathbf{r}} u_{n\mathbf{k}}(\mathbf{r})$$

where $u_{n\mathbf{k}}(\mathbf{r})$ *has the periodicity of the Bravais lattice.*

Bloch's theorem leads to a description of the energy levels of an electron in a periodic potential in terms of a family of continuous functions $\epsilon_{n\mathbf{k}}$ with the periodicity of the reciprocal lattice, i. e. the *band structure* of the solid.

B.1.5 Periodic Boundary Conditions and integration in reciprocal space

When calculating properties of an electronic system, one always considers N electrons confined to a volume Ω with dimensions L_1, L_2, L_3. This confinement is mathematically expressed by a boundary condition on the Schrodinger equation: the most frequently used boundary conditions are the so-called Periodic Boundary Conditions (or Born-von Karman boundary condition), which require the wavefunction $\psi_{\mathbf{k}}$ to be periodic with respect to the dimensions L_i.

From these conditions it also possible to obtain [53] the number of allowed k-values per unit volume of $\mathbf{k}$ space:

$$N_{\mathbf{k}} = \frac{\Omega}{(2\pi)^3}$$

This can be used to see how one can sum any smooth function $F(\mathbf{k})$ over all allowed values in $\mathbf{k}$. The volume of k-space per allowed $\mathbf{k}$ value is $\Delta\mathbf{k} = \frac{1}{N_{\mathbf{k}}} = \frac{(2\pi)^3}{\Omega}$ so it is convenient to write

$$\sum_{\mathbf{k}} F(\mathbf{k}) = \frac{8\pi^3}{\Omega} \sum_{\mathbf{k}} F(\mathbf{k})\Delta\mathbf{k}$$

for the limit $\Delta\mathbf{k} \to 0$ (that is, $\Omega \to \infty$) the sum above approaches the integral $\int \mathrm{d}\mathbf{k} F(\mathbf{k})$.
So we can write this general relation for the integration in reciprocal space

$$\lim_{\Omega\to\infty} \frac{1}{\Omega} \sum_{\mathbf{k}} F(\mathbf{k}) = \frac{1}{(2\pi)^3} \int \mathrm{d}\mathbf{k}\, F(\mathbf{k}) \tag{B.1}$$

B.2 Fourier transforms

We show now that all the properties we have resumed could be obtained also from Fourier theory [63].

B.2.1 General definitions

The Fourier transform and antitransform of a general 1D position-dependent function f are in our convention[1]

$$f(r) = \frac{1}{2\pi} \int_{-\infty}^{+\infty} \mathrm{d}k \widehat{f}(k) e^{ikr} \qquad \widehat{f}(k) = \int_{-\infty}^{+\infty} \mathrm{d}r f(r) e^{-ikr} \tag{B.2}$$

Let us apply this general definition to the particular case of a periodic function. Let f have a period L. From Eq. (B.2)

$$\begin{aligned}\widehat{f}(k) &= \int_{-\infty}^{+\infty} \mathrm{d}r f(r) e^{-ikr} = \sum_{n\in\mathbb{Z}} \int_{-\frac{L}{2}+nL}^{-\frac{L}{2}+nL} \mathrm{d}r f(r) e^{-ikr} = \\ &= \int_{-\frac{L}{2}}^{\frac{L}{2}} \mathrm{d}r f(r) e^{-ikr} \sum_{n\in\mathbb{Z}} e^{-inkL}\end{aligned}$$

The last line comes from the variable change $r' = r - nL$ and from the periodicity of $f(r)$. The last sum is nonzero if and only if kL is a multiple of 2π. This defines discrete values

$$k_n = \frac{2\pi}{L} n$$

where Fourier coefficients are non-vanishing (the reciprocal lattice).
The Fourier transform of a periodic function is nothing but a Fourier series[2]:

$$f(r) = \frac{1}{L} \sum_{n\in\mathbb{Z}} \widehat{f}(k_n) e^{ik_n r} \qquad \widehat{f}(k_n) = \int_{-\frac{L}{2}}^{\frac{L}{2}} \mathrm{d}r f(r) e^{-ik_n r}$$

[1] The ambiguity stands in the choice of the volume normalization and the sign of exponentials. This actually has no influence for the final result, as long as one is coherent with himself...

[2] To obtain this, remember that in passing from an integral to a sum, $\mathrm{d}k$ has to be replaced by $\frac{2\pi}{L}$

These expressions tend to the original Fourier transform for $L \to \infty$.
It is possibile to extend this derivation to three dimensional periodic functions with periods $\mathbf{a}_1$, $\mathbf{a}_2$ and $\mathbf{a}_3$:

$$f(\mathbf{r}) = \frac{1}{\Omega_{cell}} \sum_{\mathbf{G}} \widehat{f}(\mathbf{G}) e^{i\mathbf{G}\cdot\mathbf{r}} \qquad \widehat{f}(\mathbf{G}) = \int_{\Omega_{cell}} \mathrm{d}\mathbf{r} f(\mathbf{r}) e^{-i\mathbf{G}\cdot\mathbf{r}} \tag{B.3}$$

where Ω_{cell} is the unit cell and $\mathbf{G}$ are the vectors of the reciprocal lattice.

B.2.2 One-index periodic functions of a crystal

The crystal structure is periodic, with a unit cell of volume Ω_{cell} repeated along 3 directions N_1,N_2 and N_3 times respectively, so that the total volume is given by $\Omega = N_1 N_2 N_3 \Omega_{cell}$. All the observables of a crystal are invariant by application of the same translations, and their Fourier transforms are given by Eq.(B.3). Anyway, the wavefunctions are not observable, so they are *not* periodic functions of $\mathbf{a}_1$, $\mathbf{a}_2$ and $\mathbf{a}_3$.
The Fourier transform $\widehat{f}(\mathbf{K})$ of any function for which the PBC are adopted has $\mathbf{K}$ vectors restricted to

$$\mathbf{K} = \frac{n_1}{N_1}\mathbf{b}_1 + \frac{n_2}{N_2}\mathbf{b}_2 + \frac{n_3}{N_3}\mathbf{b}_3 \qquad n_1, n_2, n_3 \in \mathbb{Z} \tag{B.4}$$

We can write the vector $\mathbf{K}$ as a crystal reciprocal lattice vector plus a vector $\mathbf{q_r}$ that belongs to the first Brillouin zone. Then

$$f(\mathbf{r}) = \frac{1}{\Omega} \sum_{\mathbf{q_r},\mathbf{G}} \widehat{f}(\mathbf{q_r}+\mathbf{G}) e^{i(\mathbf{q_r}+\mathbf{G})\cdot\mathbf{r}} \qquad \widehat{f}(\mathbf{q_r}+\mathbf{G}) = \int_{\Omega} \mathrm{d}\mathbf{r} f(\mathbf{r}) e^{-i(\mathbf{q_r}+\mathbf{G})\cdot\mathbf{r}} \tag{B.5}$$

In this case the normalization is over the total volume $\Omega = N_1 N_2 N_3 \Omega_{cell}$: This because also a normalization over the number of $\mathbf{K}$ is needed.
Notice that this result can be obtained also by applying the relation Eq.(B.1) to the general convention in Eq.(1.21).

B.2.3 Two-index periodic functions

The Fourier transform of a periodic two-index quantity should be expressed as

$$f(\mathbf{r},\mathbf{r}') = \frac{1}{\Omega} \sum_{\mathbf{q_r},\mathbf{q}'_\mathbf{r}} \sum_{\mathbf{G},\mathbf{G}'} e^{i(\mathbf{q_r}+\mathbf{G})\cdot\mathbf{r}} \widehat{f}(\mathbf{q_r}+\mathbf{G},\mathbf{q}'_\mathbf{r}+\mathbf{G}') e^{-i(\mathbf{q}'_\mathbf{r}+\mathbf{G}')\cdot\mathbf{r}'} \tag{B.6}$$

where $\mathbf{q_r}, \mathbf{q}'_\mathbf{r}$ are restricted to the first Brillouin zone. Thanks to the translational invariance of the crystal, this expression can be simplified, and only one $\mathbf{q_r}$ is needed. Tho show this, we recall that for any vector $\mathbf{R}$ of the direct lattice the equality

$$f(\mathbf{r}+\mathbf{R},\mathbf{r}'+\mathbf{R}) = f(\mathbf{r},\mathbf{r}')$$

holds. If we Fourier transform the two sides of this last expression we get

$$\begin{aligned} \sum_{\mathbf{q_r},\mathbf{q}'_\mathbf{r}} \sum_{\mathbf{G},\mathbf{G}'} e^{i(\mathbf{q_r}+\mathbf{G})\cdot(\mathbf{r}+\mathbf{R})} \widehat{f}(\mathbf{q_r}+\mathbf{G},\mathbf{q}'_\mathbf{r}+\mathbf{G}') e^{-i(\mathbf{q}'_\mathbf{r}+\mathbf{G}')\cdot(\mathbf{r}'+\mathbf{R})} = \\ = \sum_{\mathbf{q_r},\mathbf{q}'_\mathbf{r}} \sum_{\mathbf{G},\mathbf{G}'} e^{i(\mathbf{q_r}+\mathbf{G})\cdot\mathbf{r}} \widehat{f}(\mathbf{q_r}+\mathbf{G},\mathbf{q}'_\mathbf{r}+\mathbf{G}') e^{-i(\mathbf{q}'_\mathbf{r}+\mathbf{G}')\cdot\mathbf{r}'} \end{aligned}$$

By definition of a reciprocal lattice vector we know that $e^{i\mathbf{G}\cdot\mathbf{R}} = 1$. Then

$$\sum_{\mathbf{q_r},\mathbf{q'_r}} \left[e^{i(\mathbf{q_r}-\mathbf{q'_r})\cdot\mathbf{R}} - 1\right] \cdot \sum_{\mathbf{G},\mathbf{G'}} e^{i(\mathbf{q_r}+\mathbf{G})\cdot\mathbf{r})}\, \widehat{f}(\mathbf{q_r}+\mathbf{G}, \mathbf{q'_r}+\mathbf{G'}) e^{-i(\mathbf{q'_r}+\mathbf{G'})\cdot\mathbf{r'}} = 0 \tag{B.7}$$

Since this must hold for any function $f(\mathbf{r})$, Eq.(B.7) implies for any direct lattice vector $\mathbf{R}$

$$e^{i(\mathbf{q_r}-\mathbf{q'_r})\cdot\mathbf{R}} = 1$$

which means that $\mathbf{q_r} - \mathbf{q'_r}$ is a reciprocal lattice vector. As $\mathbf{q_r}$ and $\mathbf{q'_r}$ are in the first Brillouin zone, their difference can just be the zero vector: $\mathbf{q_r} - \mathbf{q'_r} = 0$.
From this reasoning we can conclude that the expression for any two index function of a crystal can be written as

$$f(\mathbf{r},\mathbf{r'}) = \frac{1}{\Omega} \sum_{\mathbf{q_r}} \sum_{\mathbf{G},\mathbf{G'}} e^{i(\mathbf{q_r}+\mathbf{G})\cdot\mathbf{r})}\, \widehat{f}_{\mathbf{G}\mathbf{G'}}(\mathbf{q_r}) e^{-i(\mathbf{q'_r}+\mathbf{G'})\cdot\mathbf{r'}} \tag{B.8}$$

with

$$\widehat{f}_{\mathbf{G}\mathbf{G'}}(\mathbf{q'_r}) = \frac{1}{\Omega} \int_{\Omega} \mathrm{d}\mathbf{r}\mathrm{d}\mathbf{r'}\, e^{-i(\mathbf{q_r}+\mathbf{G})\cdot\mathbf{r}} f(\mathbf{r},\mathbf{r'}) e^{i(\mathbf{q_r}+\mathbf{G'})\cdot\mathbf{r'}} \tag{B.9}$$

In the case of two-index periodic functions the volume is required in both the directions of transforming, because there are actually two fourier transforms.
Examples of important two-index periodic functions are the response functions in a non-homogeneous medium, like $\varepsilon(\mathbf{r},\mathbf{r'})$ and $\chi(\mathbf{r},\mathbf{r'})$.
Indeed in the case of a crystal we may express $\chi(\mathbf{q},\mathbf{q'},\omega)$ in form of a matrix:

$$\chi_{\mathbf{G}\mathbf{G'}}(\mathbf{q_r},\omega) = \begin{bmatrix} \chi_{\mathbf{G_0}\mathbf{G_0}}(\mathbf{q_r},\omega) & \chi_{\mathbf{G_0}\mathbf{G_1}}(\mathbf{q_r},\omega) & \cdots & \chi_{\mathbf{G_0}\mathbf{G_N}}(\mathbf{q_r},\omega) \\ \chi_{\mathbf{G_1}\mathbf{G_0}}(\mathbf{q_r},\omega) & \chi_{\mathbf{G_1}\mathbf{G_1}}(\mathbf{q_r},\omega) & \cdots & \chi_{\mathbf{G_1}\mathbf{G_N}}(\mathbf{q_r},\omega) \\ \vdots & & & \\ \chi_{\mathbf{G_N}\mathbf{G_0}}(\mathbf{q_r},\omega) & \chi_{\mathbf{G_N}\mathbf{G_1}}(\mathbf{q_r},\omega) & \cdots & \chi_{\mathbf{G_N}\mathbf{G_N}}(\mathbf{q_r},\omega) \end{bmatrix}$$

This notation implies that $\chi(\mathbf{q},\mathbf{q'})$ in a crystal is nonzero only if $\mathbf{q}$ and $\mathbf{q'}$ differ by a reciprocal lattice vector.
The same formalism can be extended also to the dielectric function ε, which is closely related to χ (see expressions in §3.4).

B.3 Application: induced charge density in a crystal

Let us consider a general electronic system subject to an external perturbation V_{ext}. This potential causes an induced charge density that can be written in terms of the linear response theory (Appendix A) as

$$\rho_{ind}(\mathbf{r},t) = \int \mathrm{d}\mathbf{r'} \int \mathrm{d}t' \chi(\mathbf{r},\mathbf{r'},t-t') V_{ext}(\mathbf{r'},t') \tag{B.10}$$

where χ, the response function, is the polarisability of the electronic system.
In Eq.(B.10), V_{ext} and ρ_{ind} are real, as they have a physical meaning. The response function χ is real in the direct space, even if it is complex in reciprocal space.[3] Eq. (B.10) is the most

[3]This implies symmetry constraints on χ in reciprocal space, such as $\chi(\omega) = \chi^*(-\omega)$

general form, in which there are no hypothesis on the homogeneity of the system: this is the reason why both $\mathbf{r}$ and $\mathbf{r}'$ are present.
In Fourier space

$$\begin{aligned}\rho_{ind}(\mathbf{q},\omega) &= \frac{1}{2\pi}\int \mathrm{d}\mathbf{r}\int \mathrm{d}t e^{-i\mathbf{q}\cdot\mathbf{r}}e^{i\omega t}\rho_{ind}(\mathbf{r},t)\\ &= \frac{1}{2\pi}\int \mathrm{d}\mathbf{r}\int \mathrm{d}t\, e^{-i\mathbf{q}\cdot\mathbf{r}}e^{i\omega t}\int \mathrm{d}\mathbf{r}'\int \mathrm{d}t'\chi(\mathbf{r},\mathbf{r}',t-t')V_{ext}(\mathbf{r}',t')\end{aligned}$$

We use one of the properties of the Fourier Transform: $\mathrm{FT}[f*g]=\mathrm{FT}[f]\cdot\mathrm{FT}[g]$.

$$\frac{1}{2\pi}\int \mathrm{d}t\, e^{i\omega t}\int \mathrm{d}t'\chi(t-t')V_{ext}(t') = \chi(\omega)V_{ext}(\omega) \tag{B.11}$$

Now we see that

$$\rho_{ind}(\mathbf{q},\omega) = \int \mathrm{d}\mathbf{r}\int \mathrm{d}\mathbf{r}' e^{-i\mathbf{q}\cdot\mathbf{r}}\chi(\mathbf{r},\mathbf{r}',\omega)V_{ext}(\mathbf{r}',\omega)$$

We are now left with the Fourier transform in space. We explicitly consider a crystal and express $\mathbf{q}$ as $\mathbf{q_r}+\mathbf{G}$; using Eq.(B.8) we can write $\chi(\mathbf{r},\mathbf{r}',\omega)$ with its Fourier transform and obtain

$$\begin{aligned}\rho_{ind}(\mathbf{q_r}+\mathbf{G},\omega) &= \frac{1}{\Omega}\sum_{\mathbf{q_r}}\sum_{\mathbf{G'G''}}\int \mathrm{d}\mathbf{r}\int \mathrm{d}\mathbf{r}' e^{-i(\mathbf{q_r}+\mathbf{G})\cdot\mathbf{r}}e^{i(\mathbf{q'_r}+\mathbf{G'})\cdot\mathbf{r}}\chi_{\mathbf{G'G''}}(\mathbf{q'_r},\omega)e^{-i(\mathbf{q'_r}+\mathbf{G''})\cdot\mathbf{r}'}V_{ext}(\mathbf{r}',\omega) =\\ &= \frac{1}{\Omega}\sum_{\mathbf{q'_r}}\sum_{\mathbf{G'G''}}\int \mathrm{d}\mathbf{r}'\delta_{\mathbf{q_r q'_r}}\,\delta_{\mathbf{GG'}}\chi_{\mathbf{G'G''}}(\mathbf{q'_r},\omega)e^{-i(\mathbf{q'_r}+\mathbf{G''})\cdot\mathbf{r}'}V_{ext}(\mathbf{r}',\omega) =\\ &= \frac{1}{\Omega}\sum_{\mathbf{G''}}\int \mathrm{d}\mathbf{r}'\chi_{\mathbf{GG''}}(\mathbf{q_r},\omega)e^{-i(\mathbf{q'_r}+\mathbf{G''})\cdot\mathbf{r}'}V_{ext}(\mathbf{r}',\omega) =\\ &= \sum_{\mathbf{G'}}\chi_{\mathbf{GG'}}(\mathbf{q_r},\omega)V_{ext}(\mathbf{q_r}+\mathbf{G}',\omega)\end{aligned} \tag{B.12}$$

From Eq.(B.12) we see that if a perturbation V_{ext} with a certain $\mathbf{q_0}=\mathbf{q_r}+\mathbf{G}$ is sent on a crystal, the induced charge $\rho(\mathbf{q},\omega)$ of the system is given by a linear combination of the components (plane waves) of V_{ext} with $\mathbf{q}$'s that differ only by reciprocal lattice vectors, each weighted by the response function. An external potential with momentum $\mathbf{q_r}+\mathbf{G}_0$ can induce spatial charge fluctuations, whose momentum $\mathbf{q_r}+\mathbf{G}$ differs by any reciprocal lattice vector, and to which the system will *also* respond: these are the crystal LFE. This can be physically interpreted as Bragg scattering of internal fields. In real space, using again Eq.(B.8), this becomes

$$\begin{aligned}\rho_{ind}(\mathbf{r},t) &= \frac{1}{\Omega}\sum_{\mathbf{q_r}}\sum_{\mathbf{G}}\int \mathrm{d}\omega\rho_{ind}(\mathbf{q_r}+\mathbf{G},\omega)e^{i(\mathbf{q_r}+\mathbf{G})\cdot\mathbf{r}}e^{-i\omega t} =\\ &= \frac{1}{\Omega}\sum_{\mathbf{q_r}}\sum_{\mathbf{GG'}}\int \mathrm{d}\omega\,\chi_{\mathbf{GG'}}(\mathbf{q_r},\omega)V_{ext}(\mathbf{q_r}+\mathbf{G}',\omega)e^{i(\mathbf{q_r}+\mathbf{G})\cdot\mathbf{r}}e^{-i\omega t}\end{aligned} \tag{B.13}$$

B.4 Effect of Time reversal symmetry on $\tilde{\rho}$

The general form of $\tilde{\rho}_{nn'\mathbf{k}}(\mathbf{q}+\mathbf{G})$ is

$$\tilde{\rho}_{nn'\mathbf{k}}(\mathbf{q}+\mathbf{G}) = \langle \mathbf{k}-\mathbf{q},n'|e^{-i(\mathbf{q}+\mathbf{G})\cdot\mathbf{r}}|\mathbf{k},n\rangle = \int \mathrm{d}\mathbf{r}\,\psi^*_{\mathbf{k}-\mathbf{q},n'}(\mathbf{r})e^{-i(\mathbf{q}+\mathbf{G})\cdot\mathbf{r}}\psi_{\mathbf{k},n}(\mathbf{r})$$

where the ψ's are Bloch functions.
Time reversal symmetry implies:

$$\epsilon_{n,\mathbf{k}} = \epsilon_{n,-\mathbf{k}}$$
$$\psi_{\mathbf{k},n}(\mathbf{r}) = \psi^*_{-\mathbf{k},n}(\mathbf{r})$$

If we apply this symmetries to our initial definition we have:

$$\tilde{\rho}_{nn'\mathbf{k}}(\mathbf{q}+\mathbf{G}) = \int \mathrm{d}\mathbf{r}\, \psi^*_{-\mathbf{k},n}(\mathbf{r}) e^{-i(\mathbf{q}+\mathbf{G})\cdot\mathbf{r}} \psi_{-(\mathbf{k}-\mathbf{q}),n'}(\mathbf{r}) = \tilde{\rho}_{n'n,-(\mathbf{k}-\mathbf{q})}(\mathbf{q}+\mathbf{G})$$
$$= \left(\int \mathrm{d}\mathbf{r}\, \psi^*_{-\mathbf{k}-(-\mathbf{q}),n'}(\mathbf{r}) e^{+i(\mathbf{q}+\mathbf{G})\cdot\mathbf{r}} \psi_{-\mathbf{k},n}(\mathbf{r}) \right)^* = \tilde{\rho}^*_{nn',-\mathbf{k}}(-\mathbf{q}-\mathbf{G})$$

B.5 Alternative way to calculate an infinite integral of χ

In §6.3 we dealt with the computational problem rising from the integration in Eq.(6.9)

$$\hat{\rho}_{ind}(\mathbf{r},t) = \frac{1}{2\pi\Omega} \sum_{\mathbf{G}} e^{i(\mathbf{q}_{\mathbf{r}0}+\mathbf{G})\cdot\mathbf{r}} \int_{-\infty}^{+\infty} \mathrm{d}\omega\, \chi_{\mathbf{G}\mathbf{G}_\mathbf{0}}(\mathbf{q}_{\mathbf{r}0},\omega) e^{-i\omega(t-t_0)}$$

It is possible to reduce the infinite integration to an integration over the positive values by considering the symmetry properties of χ. We know that χ is real and then

$$\chi(\mathbf{r},\mathbf{r}',t) = \chi^*(\mathbf{r},\mathbf{r}',t)$$

which means in reciprocal space that

$$\chi(\mathbf{q},\mathbf{q}',\omega) = \chi^*(-\mathbf{q},-\mathbf{q}',-\omega)$$

Moreover, time reversal symmetry implies that

$$\chi(\mathbf{q},\mathbf{q}',\omega) = \chi^*(-\mathbf{q}',-\mathbf{q},\omega)$$

Considering these two relations together we get

$$\boxed{\chi(\mathbf{q},\mathbf{q}',\omega) = \chi^*(\mathbf{q}',\mathbf{q},-\omega)}$$

This allows us to write the frequency integral of Eq.(6.9) as

$$\int_{-\infty}^{+\infty} \mathrm{d}\omega\, \chi_{\mathbf{G}\mathbf{G}_\mathbf{0}}(\mathbf{q}_{\mathbf{r}0},\omega) e^{-i\omega t} =$$
$$= \int_{-\infty}^{0} \mathrm{d}\omega\, \chi_{\mathbf{G}\mathbf{G}_\mathbf{0}}(\mathbf{q}_{\mathbf{r}0},\omega) e^{-i\omega t} + \int_{0}^{+\infty} \mathrm{d}\omega\, \chi_{\mathbf{G}\mathbf{G}_\mathbf{0}}(\mathbf{q}_{\mathbf{r}0},\omega) e^{-i\omega t} =$$
$$= \int_{-\infty}^{0} \mathrm{d}\omega\, \chi^*_{\mathbf{G}_\mathbf{0}\mathbf{G}}(\mathbf{q}_{\mathbf{r}0},-\omega) e^{-i\omega t} + \int_{0}^{+\infty} \mathrm{d}\omega\, \chi_{\mathbf{G}\mathbf{G}_\mathbf{0}}(\mathbf{q}_{\mathbf{r}0},\omega) e^{-i\omega t} =$$
$$= \int_{0}^{+\infty} \mathrm{d}\omega\, \chi^*_{\mathbf{G}_\mathbf{0}\mathbf{G}}(\mathbf{q}_{\mathbf{r}0},\omega) e^{i\omega t} + \int_{0}^{+\infty} \mathrm{d}\omega\, \chi_{\mathbf{G}\mathbf{G}_\mathbf{0}}(\mathbf{q}_{\mathbf{r}0},\omega) e^{-i\omega t} =$$
$$= \int_{0}^{+\infty} \mathrm{d}\omega \left[\chi^*_{\mathbf{G}_\mathbf{0}\mathbf{G}}(\mathbf{q}_{\mathbf{r}0},\omega) e^{i\omega t} + \chi_{\mathbf{G}\mathbf{G}_\mathbf{0}}(\mathbf{q}_{\mathbf{r}0},\omega) e^{-i\omega t} \right]$$

The advantage of this formula is that only positive frequencies are needed. On the other hand, also the upper wing of the χ matrix needs to be given in input.

B.6 A delta in space

In §6.3 we studied the effect of a delta perturbation in time. The charge induced by a delta in space

$$\widehat{V}_{ext}(\mathbf{r},t) = \delta^{3D}(\mathbf{r}-\mathbf{r_0})e^{i\omega_0 t}$$
$$\widehat{V}_{ext}(\mathbf{q},\omega) = \delta(\omega-\omega_0)\frac{1}{(2\pi)^3}e^{-i\mathbf{q}\cdot\mathbf{r_0}}$$

would look like

$$\widehat{\rho}_{ind}(\mathbf{q_r}+\mathbf{G},\omega) = \frac{1}{(2\pi)^3}\sum_{\mathbf{G'}}\chi(\mathbf{q_r}+\mathbf{G},\mathbf{q_r}+\mathbf{G'},\omega)e^{-i\mathbf{q}\cdot\mathbf{r_0}}\delta(\omega-\omega_0)$$
$$\widehat{\rho}_{ind}(\mathbf{r},t) = \frac{1}{(2\pi)^3}e^{-i\omega_0 t}\sum_{\mathbf{GG'}}\int_{BZ}\mathrm{d}\mathbf{q_r}\int_{-\infty}^{+\infty}\mathrm{d}\omega\,\chi_{\mathbf{GG'}}(\mathbf{q_r},\omega_0)e^{i\mathbf{q_r}\cdot(\mathbf{r}-\mathbf{r_0})}e^{-i\mathbf{G'}\cdot\mathbf{r_0}}e^{i\mathbf{G}\cdot\mathbf{r}}$$

This last formula represents a huge computational problem: first, the summation over **G** vectors involves in this case all the matrix and not just the left wing. However, this is a minor complication, because DP already calculates all the $\chi_{\mathbf{GG'}}$ elements.
The biggest problem resides in the integral over all the points in the BZ, each of which would require a different DP calculation. What should be done is exploiting symmetries to take the smallest possible number of $\mathbf{q_r}$ for the integral to be converged, and also find a way to solve the problem of the **q** anisotropy around 0 [61].

C
Shells in graphite

We report here the division in shells of the first 239 **G** vectors in graphite. The **G**'s are expressed in reduced coordinates with respect to the primitive vectors of reciprocal space.

$$\mathbf{b_1} = \frac{2\pi}{a}\left(1, \frac{1}{\tan\frac{\pi}{3}}, 0\right)$$
$$\mathbf{b_2} = \frac{2\pi}{a}\left(0, \frac{1}{\sin(\frac{\pi}{3})}, 0\right)$$
$$\mathbf{b_3} = \frac{2\pi}{c}\left(0, 0, 1\right)$$

shell	G-vectors [reduced coordinates]				
1	1 (0 0 0)				
2	2 (0 0 1)	3 (0 0 -1)			
3	4 (0 0 2)	5 (0 0 -2)			
4	6 (0 0 3)	7 (0 0 -3)			
5	8 (1 0 0)	9 (0 -1 0)	10 (-1 1 0)	11 (-1 0 0)	
	12 (0 1 0)	13 (1 -1 0)			
6	14 (1 0 1)	15 (0 -1 -1)	16 (-1 1 -1)	17 (-1 1 1)	
	18 (0 -1 1)	19 (1 0 -1)	20 (-1 0 1)	21 (0 1 -1)	
	22 (1 -1 -1)	23 (1 -1 1)	24 (0 1 1)	25 (-1 0 -1)	
7	26 (1 0 2)	27 (0 -1 -2)	28 (-1 1 -2)	29 (-1 1 2)	
	30 (0 -1 2)	31 (1 0 -2)	32 (-1 0 2)	33 (0 1 -2)	
	34 (1 -1 -2)	35 (1 -1 2)	36 (0 1 2)	37 (-1 0 -2)	
8	38 (0 0 4)	39 (0 0 -4)			
9	40 (1 0 3)	41 (0 -1 -3)	42 (-1 1 -3)	43 (-1 1 3)	
	44 (0 -1 3)	45 (1 0 -3)	46 (-1 0 3)	47 (0 1 -3)	
	48 (1 -1 -3)	49 (1 -1 3)	50 (0 1 3)	51 (-1 0 -3)	
10	52 (0 0 5)	53 (0 0 -5)			
11	54 (1 0 4)	55 (0 -1 -4)	56 (-1 1 -4)	57 (-1 1 4)	
	58 (0 -1 4)	59 (1 0 -4)	60 (-1 0 4)	61 (0 1 -4)	
	62 (1 -1 -4)	63 (1 -1 4)	64 (0 1 4)	65 (-1 0 -4)	
12	66 (1 1 0)	67 (-1 -1 0)	68 (-2 1 0)	69 (-1 2 0)	
	70 (1 -2 0)	71 (2 -1 0)			
13	72 (1 1 1)	73 (-1 -1 -1)	74 (-2 1 -1)	75 (-1 2 1)	
	76 (1 -2 1)	77 (2 -1 -1)	78 (1 1 -1)	79 (-1 -1 1)	
	80 (-2 1 1)	81 (-1 2 -1)	82 (1 -2 -1)	83 (2 -1 1)	

14	84 (1 1 2)	85 (-1 -1 -2)	86 (-2 1 -2)	87 (-1 2 2)
	88 (1 -2 2)	89 (2 -1 -2)	90 (1 1 -2)	91 (-1 -1 2)
	92 (-2 1 2)	93 (-1 2 -2)	94 (1 -2 -2)	95 (2 -1 2)
15	96 (1 0 5)	97 (0 -1 -5)	98 (-1 1 -5)	99 (-1 1 5)
	100 (0 -1 5)	101 (1 0 -5)	102 (-1 0 5)	103 (0 1 -5)
	104 (1 -1 -5)	105 (1 -1 5)	106 (0 1 5)	107 (-1 0 -5)
16	108 (0 0 6)	109 (0 0 -6)		
17	110 (1 1 3)	111 (-1 -1 -3)	112 (-2 1 -3)	113 (-1 2 3)
	114 (1 -2 3)	115 (2 -1 -3)	116 (1 1 -3)	117 (-1 -1 3)
	118 (-2 1 3)	119 (-1 2 -3)	120 (1 -2 -3)	121 (2 -1 3)
18	122 (2 0 0)	123 (0 -2 0)	124 (-2 2 0)	125 (-2 0 0)
	126 (0 2 0)	127 (2 -2 0)		
19	128 (2 0 1)	129 (0 -2 -1)	130 (-2 2 -1)	131 (-2 2 1)
	132 (0 -2 1)	133 (2 0 -1)	134 (-2 0 1)	135 (0 2 -1)
	136 (2 -2 -1)	137 (2 -2 1)	138 (0 2 1)	139 (-2 0 -1)
20	140 (2 0 2)	141 (0 -2 -2)	142 (-2 2 -2)	143 (-2 2 2)
	144 (0 -2 2)	145 (2 0 -2)	146 (-2 0 2)	147 (0 2 -2)
	148 (2 -2 -2)	149 (2 -2 2)	150 (0 2 2)	151 (-2 0 -2)
21	152 (1 1 4)	153 (-1 -1 -4)	154 (-2 1 -4)	155 (-1 2 4)
	156 (1 -2 4)	157 (2 -1 -4)	158 (1 1 -4)	159 (-1 -1 4)
	160 (-2 1 4)	161 (-1 2 -4)	162 (1 -2 -4)	163 (2 -1 4)
22	164 (1 0 6)	165 (0 -1 -6)	166 (-1 1 -6)	167 (-1 1 6)
	168 (0 -1 6)	169 (1 0 -6)	170 (-1 0 6)	171 (0 1 -6)
	172 (1 -1 -6)	173 (1 -1 6)	174 (0 1 6)	175 (-1 0 -6)
23	176 (2 0 3)	177 (0 -2 -3)	178 (-2 2 -3)	179 (-2 2 3)
	180 (0 -2 3)	181 (2 0 -3)	182 (-2 0 3)	183 (0 2 -3)
	184 (2 -2 -3)	185 (2 -2 3)	186 (0 2 3)	187 (-2 0 -3)
24	188 (0 0 7)	189 (0 0 -7)		
25	190 (1 1 5)	191 (-1 -1 -5)	192 (-2 1 -5)	193 (-1 2 5)
	194 (1 -2 5)	195 (2 -1 -5)	196 (1 1 -5)	197 (-1 -1 5)
	198 (-2 1 5)	199 (-1 2 -5)	200 (1 -2 -5)	201 (2 -1 5)
26	202 (2 0 4)	203 (0 -2 -4)	204 (-2 2 -4)	205 (-2 2 4)
	206 (0 -2 4)	207 (2 0 -4)	208 (-2 0 4)	209 (0 2 -4)
	210 (2 -2 -4)	211 (2 -2 4)	212 (0 2 4)	213 (-2 0 -4)
27	214 (1 0 7)	215 (0 -1 -7)	216 (-1 1 -7)	217 (-1 1 7)
	218 (0 -1 7)	219 (1 0 -7)	220 (-1 0 7)	221 (0 1 -7)
	222 (1 -1 -7)	223 (1 -1 7)	224 (0 1 7)	225 (-1 0 -7)
28	226 (0 0 8)	227 (0 0 -8)		
29	228 (2 0 5)	229 (0 -2 -5)	230 (-2 2 -5)	231 (-2 2 5)
	232 (0 -2 5)	233 (2 0 -5)	234 (-2 0 5)	235 (0 2 -5)
	236 (2 -2 -5)	237 (2 -2 5)	238 (0 2 5)	239 (-2 0 -5)

D
High-frequency polarizabilities

One of the problems of the expression (6.9) is the infinite extension of the integral: we have at our disposal $\chi(\omega)$ as calculated by DP and not an anaytical expression. To improve our results, we want to study in more detail the high frequency part of the polarizability we are excluding from the integral by using a finite range of frequencies.

D.1 χ and χ_0 at high frequencies

Let us consider again the independent particle polarizability in the general case

$$\chi^0(\mathbf{q},\mathbf{G},\mathbf{G}',\omega) = \frac{2}{N_{\mathbf{k}}\cdot\Omega_{cell}}\sum_{i,j,\mathbf{k}}\frac{(f_{j,\mathbf{k+q}}-f_{i,\mathbf{k}})\tilde{\rho}_{ij\mathbf{k}}(\mathbf{q},\mathbf{G})\tilde{\rho}^*_{ij\mathbf{k}}(\mathbf{q},\mathbf{G}')}{\omega-(\epsilon_{j,\mathbf{k+q}}-\epsilon_{i,\mathbf{k}})+i\eta}$$

and the diagonal version (no LFE) for the full polarizability χ

$$\begin{aligned}\chi &= \frac{\chi^0}{1-v\chi^0} = \\ &= \frac{2}{N_{\mathbf{k}}\cdot\Omega_{cell}}\sum_{i,j,\mathbf{k}}\frac{(f_{j,\mathbf{k+q}}-f_{i,\mathbf{k}})\tilde{\rho}_{ij\mathbf{k}}(\mathbf{q},\mathbf{G})\tilde{\rho}^*_{ij\mathbf{k}}(\mathbf{q},\mathbf{G}')}{\omega-(\epsilon_{j,\mathbf{k+q}}-\epsilon_{i,\mathbf{k}})+i\eta}\cdot \\ &\cdot\left[1-v\frac{2}{N_{\mathbf{k}}\cdot\Omega_{cell}}\sum_{i,j,\mathbf{k}}\frac{(f_{j,\mathbf{k+q}}-f_{i,\mathbf{k}})\tilde{\rho}_{ij\mathbf{k}}(\mathbf{q},\mathbf{G})\tilde{\rho}^*_{ij\mathbf{k}}(\mathbf{q},\mathbf{G}')}{\omega-(\epsilon_{j,\mathbf{k+q}}-\epsilon_{i,\mathbf{k}})+i\eta}\right]^{-1}\end{aligned}$$

If $\omega\to\infty$, the term in square brakets tends to 1, and $\chi\to\chi^0$. Notice that in this way the Coulomb interaction loses its influence: for high frequencies (and so high energies) the interaction between particles results negligible, and the full polarizability tends to the independent particle one.
This can be seen also from the usual Dyson equation 3.30 in RPA:

$$\begin{aligned}\chi &= \chi^0+\chi^0 v\chi = \\ &= \chi^0+\chi^0 v\chi^0+\chi^0 v\chi^0 v\chi^0+\dots\end{aligned}$$

Then when χ^0 is small (for high frequencies) the two are at first order the same.

In particular we are interested in the left wing of the χ matrix, i.e. the elements $\chi_{\mathbf{G}0}$.

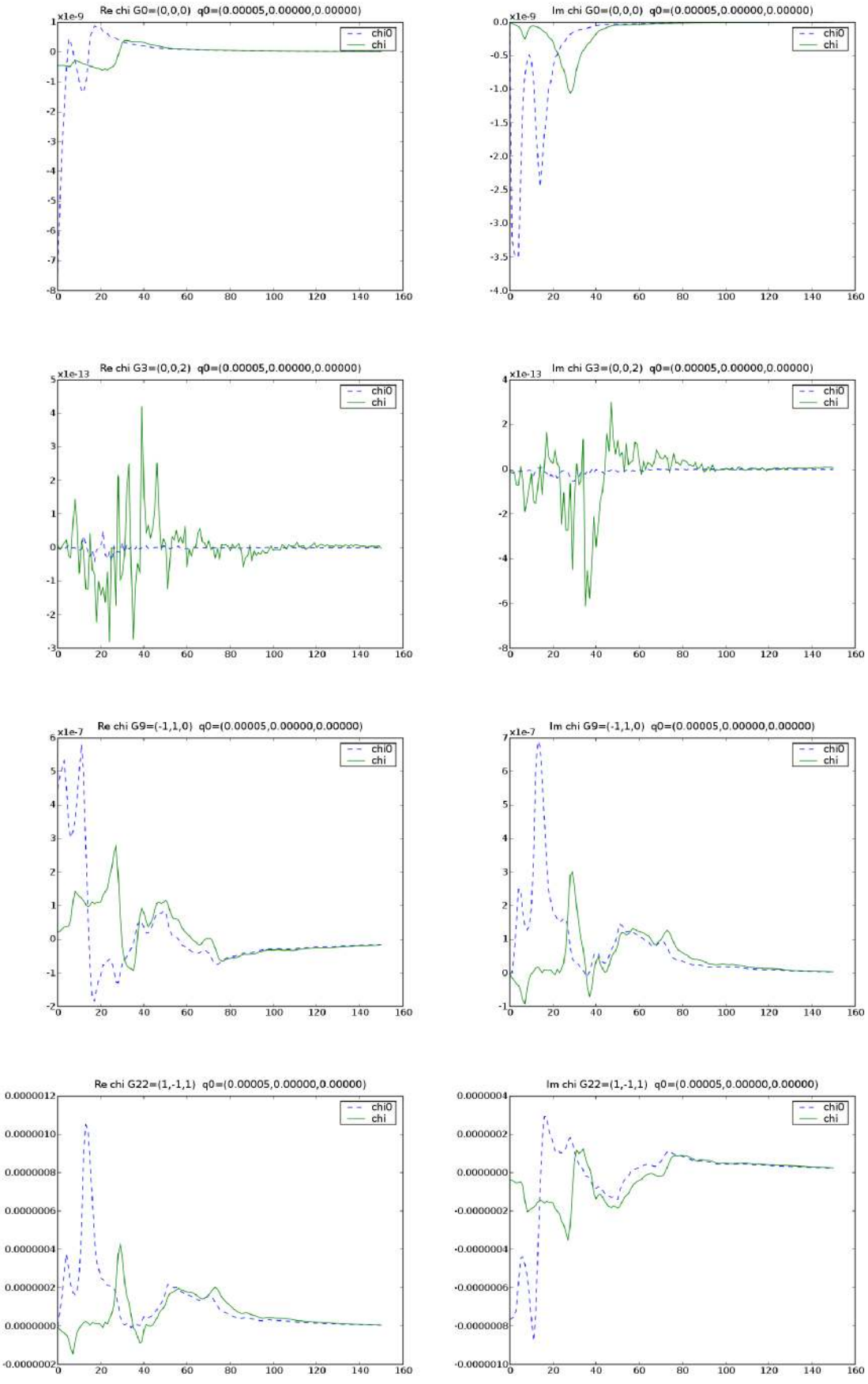

Figure D.1: Real and imaginary part of some $\chi^0_{\mathbf{G0}}$ and $\chi_{\mathbf{G0}}$'s, $\mathbf{q_0} \to 0$

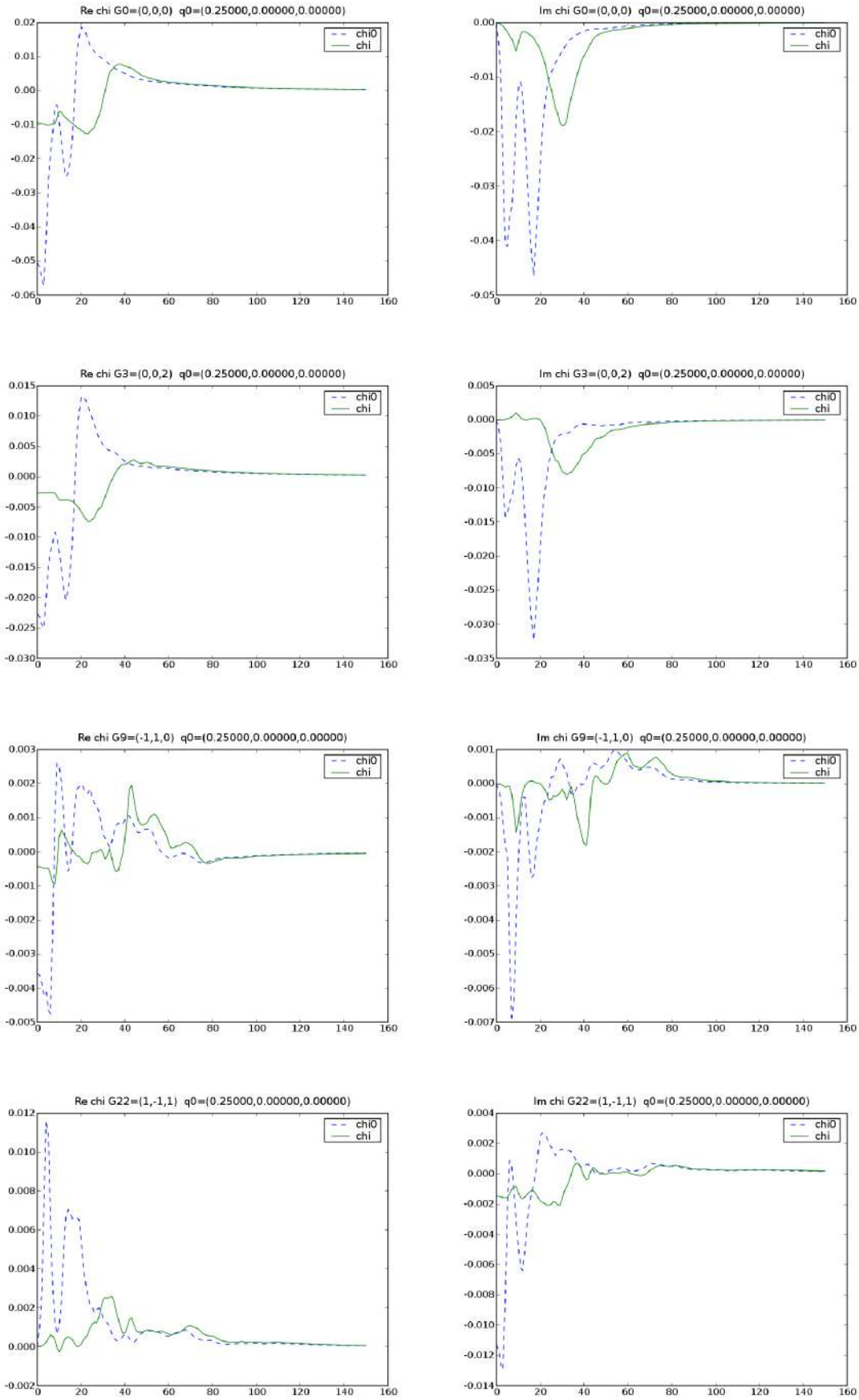

Figure D.2: Real and imaginary part of some $\chi^0_{\mathbf{G0}}$ and $\chi_{\mathbf{G0}}$'s, $\mathbf{q_0} \neq 0$

Figs. D.1 and D.2 represent some examples of the behaviour of the real (on the left) and imaginary part (on the right) of $\chi^0_{\mathbf{G}0}(\omega)$ and $\chi_{\mathbf{G}0}(\omega)$.
We can see that in general the equivalence $\chi^0_{\mathbf{G}0}(\omega) \sim \chi_{\mathbf{G}0}(\omega)$ is valid after $\omega = 80$ eV.
Incidentally, the fact that the matrix elements for $G = (0, 0, 2)$ are nearly zero in the case $\mathbf{q_0} \to 0$ agrees with the results in [55].

D.2 Extrapolation of χ^0

By looking at the Lehmann form of χ^0 (see for example Eq.(6.14)) one can derive that the asymptotic behaviour for $\omega \to \infty$ of χ^0 is

$$\chi^0 \sim \frac{1}{\omega^2}$$

This actually also recalls the form of ε for high frequencies, which is known to be [53]

$$\lim_{\omega\to\infty} \varepsilon_M = 1 - \frac{\omega_P^2}{\omega^2}$$

where ω_P is the plasma frequency. Actually it can be shown [58, 59] that a microscopic matricial form for this asymptotic behaviour is given by

$$\lim_{\omega\to\infty} \varepsilon_{\mathbf{G},\mathbf{G}'}(\mathbf{q_r}, \omega) = \delta_{\mathbf{G}\mathbf{G}'} - \frac{\omega_P^2}{\omega^2} f(\mathbf{G} - \mathbf{G}') \frac{(\mathbf{q_r} + \mathbf{G}) \cdot (\mathbf{q_r} + \mathbf{G}')}{|\mathbf{q_r} + \mathbf{G}|^2} \tag{D.1}$$

where

$$\begin{aligned} f(\mathbf{G}) &= \frac{1}{n} \sum_{\mathbf{k},l} f_0[\epsilon_l(\mathbf{k})] \langle \mathbf{k}, l | e^{i\mathbf{G}\cdot\mathbf{r}} | \mathbf{k}, l \rangle \\ &= \frac{1}{n} \tilde{\rho}(\mathbf{G}) \end{aligned}$$

is the Fourier transform of the electronic density normalized to $f(0) = 1$[1]. We are working in the RPA approximation, so that

$$\varepsilon_{\mathbf{G}\mathbf{G}'}(\mathbf{q_r}, \omega) = \delta_{\mathbf{G}\mathbf{G}'} - v_{\mathbf{G}}(\mathbf{q_r}) \chi^0_{\mathbf{G}\mathbf{G}'}(\mathbf{q_r}, \omega) \tag{D.2}$$

If now we compare Eqs.(D.2) and (D.1) we get an expression for χ^0:

$$\begin{aligned} \chi^0_{\mathbf{G}\mathbf{G}'}(\mathbf{q_r}, \omega) &= \frac{\omega_P^2}{\omega^2} \frac{|\mathbf{q_r} + \mathbf{G}|^2}{4\pi} f(\mathbf{G} - \mathbf{G}') \frac{(\mathbf{q_r} + \mathbf{G}) \cdot (\mathbf{q_r} + \mathbf{G}')}{|\mathbf{q_r} + \mathbf{G}|^2} \\ &= \frac{4\pi n}{\omega^2} \frac{(\mathbf{q_r} + \mathbf{G}) \cdot (\mathbf{q_r} + \mathbf{G}')}{4\pi} \frac{1}{n} \hat{\rho}(\mathbf{G} - \mathbf{G}') = \\ &= \frac{(\mathbf{q_r} + \mathbf{G}) \cdot (\mathbf{q_r} + \mathbf{G}')}{\omega^2} \hat{\rho}(\mathbf{G} - \mathbf{G}') \end{aligned} \tag{D.3}$$

We would like to use the correspondance between the two polarizabilities at high frequencies and this formula to complete the integral in Eq.(6.9).
Let us compare the result of the extrapolation using Eq. (D.3) with the tails of $\chi^0_{\mathbf{G}0}$ and $\chi_{\mathbf{G}0}$ and with a $\frac{1}{\omega^2}$ fit.

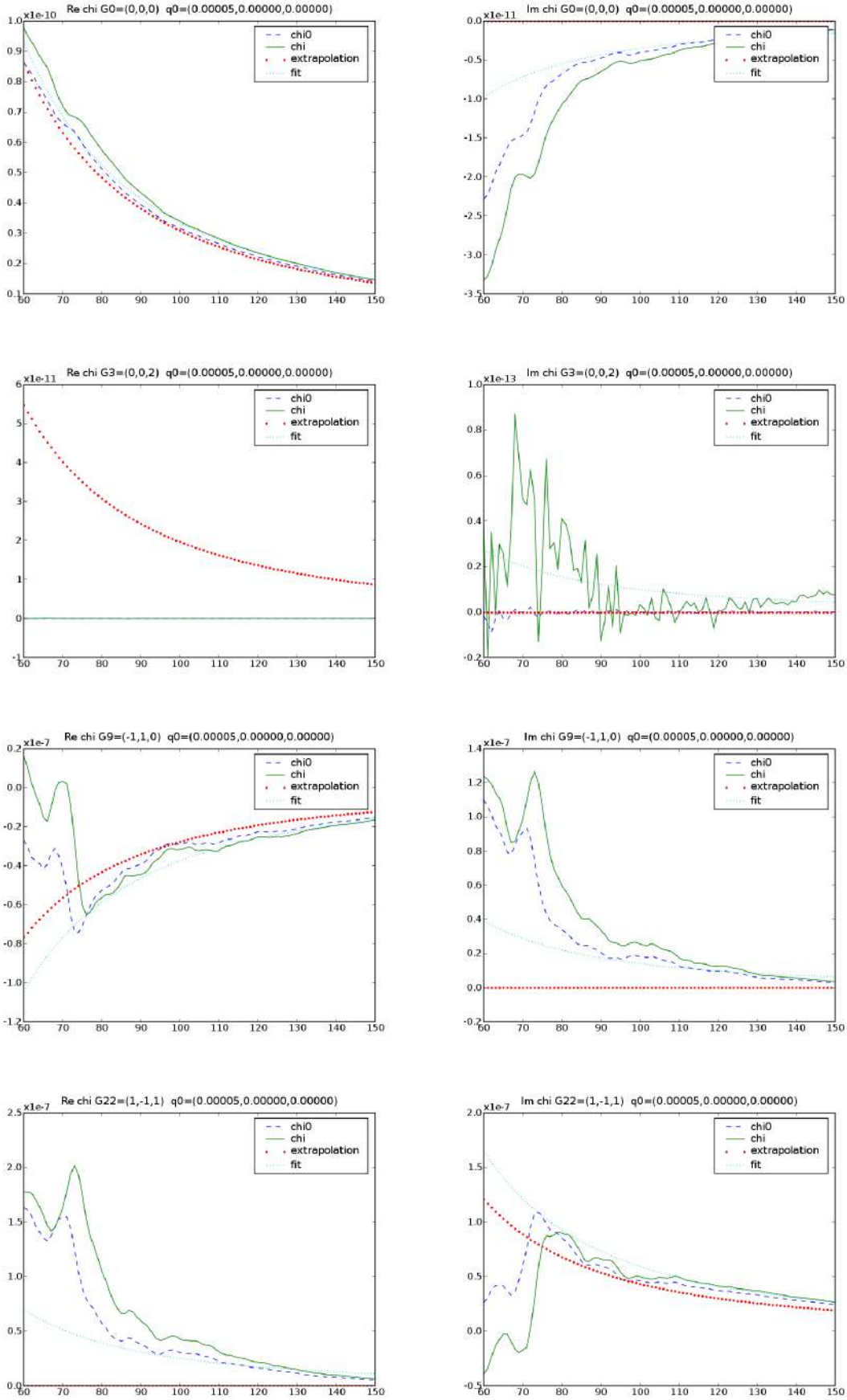

Figure D.3: Tail of $\chi^0_{\mathbf{G0}}$ and $\chi_{\mathbf{G0}}$'s of Fig.D.1, extrapolation of Eq. (D.3) and $\frac{1}{\omega^2}$ fit, $\mathbf{q_0} \to 0$

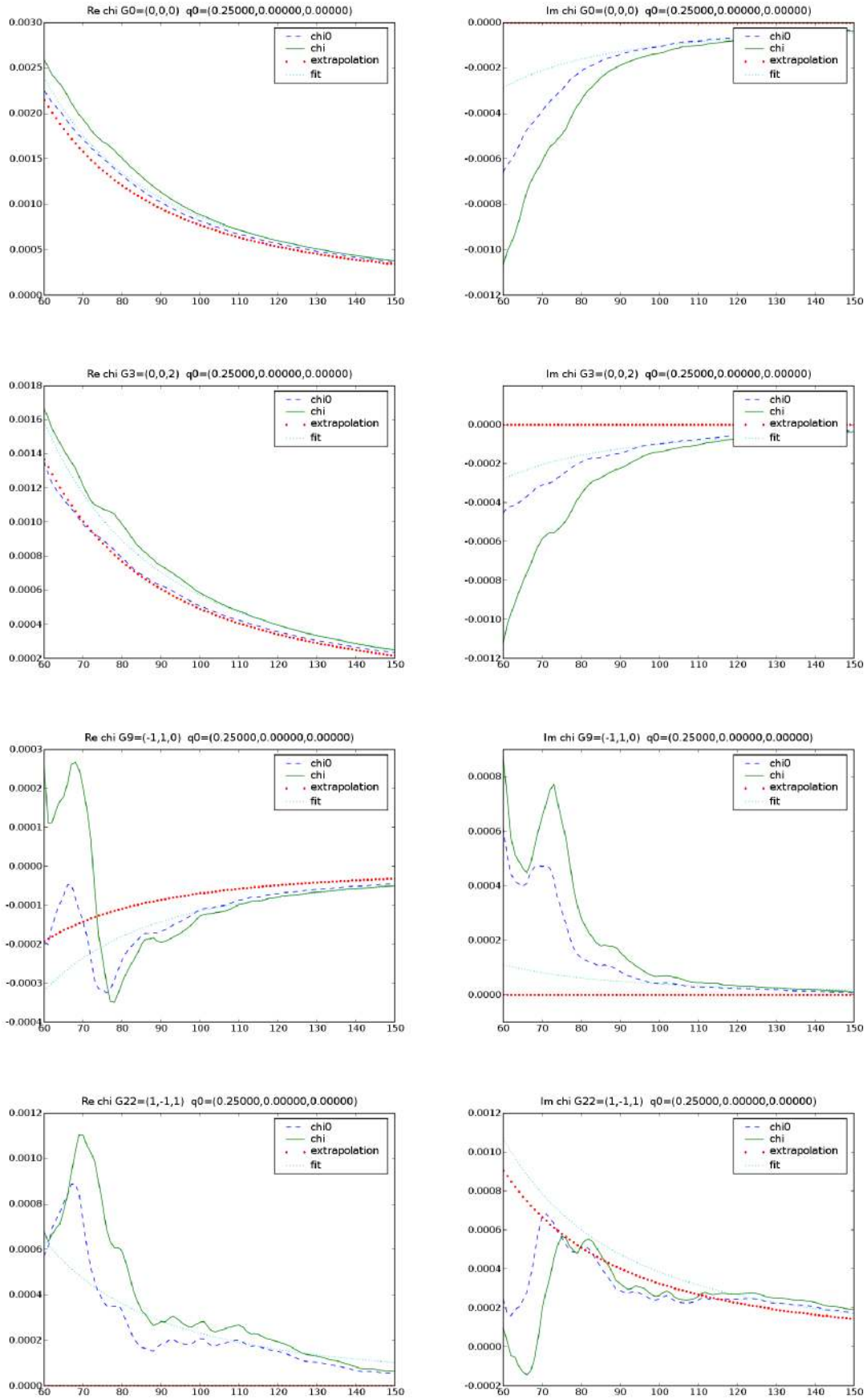

Figure D.4: Tail of $\chi^0_{\mathbf{G0}}$ and $\chi_{\mathbf{G0}}$'s Fig.D.2, extrapolation of Eq. (D.3) and $\frac{1}{\omega^2}$ fit, , $\mathbf{q_0} \neq 0$

With a look at the results in Figs. D.3 and D.4 it appears that the extrapolation seems to work well just in certain cases, while the $\frac{1}{\omega^2}$ fit generally does. This is probably because the starting energy should be bigger for the hypothesis of high frequency to be always satisfied. Another reason could lie in the fact that we are using a non-local potential, and this is in contrast with the hypothesis used in [58, 59].
Unfortunately, this means that we cannot exploit the formula (D.3) for our integration. By the way, this kind of technique may be successfully applied to other systems.

[1]The density operator in reciprocal space is a plane wave: this has already appeared in §5.1.1

References

[1] F. Krausz and M. Ivanov. Attosecond physics. *Reviews of Modern Physics*, 81(109):163, January-March 2009.

[2] P. Abbamonte, K.D. Finkelstein, M.D. Collins, and S.M. Gruner. Imaging density disturbances in water with a 41.3-attosecond time resolution. *Physical Review Letters*, 92(23): 237401, June 2004.

[3] See e.g. URL `http://www.etsf.eu`.

[4] A.G. Marinopoulos, L.Reining, V. Olevano, and A. Rubio. Anisotropy and interplane interactions in the dielectric response of graphite. *Physical Review Letters*, 89(7):076402, August 2002.

[5] A. G. Marinopoulos, L. Reining, A. Rubio, and V. Olevano. Ab initio study of the optical absorption and wave-vector-dependent dielectric response of graphite. *Physical Review B*, 69:245419, June 2004.

[6] J. D. Jackson. *Classical Electrodynamics*. Wiley, 1998.

[7] F. Wooten. *Optical Properties of Solids*. Academic Press, 1972.

[8] V. Lucarini, F. Bassani, K.-E. Peiponen, and J.J. Saarinen. Dispersion theory and sum rules in linear and nonlinear optics. *Rivista del Nuovo Cimento*, 2003.

[9] F. Sottile. *Response functions of semiconductors and insulators: from the Bethe-Salpeter equation to time-dependent density functional theory*. PhD thesis, Ecole Polytechnique, September 2003.

[10] V. Veniard. Microscopic-macroscopic connection. In *CECAM Tutorial - Theoretical Spectroscopy Lectures*, May 2009.

[11] S. Adler. Quantum theory of the dielectric constant in real solids. *Physical Review*, 126(2): 413, April 1962.

[12] N. Wiser. Dielectric constant with local fields effects included. *Physical Review*, 129(1):62, January 1963.

[13] H. Ehrenreich. Electromagnetic transport in solids: Optical properties and plasma effects.

[14] P. Hohenberg and W. Kohn. Inhomogeneous electron gas. *Physical Review*, 136(3B):864, November 1964.

[15] J.E. Inglesfield. *Density Functional Theory*, 1993.

[16] W. Kohn and J. Sham. Self-consistent equations including exchange and correlation effects. *Physical Review*, 140(4A):A1133, November 1965.

[17] M. C. Payne et al. Ab initio iterative minimization techniques. *Reviews of Modern Physics*, 64(4):1051, October 1992.

[18] E. Runge and E. K. U. Gross. Density-functional theory for time-dependent systems. *Physical Review Letters*, 52(12):997, March 1984.

[19] E. K. U. Gross and W. Kohn. Local density-functional theory of frequency-dependent linear response. *Physical Review Letters*, 55(26):2850, December 1985.

[20] M. Born and M. Oppenheimer. Zur quantentheorie der molekœãln. *Annalen der Physik*, 84(457), 1927.

[21] B.H. Bransden and C.J. Joachain. *Physics of Atoms and Molecules*. Prentice Hall, 2003.

[22] D.M. Ceperley and B.J. Adler. Ground state of the electron gas by a stochastic method. *Physical Review Letters*, 45(7):566, August 1980.

[23] S. Moroni, D.M. Ceperley, and G. Senatore. Static response and local field factor of the electron gas. *Physical Review Letters*, 75(4):689, July 1995.

[24] G. Ortiz, M. Harris, and P. Ballone. Zero temperature phases of the electron gas. *Physical Review Letters*, 82(26):5317, June 1999.

[25] J.P. Perdew and M.R. Norman. Electron removal energies in Kohn-Sham density-functional theory. *Physical Review B*, 26(10):5445, November 1982.

[26] C.O. Almbladh and U. von Barth. Exact results for the charge and spin densities, exchange-correlation potentials, and density-functional eigenvalues. *Physical Review B*, 31(6):3231, March 1985.

[27] J. F. Janak. Proof that $\frac{\partial e}{\partial n_i} = \epsilon_i$ in density-functional theory. *Physical Review B*, 18(2): 7165, December 1978.

[28] R. W. Godby. *Unoccupied Electronic States*. Springer-Verlag, 1992.

[29] Y.M. Juan and E. Kaxiras. Application of gradient corrections to density-functional theory for atoms and solids. *Physical Review B*, 48(20):14944, November 1993.

[30] P. Giannozzi. Lecture notes per il corso di struttura della materia. 2005.

[31] M. Petersilka, U. J. Grossman, and E. K. U. Gross. Excitations energies from time-dependent density-functional theory. *Physical Review Letters*, 76(8):1212, February 1996.

[32] H. Appel, E. K. U. Gross, and K. Burke. Excitations in time-dependent density-functional theory. *Physical Review Letters*, 90(4):2003, January 2003.

[33] X. Gonze et al. First-principles computation of material properties: the ABINIT software project. *Computational Materials Science*, 25:478, 2002.

[34] URL `http://www.abinit.org/`.

[35] S. Albrecht. *Absorption Optique des semi-conducteurs et isolants: calculs ab-initio des effets à plusieurs corps*. PhD thesis, Ecole Polytechnique, January 1999.

[36] X. Gonze. Density functional theory: Formalism and implementation. In *CECAM Tutorial - Theoretical Spectroscopy Lectures*, 2009.

[37] H.J. Monkhorst and J.D. Pack. Special points for Brillouin-zone integrations. *Physical Review B*, 13(12):5189, June 1976.

[38] J.C. Phillips. Energy-band interpolation scheme based on a pseudopotential. *Physical Review*, 112(3):685, November 1958.

[39] M.T. Yin and M.L. Cohen. Theory of ab-initio pseudopotential calculations. *Physical Review B*, 25(12):7403, June 1982.

[40] W.E. Pickett. Pseudopotential methods in condensed matter applications. *Computer Physics Reports*, 9(3):116, April 1989.

[41] J.C. Phillips and L. Kleinman. New method for calculating wave functions in crystals and molecules. *Physical Review*, 116(2):287, October 1959.

[42] D.R. Hamann, M. Schluter, and C. Chiang. Norm-conserving pseudopotentials. *Physical Review Letters*, 43(20):1494, November 1979.

[43] N. Troullier and J.L. Martins. Efficient pseudopotentials for plane-wave calculations. *Physical Review B*, 43(3):1993, January 1991.

[44] Y. X. Zhao and I. L. Spain. X-ray diffraction data for graphite to 20 gpa. *Physical Review B*, 40(2):993, July 1989.

[45] A. H. Castro Neto, F. Guinea, N. M. R. Peres, K. S. Novoselov, and A. K. Geim. The electronic properties of graphene. *Reviews of Modern Physics*, 81(109), January-March 2009.

[46] K. S. Novoselov, A. K. Geim, S. V. Morozov, D. Jiang, M. I. Katsnelson, I. V. Grigorieva, S. V. Dubonos, and A. A. Firsov. Two-dimensional gas of massless dirac fermions in graphene. *Nature*, 438(19):197, November 2005.

[47] S. Y. Zhou, G. h. Gweon, J. Graf, A. V. Fedorov, C. D. Spataru, R. D. Diehland Y. Kopelevich, D. h. Lee, Steven G. Louie, and A. Lanzara. First direct observation of Dirac fermions in graphite. *Nature Physics*, 2:595, September 2006.

[48] URL `http://www.dp-code.org`.

[49] URL `http://www.tddft.org/programs/octopus/wiki/index.php/Main_Page`.

[50] D. Pines. *Elementary Excitations in Solids*. Benjamin Cummings, 1963.

[51] D. Pines and D. Bohm. A collective description of electron interactions: II collective vs individual particle aspects of the interactions. *Physical Review*, 85(2):338, January 1952.

[52] D. Bohm and D. Pines. A collective description of electron interactions: III Coulomb interactions in a degenerate electron gas. *Physical Review*, 92(3):609, November 1953.

[53] N.W. Ashcroft and N.D. Mermin. *Solid State Physics*. Brooks/Cole, 1976.

[54] L. Van Hove. Correlations in space and time and Born approximation scattering in systems of interacting particles. *Physical Review*, 95(1):249, 1954 1954.

[55] R. Hambach, C. Giorgetti, N. Hiraoka, Y. Q. Cai, F. Sottile, A. G. Marinopoulos, F. Bechstedt, and L. Reining. Anomalous angular dependence of the dynamic structure factor near Bragg reflections: Graphite. *Physical Review Letters*, 101(26):266406, December 2008.

[56] K. Zeppenfeld. Nichtsenkrechte interbandubergange in graphit durch unelastische elektronenstreuung. *Z. fur Physik A*, 243(3):229, June 1971.

[57] URL `http://www.python.org/`.

[58] D. L. Johnson. Local field effects and the dielectric response matrix of insulators: a model. *Physical Review B*, 9(10):4475, May 1974.

[59] D. L. Johnson. Local-field effects, x-ray diffraction, and the possibility of observing the optical Borrmann effect: Solutions to Maxwell's equations in perfect crystals. *Physical Review B*, 12(8):3428, October 1975.

[60] J. Bak and D. J. Newman. *Complex Analysis*. Springer, second edition, 1997.

[61] Christoph Freysoldt, Philipp Eggert, Patrick Rinke, Arno Schindlmayr, R.W. Godby, and Matthias Scheffler. Dielectric anisotropy in the GW space-time method. *Computer Physics Communications*, 176:1, September 2007.

[62] J. S. Toll. Causality and the dispersion relation: Logical foundations. *Physical Review*, 104 (6):1760, December 1956.

[63] F. Bruneval. *Exchange and Correlation in the Electronic Structure of Solids, from Silicon to Cuprous Oxide: GW Approximation and beyond*. PhD thesis, Ecole Polytechnique, October 2005.